UNIVERSITÀ DI SIENA 1240

Dipartimento di Biotecnologie, Chimica e Farmacia

Dottorato in Chemical and Pharmaceutical Sciences

XXXVI Ciclo

Coordinatore: Prof. Maurizio Taddei

Identification and characterization of natural bioactive molecules and their liposomal formulation

Settore scientifico disciplinare: CHIM-02

Candidato

Dott. Lorenzo Cangeloni

Dip. Biotecnologie Chimica e Farmacia

Firma digitale del candidato

Firmato digitalmente da:
LORENZO
CANGELONI

Supervisore

Prof. Claudio Rossi

Dip. Biotecnologie Chimica e Farmacia

Co-supervisore

Prof.ssa Gabriella Tamasi

Dip. Biotecnologie Chimica e Farmacia

Anno accademico di conseguimento del titolo di Dottore di ricerca

2022/2023

Università di Siena
Dottorato in Chemical and Pharmaceutical Sciences
XXXVI Ciclo

Data dell'esame finale
28/03/2024

Commissione giudicatrice

Supplenti

Summary

Abstract

Growing concerns about the environmental impact of agricultural and agro-industrial waste have promoted exploration towards creating novel natural products that feature additional health benefits. This includes the formulation of novel foods, nutraceuticals, cosmetics, and biocides, all enriched with bioactive compounds derived from materials currently estimated as waste. The focus is on transforming what is traditionally considered waste into valuable resources for the development of products that promote well-being and sustainability. The main target of this thesis is to characterize selected plant matrices to extract specific metabolites that possess bioactive capabilities. The selected matrices are usually considered non relevant products or agricultural waste.

Coffea arabica L. leaves represent a viable alternative to the canonical matrices used for preparation of beverages, such as tea leaves and grounded coffee beans. Coffee leaves infusions are rich in antioxidant phenolic compounds and have a lower concentration of caffeine. Due to increasing interest in this field, a complete study of the bioactive compounds as chlorogenic acids, xanthones and alkaloids is noteworthy. The study was conducted using a combination of spectroscopic techniques as ^{1}H NMR and chromatographic/spectroscopic techniques as HPLC-MS.

Laboratory-scale methods for obtaining bioactive complexes have been developed and optimized, incorporating non-conventional extraction techniques like ultrasound-assisted extraction. These approaches overcome the classical weaknesses of traditional extraction methods. The extraction of 1-DNJ from Morus leaves was optimized using Experimental Desing together with a HILIC chromatography HPLC-MS method. The by-products of the agricultural industry can pose both economic and environmental challenges since they are often destined for disposal, contributing to increased emissions in the production process. The reuse of these by-products is a fundamental aspect of circular economy approaches. Tomato and potato leaves have been studied for their reuse to extract important molecules such as steroidal alkaloids. To quantify these molecules in these matrices, an HPLC-MS method was developed. To deliver the previously studied bioactive compounds and enhance their bioavailability, two formulations of liposomes loaded with extracts of *Coffea arabica* and chlorogenic acid have been synthesized. These systems were characterized through physico-chemical techniques, and the encapsulation efficiency value was also assessed through HPLC-MS and UV-visible analysis.

Chapter I

Introduction

In the contemporary world, a heightened awareness regarding the imperative need for valuable materials is present, given the expanding global population and increasing affluence. One promising opportunity involves the comprehensive utilization of agricultural and agro-industrial by-products within the context of a circular bioeconomy. This approach aims to address environmental, economic, and social concerns. These by-products are often relegated to disposal in fields or employed in energy processes. Despite being perceived as waste, these residues harbor bioactive molecules of considerable value.

The recovery of bioactive compounds from these agricultural and agro-industrial by-products represents a strategic effort with dual benefits: enhancing human health and yielding economic resources. Extracts and purified compounds derived from these so-called wastes present opportunities for formulating new enriched foods, feeds and cosmetics. The primary goal of this thesis is to investigate vegetal matrices for the recovery of components from agricultural and agro-industrial by-products. This approach holds the potential to establish new value chains. Such initiatives can offer economic returns to farmers and industries, while also encouraging employment and improving life quality. Moreover, this strategy aligns with the principles of a circular economy, leading to reduced harmful waste and greenhouse gas emissions in the agri-food sector. The recovery of bioactive compounds from underestimated vegetal components emerges as a novel strategy to fortify and sustain agro-industrial activities. This challenge visualizes a smart and inclusive growth trajectory for the Italian economy. These methodologies aim to restrict or eliminate the production of feedstock by-products and the usage of pollutants detrimental to human and environmental health.

The central focus of the thesis is to maximize the recovery of secondary metabolites, including glycoalkaloids, flavonoids, xanthones, and iminosugars, from agricultural and agro-industrial side products to generate “green” bioactive compounds.

Procedures for the extraction and quantitation of bioactive complexes have been defined and validated, conforming to the principles of green chemistry. Non-conventional extraction methodologies, particularly ultrasound-assisted extraction (UAE) and microwave assisted extraction have been developed and validated for the recovery of bioactive molecules. UAE exploits cavitation phenomena induced by ultrasound waves to agitate the extracting mixture and facilitate the extraction process.

The first vegetal matrix investigated are *Coffea arabica* leaves. Coffee leaves, often overshadowed by the attention given to coffee beans, are emerging as a valuable source of bioactive compounds with potential health benefits.(Campa et al., 2012) These leaves contain a rich array of polyphenols, alkaloids, and other phytochemicals that contribute to their

medicinal properties. One key bioactive compound found in coffee leaves is chlorogenic acid, which is renowned for its antioxidant properties.(X. Chen, 2019) Chlorogenic acid has been associated with various health benefits, including anti-inflammatory effects and the potential to reduce the risk of chronic diseases such as cardiovascular disorders(Ngamsuk et al., 2019a). Moreover, coffee leaves contain catechins, similar to those found in green tea, known for their antioxidant and anti-inflammatory properties. These compounds may play a role in supporting overall well-being and potentially aiding in the prevention of oxidative stress-related conditions. Research suggests that coffee leaf extracts may have antimicrobial properties, contributing to their traditional use in some cultures for medicinal purposes. Additionally, coffee leaves are being explored for their potential role in managing blood sugar levels and improving insulin sensitivity. The importance of understanding and harnessing the bioactive compounds in coffee leaves lies not only in their potential health-promoting effects but also in diversifying the use of coffee plants. By exploring the nutritional and medicinal value of coffee leaves, we can gain a more comprehensive understanding of the plant's benefits beyond the well-known beverage derived from its beans. Further research is ongoing to unlock the full spectrum of bioactive compounds in coffee leaves and their impact on human health.

The thesis primarily targets bioactive molecules known for their health-promoting properties. For instance, *Solanaceae* vegetables, such as potatoes and tomatoes, are rich in glycoalkaloids, which exhibit diverse bioactivities in the human body. The recovery and utilization of glycoalkaloids from potato (*Solanum tuberosum*) and tomato (*Solanum lycopersicum*) leaves, discarded after fruit production, present a viable solution to minimize waste. Potato plants, synthesize two major glycoalkaloids. Solanine and chaconine despite their similar chemical structures differ slightly in their characteristics and potential effects on human health. Solanine is a toxic steroidal glycoside that occurs in Solanaceae plants, particularly in potatoes, especially when exposed to sunlight or subjected to mechanical damage. Like solanine, chaconine can cause adverse effects on human health. Its toxicity is associated with its ability to interfere with the nervous system, leading to symptoms similar to those caused by solanine, such as gastrointestinal and neurological disorders. Both alkaloids play a defensive role for the plants that produce them, providing a form of protection against predators and parasites. These compounds can be used as potential biocides. The interaction mechanism involves the inhibition of enzymes and the ability to disrupt membranes in pathogens(Clemente et al., 2023). In addition, potato glycoalkaloids were studied as potential anticarcinogenic treatment in in vitro testing(Friedman, 2015). Tomato glycoalkaloids protect plants from insects and fungal pathogens, acting on cell membranes. Bioactive compounds in tomatoes exhibit various

beneficial effects, including antioxidant, anti-inflammatory, cardiovascular, and immunostimulant effects(Marcolongo et al., 2020).

Another focus of the thesis involves iminosugars, a unique class of vegetable secondary metabolites abundant in *Morus* crops. The most important iminosugar in mulberry leaves is 1-deoxynojirimycin (1-DNJ)(Rohela et al., 2020). These compounds possess diverse biological activities, including antioxidant and antimicrobial properties. This molecule has gained attention due to its inhibitory effects on alpha-glucosidase, an enzyme involved in carbohydrate digestion(C. Chen et al., 2021). As a result, DNJ has been explored for its potential in managing conditions such as diabetes, as it could help regulate blood sugar levels by slowing down the absorption of carbohydrates. Additionally, 1-deoxynojirimycin has been studied for its potential antiviral properties, particularly against certain enveloped viruses. It works by inhibiting the processing of viral glycoproteins, affecting the maturation of the virus and potentially limiting its ability to infect host cells(Ramappa et al., 2020; Yuan & Zhao, 2017). The thesis focuses on the optimization of the DNJ extraction using design of experiments techniques and a HPLC-MS validated method.

Furthermore, the thesis delves into the application of liposomes as nutraceutical delivery systems. Liposomes, as carriers, aim to transport bioactive molecules to targeted tissues, reducing potential side effects and protecting encapsulated compounds from enzymatic metabolic processes. Liposomes, investigated as nutraceutical delivery systems for phenolic compounds from *Coffea arabica* leaves extracts, hold promise in enhancing bioavailability and targeted delivery. Two cationic liposomes were formulated and used for including polyphenols, chlorogenic acids, xanthones and alkaloids as caffeine have demonstrated various health benefits, and their encapsulation in liposomes could enhance their therapeutic efficacy.

In conclusion, the thesis not only advances sustainable methodologies for recovering bioactive compounds from agricultural and agro-industrial by-products but also explores the potential therapeutic applications of these compounds. The multifaceted nature of these bioactive natural compounds suggests a promising future in the development of therapeutics, further emphasizing the significance of a circular and sustainable bioeconomy in development both economic and health-related advancements.

Chapter II

Coffea arabica L.

II.1 Introduction

The *Coffea arabica L.* is the most prestigious species of the Rubiaceae, perennial plants from whose fruit, the coffee beans are obtained. The family includes several genus and species, but the greatest production of coffee is from *C. arabica* beans, which represent the most diffused variety, at 59%. South America has been, for the last hundred years and still today, the main production area. Currently, the American continent accounts for more than 50% of the world coffee production, with Brazil, Honduras, Mexico, Peru and especially Colombia among the major contributors to the world supply of coffee. During the last years, there has been a continuous and progressive interest increase in coffee leaves applications as a potential alternative to tea, and as food supplement (Campa et al., 2012). Coffee leaves contain several phytochemical molecules such as alkaloids, flavonoids, terpenes, tannins, xanthonoids, phenolic acids, phytosterol, amino acids and carotenoids, which help to give coffee its antioxidant, anti-inflammatory, antihypertensive, anticancer, antibacterial and antifungal properties (X. Chen, 2019; Ngamsuk et al., 2019b). Furthermore, mangiferin has been previously investigated in relation to heart diseases. In particular, natural bioactive molecules have been studied as possible alternatives to synthetic drugs as potential inhibitors of the processes of activation and platelet aggregation (Alañón et al., 2019; Bonechi et al., 2018).

The phytochemical profile of plants varies according to the cultivar, the growth region, the climate and the vegetation stage of the plants, together with the agronomical processes. Several studies have been already published in this field for vegetable species (Tamasi et al., 2021) and for coffee leaves(Monteiro et al., 2020). The post-harvesting processes also affect the overall profile of bioactive molecules in the vegetable(Pardini et al., 2021). As regards coffee beans, they commonly undergo fermentation and roasting procedures to finally obtain the commercial ground coffee powder, that is usually used to make coffee beverages. These processes cause the degradation of most of the chlorogenic acids and other bioactive species that are initially present in the fruits(Perrone et al., 2010). On the contrary, the simpler drying procedures to obtain commercial coffee leaves, can allow the preservation of these bioactive molecules. Additionally, the xanthones family member mangiferin, a potent antioxidant molecule, has been detected and measured in the leaves of *C. arabica.* Its presence in the pulp and peels of coffee berries was previously revealed (Esquivel et al., 2020), but it was never detected before in coffee leaves.

This suggests that coffee leaves have a potentially beneficial profile that is much more important than the most well-known beans. Furthermore, the assessment of the antioxidant and other bioactive properties of the identified and quantified molecules is a very important topic

already studied and reported in many papers(X. M. Chen et al., 2018; Dar et al., 2005; Segheto et al., 2018). Considering the promising beneficial effects on human health and the growing interest in the applications of coffee leaves, it is necessary to fully understand the profile of bioactive components. An important feature of coffee leaf infusions is related to the low concentration of caffeine with respect to regular tea leaves infusion beverages(Boros et al., 2016; Choung et al., 2014). This feature does not affect the polyphenolic concentration and other beneficial bioactive compounds. An infusion of coffee leaves constitutes a potentially healthier option to both coffee and tea. Coffee leaves are rich in phenolic compounds such as mangiferin and the esters of hydroxycinnamic acids (HCEs), which are not present in tea or coffee (Campa et al., 2012).

The present chapter reports on the study that aims to characterize coffee leaf extracts from *C. arabica L.* cultivar, belong the Castillo variety to increase knowledge on antioxidant compounds present in coffee leaves using untargeted high throughput techniques, such as tandem mass spectrometry coupled with high performance liquid chromatography (HPLC-MS^n) and nuclear magnetic resonance spectroscopy (NMR). This experimental design has previously been applied for the study of different plant matrices such as *Olea europaea* L. and *Solanum lycopersicum L.* (Segheto et al., 2018; Tamasi, Baratto, et al., 2019; Tamasi, Pardini, et al., 2019). The novelty of this paper focuses on the optimization of a combined approach, of the two main spectroscopic and spectrometric techniques commonly processed for untargeted metabolomic studies, allowing high throughput. This is intended to avoid, as much as possible, potential critical biases in secondary metabolite identification that are often present in low concentrations, and to characterize the vegetable matrices in their natural complexity. After identification, the main categories of compounds were quantified to assess the concentration of bioactive compounds in *C. arabica L.* leaves.

II.2 Materials and methods

II.2.1 Reagents and standards

All the reagents and solvents listed below were purchased from Sigma-Aldrich (Milan, Italy) and were used without any further purification: mangiferin (≥98.0%), sinapic acid (≥98.0%), quinic acid (≥96.0%), 3,5-dicaffeoylquinic acid (≥95.0%), chlorogenic acid (5 CGA, ≥95.0%), neo-chlorogenic acid (3-CGA, ≥98.0%), crypto-chlorogenic acid (4-CGA, ≥98.0%), quercetin (≥95.0%), quercetin-3β-(D)-glucoside (≥98.0%), trigonelline hydrochloride (≥95.0%), nicotinic acid (≥99.5%), theophylline (≥98.0%), methanol (MeOH, LC-MS grade 99.9%), ethanol (EtOH, LC-MS grade 99.9%), acetonitrile (CH_3CN, ACN, LC-MS grade), formic acid (HCOOH, LC-MS grade 98.5%), deuterated methanol (CD_3OD, MeOD-d_4; 99.8 atom % D). Caffeine (≥98%) was purchased from Extrasynthese (Lyon, France). Ultrapure water (18.2 MΩ·cm) was obtained from a Rephile Direct-Pure water purifier.

II.2.2 Plant material collection, pre-treatment and extraction

The *Coffea arabica L.* leaves were collected in Colombia, in the Department of Huila at Garzon, located in the central part of the country at an altitude of about 1700 m asl, on a cultivation of Castillo variety. Once collected, the coffee leaves underwent a freeze-drying procedure, to allow the conservation of the bioactive components over time. The leaves were frozen under liquid nitrogen and then freeze-dried (-48 ± 2 °C, 450 ± 50 μBar) for 96 h. After freeze-drying, the samples were cold crushed in a knife mill using liquid nitrogen (Pulverisette 11, Fritsch) and sieved to obtain a particle size <500 μm. The ground leaves were stored at –20 ± 1 °C before subsequent analyses. The extraction protocol was optimized based on procedures previously reported, with some modifications (Alañón et al., 2019; Boros et al., 2016; Pardini et al., 2021). Aliquots of 0.500 g of lyophilized sample were treated with 10 mL of a solvent mixture consisting of EtOH/H_2O (70:30, v/v). The extraction process was assisted by ultrasound sonication using an ultrasonic bath (10 min, 20 ± 1 °C; nominal power 120 W; ultrasound frequency 35 kHz; Branson Ultrasonics Corporation, Danbury, CT, USA). The suspension was then centrifuged (5 min, 1882 g; Thermo Electron Corporation PK 110 centrifuge). The supernatant was carefully separated from the solid residue and then transferred into a polypropylene tube. The extraction procedure was repeated three times, using 10 mL of mixture (each time) on the residual solid phase. The aliquots of extracts were combined (total volume,

30 mL) and the extract was dried overnight under a gentle nitrogen flow, and finally stored in polyethylene tubes at –20 ± 1 °C before subsequent analyses.

II.2.3 Nuclear Magnetic Resonance (NMR) experiments.

NMR experiments were performed using a Bruker DRX-600 Avance spectrometer operating at 600.13 MHz for ^{1}H, equipped with an xyz gradient unit. Spectra were processed using Bruker TopSpin software (version 3.6.1, Bruker, Bremen, Germany). The dried extract was freeze dried to remove the eventual humidity, and then reconstituted in deuterated methanol (MeOD-d_4) for NMR analysis.

II.2.4 Chromatographic conditions

The coffee leaves extract was resuspended in MeOH/H_2O mixture (40:60 %v/v) and the analyses were performed using an HPLC instrument (Thermo Fisher Scientific UltiMate 3000) coupled to a linear ion trap mass spectrometer (Thermo Fisher Scientific LTQ XL), equipped with an electrospray ion source (ESI). The spectra were acquired and processed using Xcalibur software (Thermo Fisher Scientific, Waltham, MA, USA). A biphenyl column was used for the analysis (Biphenyl Phenomenex Kinetex, 100 × 2.1 mm; particle diameter 2.6 μm; porosity 100 Å) with a phenyl Security Guard pre-column (4.0 × 2.0 mm, Phenomenex, Torrance, CA, USA). The column temperature was 35 ± 1 °C. The eluents were (A) H_2O and (B) MeOH, both acidified with formic acid (0.1%), and the gradient of elution was optimized based on subsequent positive or negative ESI process, as hereafter reported. Gradient for ESI negative mode: from 0 to 15.0 min 10–15% B (linear); from 15.0 to 25.0 min 15–50% B (linear); 25.0 to 35.0 min 50–95% B (linear). Gradient for ESI positive mode: from 0.0 to 5.0 min 0% B (isocratic); from 5.0 to 45.0 min 0–70% B (linear). In both cases, the injected volumes were 3 μL, and the flow rate was 0.4 mL/min. Each standard and sample was injected and analyzed in triplicate.

II.2.5 HPLC-MS^n method for qualitative and quantitative analysis of the extracts

To identify the analytes in the extracts, the MS^n spectra products from the sequentially fragmented molecules within the ion trap were compared with the spectra of the characteristic fragments obtained from the standards and spectra reported in literature. The main feature of this method is to take advantage of the linear ion trap ability to fragment a specific ion inside the trap, separating it in time, unlike what happens in other analyzers that separate in space (Q, TOF, EB).

To characterize the extracts, a preliminary approach was used to collect information on the structure and the fragmentation of the various analytes by using a data dependent acquisition approach. Each MS scan in both positive and negative modes above a specific threshold level was collected and the most abundant ion was fragmented through CID (collision induced dissociation) using He as a collision gas, generating a MS^2 spectra; the first and second most abundant ions were then fragmented again in two separate steps, generating two different MS^3 spectra. The generated spectral fragmentation tree was used to preliminarily identify the constituents of the extracts. All the identified constituents were compared with spectral databases (MassBank, mzcloud, HMDB) and the relative standard compounds when available. The MS full scan analyses were in the range of *m/z* 100–1000. The collision energies were 35 nCE (normalized collision energy) and 45 nCE, respectively for MS^2 and MS^3 fragmentation steps.

The ESI parameters were optimized in both positive and negative modes through direct injection of the standards of the major components of the extracts: pure caffeine, chlorogenic acid, mangiferin and rutin, dissolved in a MeOH/H_2O (60:40, %v/v) mixture. For negative ionization, the following parameters were optimized: spray voltage 3000 V, sheath gas and auxiliary gas pressure of 35 and 25 arbitrary units, respectively, capillary temperature 350 °C. For positive ionization, the following parameters were optimized: spray voltage 3500 V, sheath gas and auxiliary gas pressure of 20 and 12 arbitrary units, respectively, capillary temperature 300 °C.

The single ion monitoring (SIM) method was used for the quantitation of all caffeoylquinic derivatives, mangiferin and alkaloids, selecting ions with the values of *m/z*, as shown in Table II.1. All molecules except alkaloids were quantified in negative mode via external calibration method using the external calibration method with internal standards. The calibration curves of the analytes were acquired in triplicate and obtained by plotting the area ratio of the analytes normalized by the internal standard against the analyte concentration in the linearity ranges

(Table II.1). Chlorogenic acids were quantified using the calibration curve built from 5-caffeoylquinic acid, while mangiferin isomers were quantified on the curve obtained from a standard of mangiferin. For the quantitation of dicaffeoylquinic acids, a calibration curve obtained from 3,5 dicaffeoylquinic acid was used. For the alkaloids, each molecule was quantified on its relative standard. The results were expressed as g/kg of sample dry weight (DW).

Table II.1: List of quantified compounds in the *C. arabica* extracts with the relative internal standards and ESI ionization mode and calibration curve parameters.

No.	Compound	Internal Standard	ESI Mode	$[MH]^-$ $[MH]^+$	Equation	R^2	Linearity Range (µg/mL)	LoD//LoQ (µg/mL)
1	3-CGA	Sinapic acid	(−)	353	y = 0.741x	0.9986	0.500–10.0	0.07//0.30
3	4-CGA							
4	5-CGA							
34	3,5-dCQA		(−)	515	Y = 0.395	0.9961	0.500–10.0	0.10//0.35
33	3,4-dCQA							
36	4,5-dCQA							
5	Mangiferin	Quercetin	(−)	421	y = 2.962x	0.9995	0.025–2.50	0.007//0.023
22	Isomangiferin							
39	Caffeine	Theophylline	(+)	138	y = 6.530x	0.9997	0.025–12.5	0.004//0.010
38	Trigonelline	Nicotinic acid	(+)	195	y = 0.892x	0.9983	0.100–12.5	0.02//0.06

II.3 Results and discussion

II.3.1 ^{1}H NMR analysis of *Coffea arabica* leaves extract

NMR spectroscopy was used to characterize the main components of the extract without any further purification. The acquired ^{1}H spectrum for the coffee leaf extract reconstituted in CD_3OD is reported in Figure II.1. The signals reported in the spectrum were analyzed and compared with the available standards in already published papers (Choung et al., 2014; Tamasi, Baratto, et al., 2019) and databases (HMDB, BMRB) (Ulrich et al., 2007; Wishart et al., 2022).The spectrum can be divided into three main sections based upon the chemical shift values of the principal compounds.

The assignment of the signals is reported in Figure II.2 and the chemical shift values are reported in Table II.2, together with the multiplicities and coupling constants.

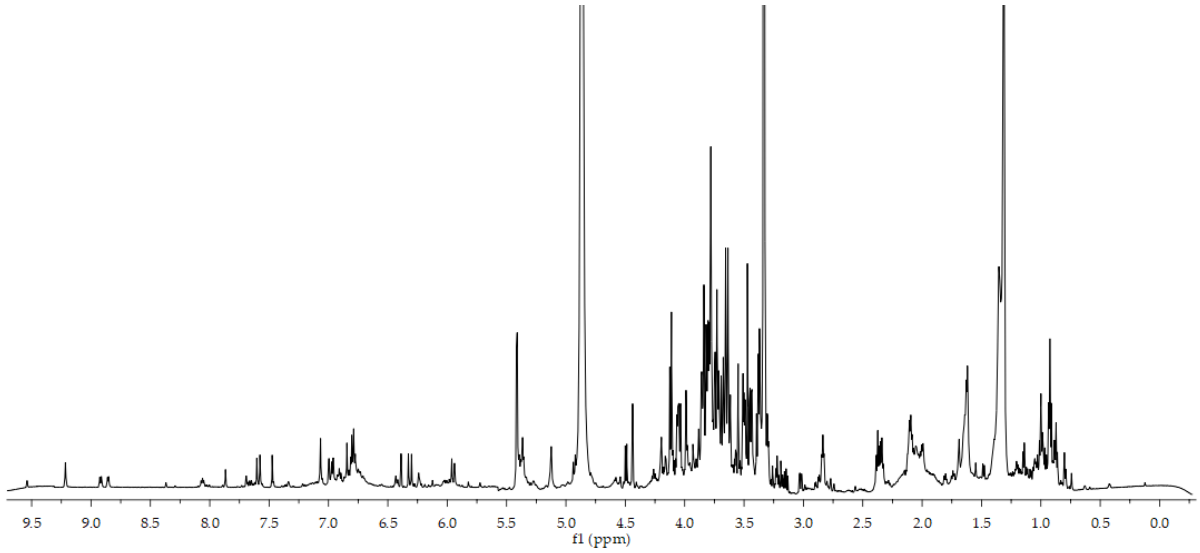

Figure II.1: ^{1}H NMR (600 MHz) spectrum of *Coffea arabica L.* leaf extract resuspended in deuterated methanol.

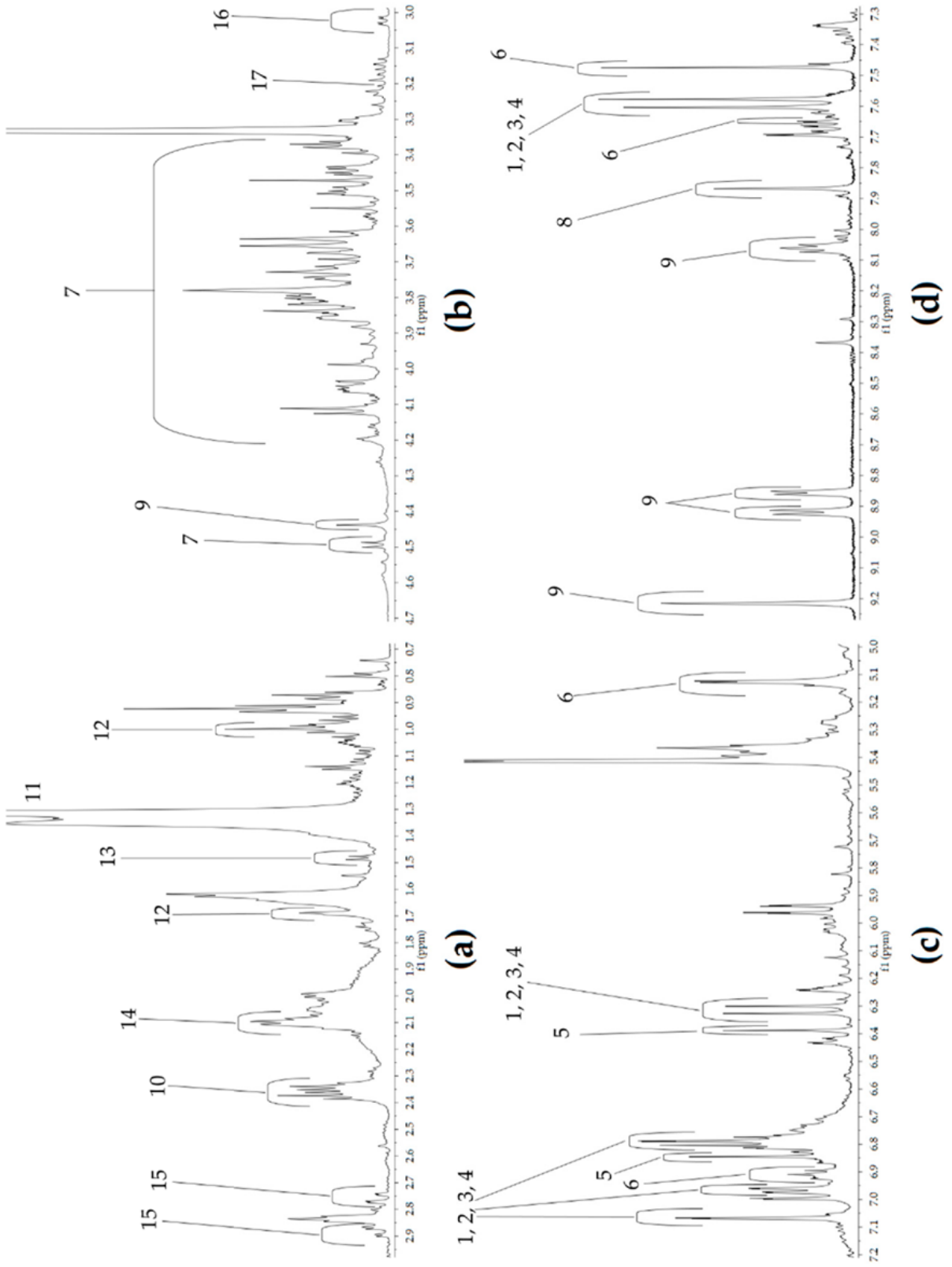

Figure II.2: Magnification of the four main section of the ^{1}H NMR spectrum of *C. arabica L.* leaf extract: (a) 0.0–3.0 ppm, (b) 3.0–5.0 ppm, (c) 5.0–7.2 ppm, (d) 7.3–9.3 ppm.

Table II.2: Assignment of ^{1}H NMR signals in *C. arabica L.* leaf extracts.

No.	Compound	^{1}H Chemical Shifts (ppm) [J-Coupling Values (Hz)]
1, 2, 3, 4	Chlorogenic acids	6.32 (d, 15.74), 6.80 (d, 8.14), 6.97 (dd, 1.9,1.9), 7.07 (d, 2.0), 7.59 (d, 15.9)
5	Mangiferin	6.39 (s), 6.84 (s)
6	Rutin	5.13 (d, 3.62), 7.65 (d, 2.4) 6.90 (m), 7.48 (s)
7	Saccharides	4.50 (d, 7.7), 3.3–4.2
8	Caffeine	7.87 (s)
9	Trigonelline	8.06 (t, 7.61), 9.22 (s), 8.86 (d, 5.9), 8.92 (d, 7.8), 4.47 (s)
10	Malic acid	2.37 (dd,15.3, 10.0)
11	Lactic acid	1.34 (d, 10.5)
12	Leucine	0.98 (t, 7.2), 1.69 (m)
13	Alanine	1.46 (d, 7.2)
14	Glutamine	2.12 (m)
15	Aspartic acid	2.75 (dd, 15.2, 8.3), 2.85 (dd, 17.3, 4.1)
16	Cystein	3.03 (dd, 2.7, 2.8)
17	Choline	3.22 (s)

The first section (0.0–3.0 ppm, Figure II.2a) corresponds to the region usually associated with aliphatic compounds, amino acids and organic acids (Gogna et al., 2015) In this part of the spectrum are located the signals of compounds 12–17, respectively assigned to malic and lactic acid, Leu, Ala, Glu, and Asp. The most intense signals are located in the central part of the spectrum, from 3.0 to 5.0 ppm (Figure II.2b): This section is dominated by carbohydrates signals, principally attributed to hexose, deoxyhexose and pentose monosaccharides involved in the glycosylation of the main compounds. In addition, Cys (18) and choline (19) are assigned in this interval at chemical shift values of 3.0 and 3.2 ppm, respectively. The downfield section (5.0–10.0 ppm; Figure II.2c, d) contains signals that arise from aromatic molecules; the main components identified are phenolic compounds as chlorogenic acids (compounds 1, 2, 3, 4), caffeic acid (5), the flavonoid rutin (7) and the xanthone mangiferin (6). Another important class of compounds identified in this spectral section correspond to alkaloids, specifically caffeine (10) and trigonelline (11), located in the most downfield section of the spectrum (7.0–9.5 ppm, Figure II.2d).

II.3.2 HPLC-ESI (−)-MS^n profiling of *Coffea arabica* leaf extract

The dried extracts were resuspended in MeOH/H_2O (60:40, % v/v) filtered through a 0.2 μm PTFE syringe filter (Whatman) before injection, and analyzed through data dependent analysis, resulting in the chromatogram reported in Figure II.3.

The identified compounds are members of different categories of phenolic compounds—xanthones, flavonoids, chlorogenic acids, and lignans—except the first compound (18) with *m/z* 191, which was not retained in the chromatographic elution. After accurate analysis of the product ions generated from MS^2 fragmentation shown in Table II.3, the compound was identified as quinic acid; this was confirmed through comparison with the available standard.

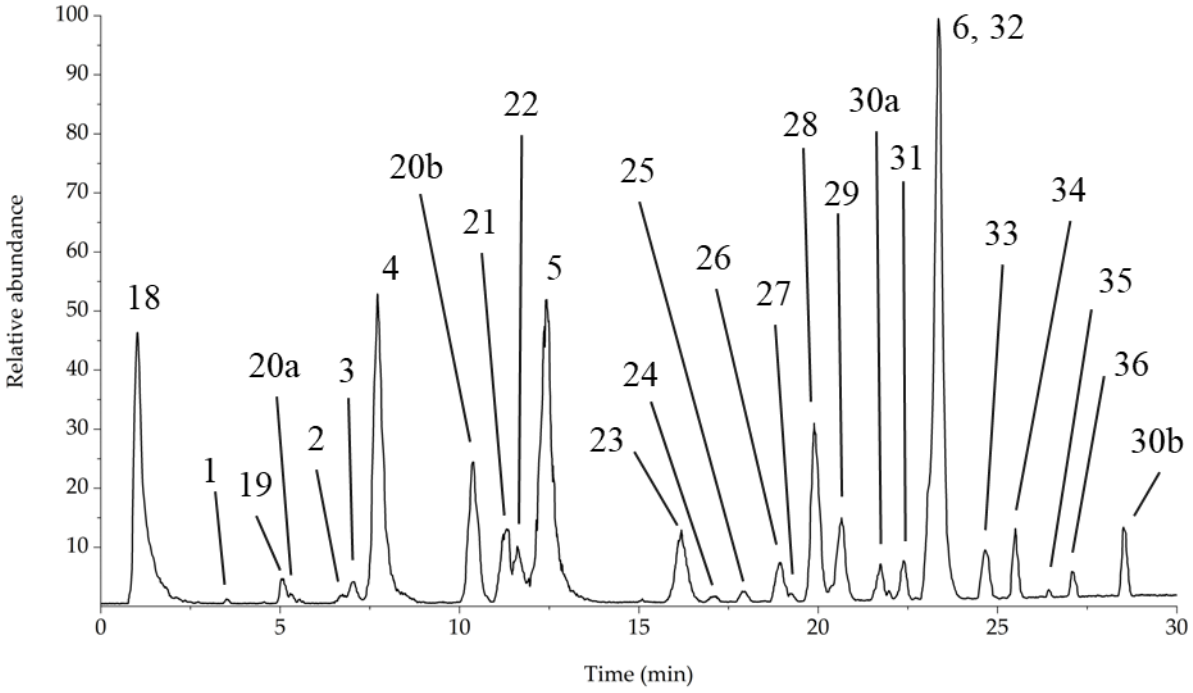

Figure II.3: HPLC-ESI(−) chromatogram of coffee leaves extract. The identified compounds are numbered as also reported in Table II.3.

Table II.3: Assignment of identified compounds in HPLC-ESI chromatograms of coffee leaf extracts. The *m/z* values reported in bold represent the base peak of each spectrum. In MS^2 spectra the base peak was fragmented to generate the MS^3 fragmentation spectra. The MS^2 and MS^3 fragmentations are from HPLC-ESI chromatograms acquired in negative mode. (1) identified as double charged, (2) identified in ESI+ mode.

No.	Compound	Rt (min)	$[M-H]^-$	$[M+H]^+$	MS^2	MS^3
18	Quinic acid	1.00	191		127–**173**–111–93	-
1	3-Caffeoyl-quinic acid	3.51	353	355	179–**191**	**126**–173–171
19	Iriflophenone 3-C-glucoside	5.07	407	-	317–**287**	243–**193**–167
20a	Catechin/Epicatechin	5.28	289	291	271–**245**–205–179	227–**203**–161
2	1-Caffeoyl-quinic acid	6.69	353	355	**191**–173–179	173–171–**126**
3	4-Caffeoyl-quinic acid	7.06	353	355	**173**–179–191	**155**
4	5-Caffeoyl-quinic acid	7.70	353	355	**191**	173–171–**126**
20b	Catechin/Epicatechin	10.38	289	291	271–**245**–205–179	227–**203**–161
21	Procyanidin B	11.22	577	579	**425**–407–289	**407**–273
22	Isomangiferin	11.63	421	423	**301**–331	273–**258**
5	Mangiferin	12.42	421	423	**301**–331–403	273–**258**
23	Procyanidin trimer A-type	16.19	863	865	**711**–573–451–411	**693**
24	Procyanidin tetramer B-type [1]	17.10	576	-	**500**–491–289–567–559–451	-
25	Apigenin 6,8-di-C-glucoside	17.91	593	-	**473**–503–383–353	383–**353**
26	Procyanidin C	18.95	865	-	739–**695**–577–847–449–425	677–**543**–525–451–405–289
27	5-Feruloyl-quinic acid	19.25	367	-	**191**–163	173–171–**127**
28	Rutin glycoside	19.89	771	773	753–609–**591**–301–300–271	547–445–409–367–**355**–301
29	Quercetin sophoroside	20.70	625	627	505–463–445–**301**	**271**–255–179
30a	Cinchonain I isomer	21.75	451	-	**341**	231–**217**
31	Kaempferol triglycoside	22.41	755	-	**575**–285	393–**339**
6	Rutin	23.36	609	611	**301**	271–**179**–151
32	3,4-Dicaffeoyl-quinic acid	24.00	515	-	**353**–335	191–179–**173**
33	3,5-Dicaffeoyl-quinic acid	24.62	515	-	**353**	**191**–179–173
34	Kaempferol-3-O-rhamnoglucoside	25.50	593	-	**285**	267–**257**–241
35	4,5-Dicaffeoyl-quinic acid	26.44	515	-	**353**	**191**–179–173
36	6-O-(p-hydroxybenzoyl)mangiferin	27.10	541	-	**331**–301	**313**–301–271–259
30b	Cinchonain I isomer	28.52	451	-	**341**	231–**217**
37	Trigonelline [2]	1.11	-	138	**121**	-
38	Caffeine [2]	20.69	-	195	**138**	**121**

II.3.2.1 Xanthones

The first compound related to the xanthone structure was compound 19. The deprotonated molecule shows a $[M-H]^-$ ion at *m/z* 407, producing ions at *m/z* 287 and 317 in MS^2 and 193, 243, 167 in MS^3 fragmentations. The compound was identified as iriflophenone-3-C-glucoside (Figure II.4a), in agreement with database spectra and previous published papers (Malherbe et al., 2014). Other xanthone molecules were eluted at Rt of 11.63 and 12.42 min, respectively; the molecules show the same MS^n fragmentation with a $[M-H]^-$ ion at *m/z* 421, and were identified as isomangiferin (22, Figure II.4b) and mangiferin (5, Figure II.4c). The same fragmentation pattern of the two molecules required the optimization of the chromatographic separation, and the consequent structure assignment was based on comparison with Rt and MS^n fragments of the standard mangiferin. The last compound identified as xanthone was eluted at Rt 27.10 min; the deprotonated molecule shows *m/z* 541 and the most abundant ions in MS2 spectrum were at *m/z* 331 and 301, as reported for compounds 22 and 5. The ion at *m/z* 331 was consequently fragmented, generating product ions at *m/z* 313, 301, 271 and 259. These fragmentations led to the identification of compound 37 as 6-O-(p-hydroxybenzoyl) mangiferin (Figure II.4d), in agreement with database spectra and previous published papers(Barreto et al., 2008).

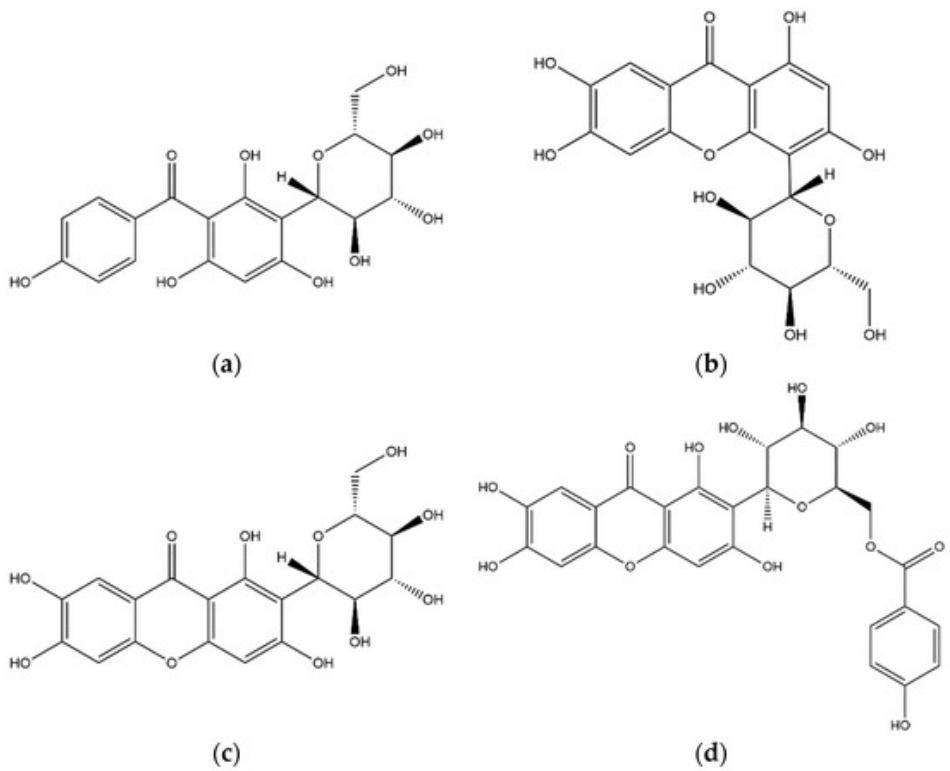

Figure II.4: Structures of selected xanthones identified in the coffee leaf extract:
(a) iriflophenone-3-C-glucoside, (b) isomangiferin, (c) mangiferin, (d) 6-O-(p-hydroxybenzoyl) mangiferin.

II.3.2.2 Chlorogenic acids

This class of molecules is represented by 5-caffeoyl-quinic acids and is composed by esters of hydroxycinnamic acids (ferulic, caffeic, p-coumaric acids) with quinic acid. They are widely studied (de Almeida et al., 2019a; Jaiswal et al., 2010; Kazuno et al., 2005; Panche et al., 2016a; Salerno et al., 2016) for their antioxidant properties and high concentrations in plant matrices. Mono caffeoyl-quinic acids have $[M-H]^-$ ions at *m/z* 353 and their differentiation is based upon the MS2 fragmentation as reported from literature(Clifford et al., 2003, 2008). In this study, four different species were isolated at Rt values, as reported in Table II.3; the species identified are 3-CGA (1), 1-CGA (2), 4-CGA (3) and 5-CGA (4). The structural assignment was based on the comparison with the relative standards for compounds 1, 3 and 4, while for compound 2, the tentative structural identification was based on literature(Clifford et al., 2003). The MS2 fragmentation of mono caffeoyl-quinic acids is reported in Figure II.5.

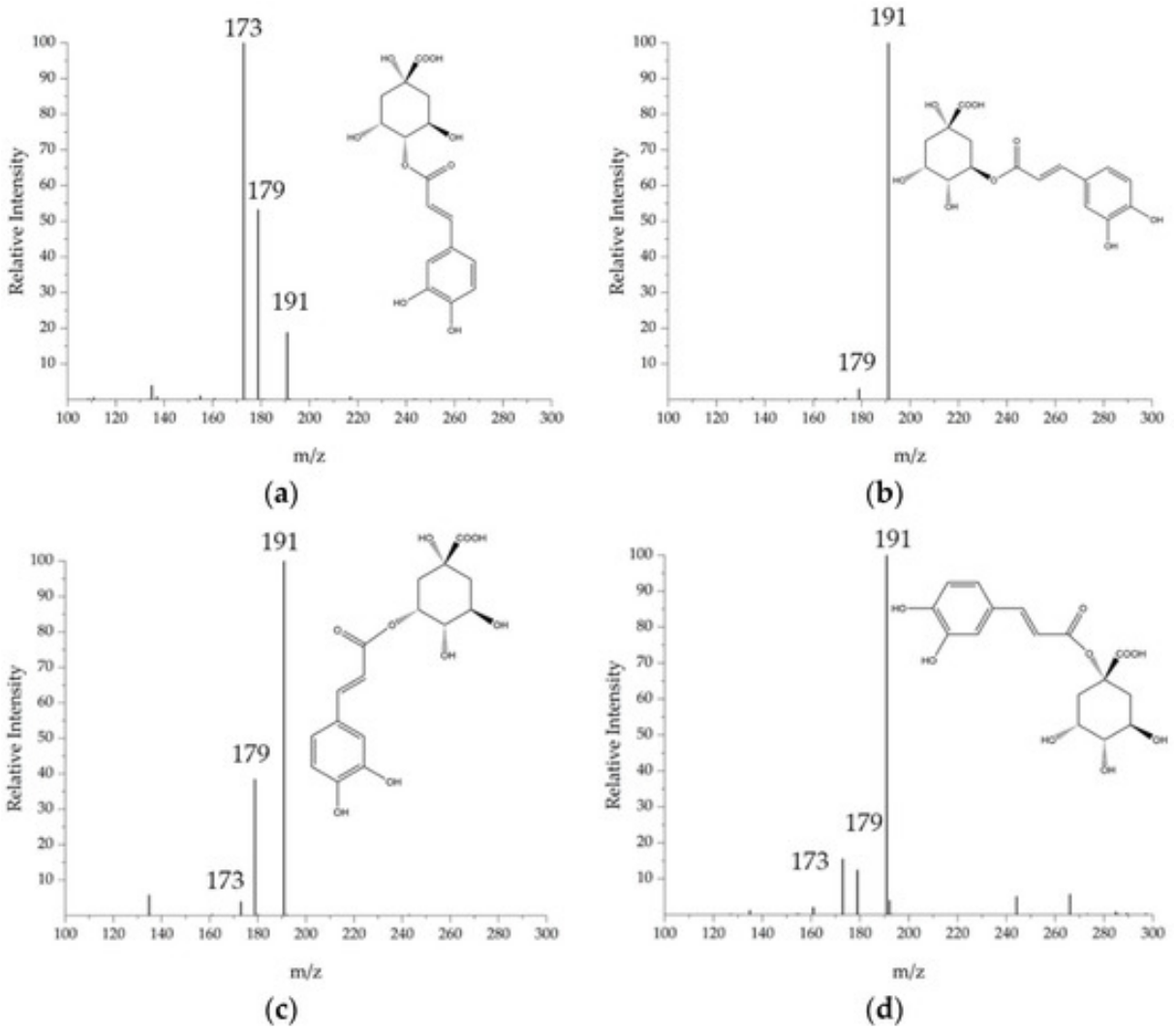

Figure II.5: Tandem mass spectra of the compounds 1, 2, 3, and 4, identified as chlorogenic acids: (a) 4-CGA, (b) 5-CGA, (c) 3-CGA, (d) 1-CGA.

Compound 28 was eluted at Rt 19.25 min with a $[M-H]^-$ ion at *m/z* 367; after the first fragmentation, the MS^2 full scan spectrum presented two main fragments at *m/z* values of 191 and 16; the following fragmentation of the *m/z* 191 ion produced three fragment ions at *m/z* values 127, 173 and 171. The compound 28 was identified as 5-feruloyl-quinic acid (5-FQA, Figure II.6a) by comparison with data previously reported (Clifford et al., 2003).

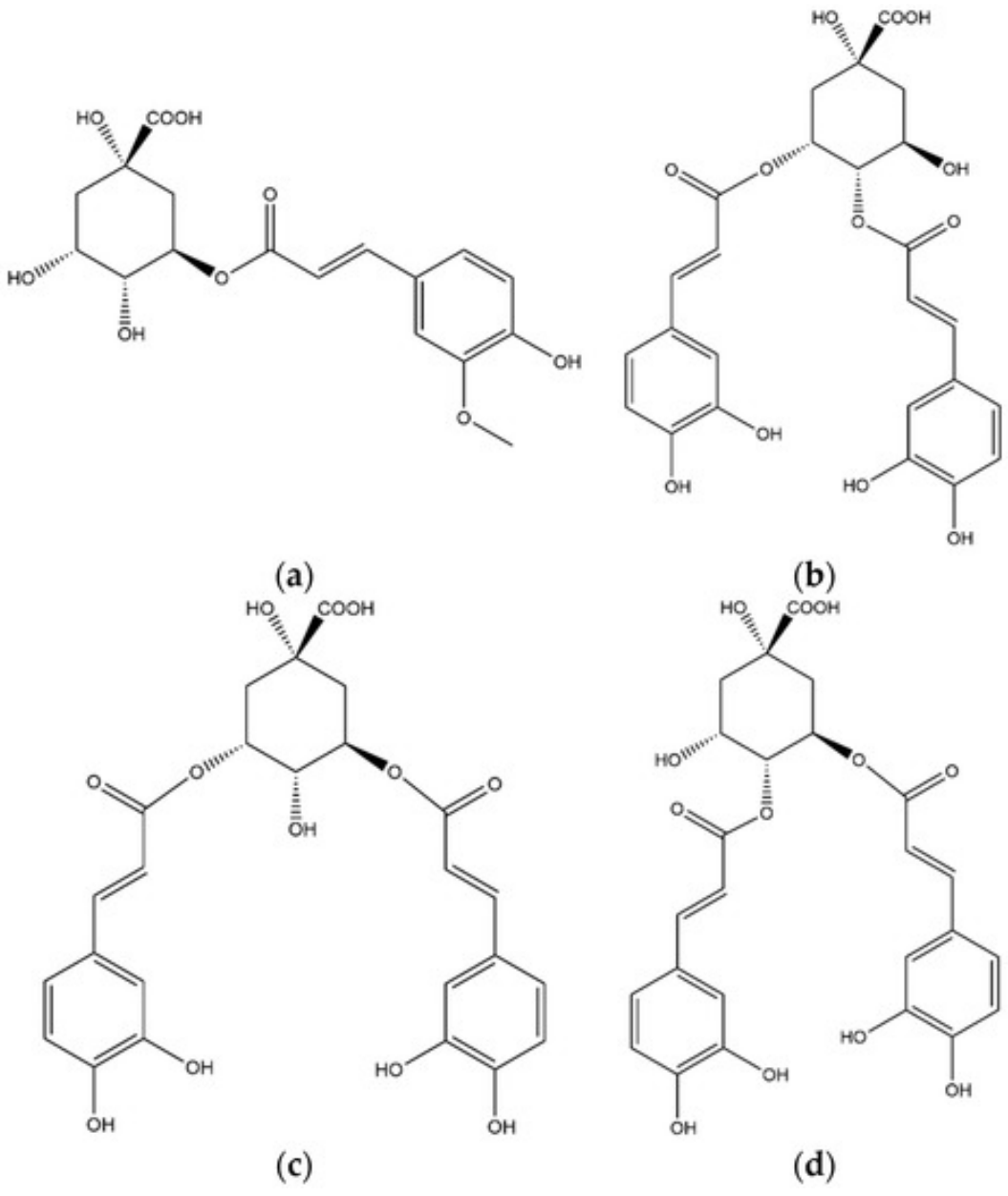

Figure II.6: Structures of the chlorogenic acids identified in the coffee leaf extract: (a) 5-feruloyl-quinic acid, (b) 3,4-dicaffeoyl-quinic acid, (c) 3,5-dicaffeoyl-quinic acid, (d) 4,5-dicaffeoyl-quinic acid.

The dicaffeoyl-quinic acids are represented by the ion $[M-H]^-$ at *m/z* 515; in the present study three compounds with the same *m/z* value were eluted at Rt 24.00 (33), 24.62 (34), and 26.44 (36) min, respectively. The three compounds were identified, as reported in literature(Tamasi, Pardini, et al., 2019), as 3,4-dicaffeoylquinic acid (33, Figure II.6b), 3,5-dicaffeoylquinic acid (34, Figure II.6c) and 4,5-dicaffeoylquinic acid (36, Figure II.6d).

II.3.2.3 Flavonoids

Flavonoids are a class of phenolic molecules widely distributed in plant matrices that have important antioxidant activities(de Almeida et al., 2019a). The compound 26 was eluted at 17.91 min with a $[M-H]^-$ ion at *m/z* 593. The fragmentation of the deprotonated molecule produced a MS^2 spectra with the base peak at *m/z* 473, together with the ions at *m/z* 503, 383 and 353. The main neutral loss of 120 Da was addressed as a loss of C-glucoside moiety. This fragmentation pattern, connected with the absence of the regular neutral loss of 162 Da previously observed for O-glycosides (Kazuno et al., 2005; Panche et al., 2016b), allowed the identification of the compound as a C-glucoside derivative. The *m/z* 473 ion was then fragmented, producing an MS^3 spectrum with a base peak at *m/z* 353, confirming a consecutive loss of C-glucoside moiety. The comparison of these fragmentation patterns with data previously published (Salerno et al., 2016) and with databases (mzcloud) allowed the identification of compound 26 as apigenin 6,8-di-C-glucoside (Figure II.7a).

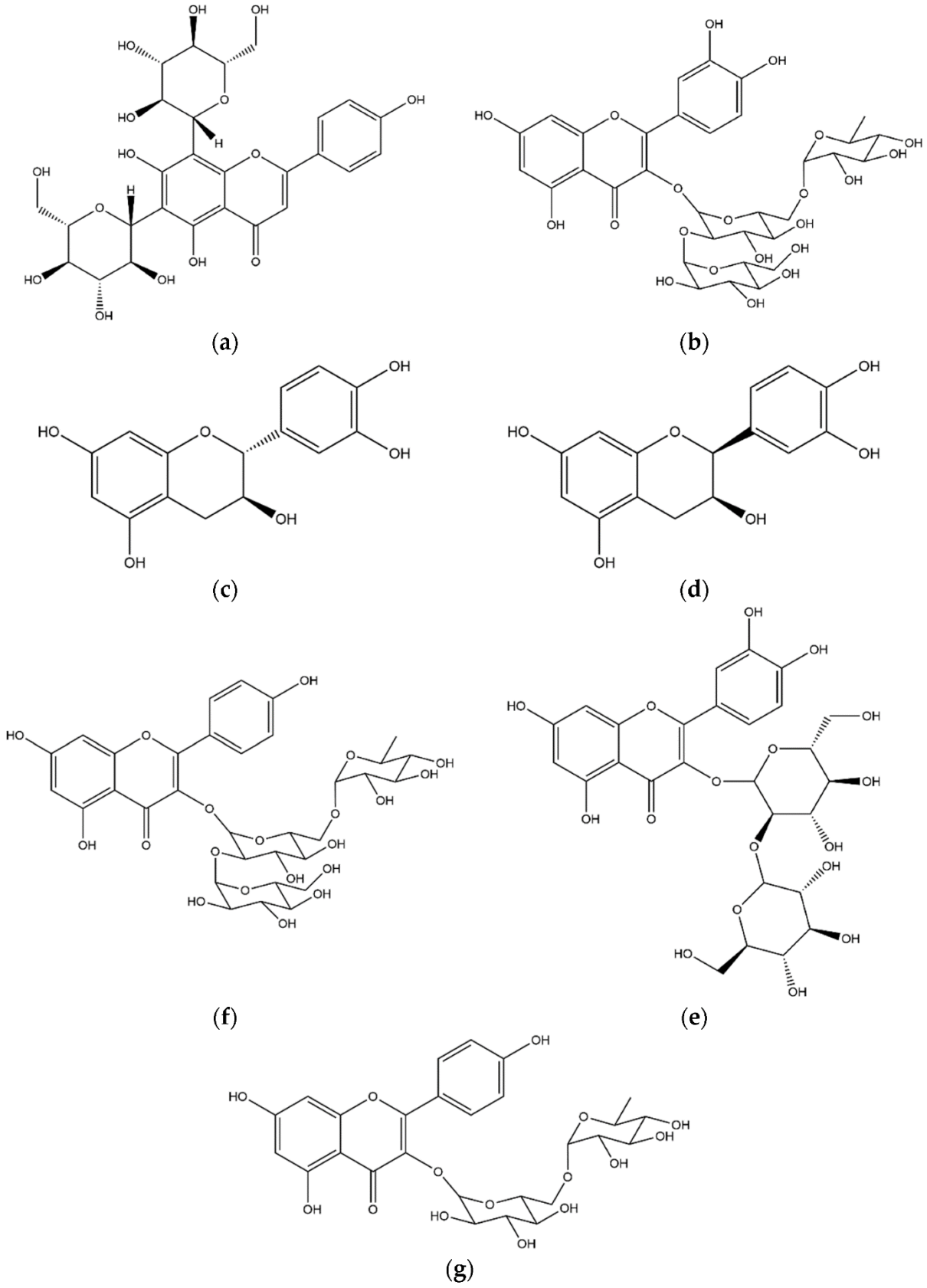

Figure II.7: Structures of the main flavonoids identified in the coffee leaf extract: (a) apigenin 6,8-di-C-glucoside, (b) rutin glycoside, (c) (+)catechin, (d) (+)epicatechin, (e) quercetin sophoroside, (f) kaempferol triglycoside, (g) kaempferol rhamnoglucoside.

The second flavonoid was eluted at Rt 19.89 min (compound 29) with a base peak ion at *m/z* 771. The fragmentation produced a MS^2 spectra reporting the classic main losses of O-glycosylated flavonoids, producing the ions at *m/z* 609 ([M−Hexose−H]$^-$), 591 ([M−Hexose−H2O−H]$^-$) and 301 ([M−2Hexose−Deoxyhexose−H]$^-$). The MS^3 fragmentation of the MS^2 base peak at *m/z* 591 produced several fragments consistent with the identification of a glycosylated rutin molecule (quercetin rutinoside). The identification of compound 29 as rutin glycoside (Figure II.7b) was also suggested (de Almeida et al., 2019b).

Two compounds with the same [M−H]$^-$ ion at *m/z* 289 were eluted at Rt 5.28 min and 10.38 min. The two compounds show the same fragmentation pattern in both MS^2 and MS^3 fragmentation steps. The fragmentation was compatible with the one obtained for the catechin and epicatechin standards and was compared with databases and literature (Stöggl et al., 2004). Compounds 20a and 20b were identified as catechin/epicatechin (Figure II.7c, d).

Compound 30 showed a Rt 20.70 min and a base peak ion at *m/z* 625; the compound was identified as quercetin sophoroside (Figure II.7e) based on the relative abundances and the values of the neutral losses in MS^2 and MS^3 spectra. In MS^2, four main product ions were identified as [M−Hexose−H]$^-$ (*m/z* 463), [M−Hexose−H2O−H]$^-$ (*m/z* 445) and [M−2Hexose−H]$^-$ (*m/z* 301). The MS^3 fragmentation was performed on the ion at *m/z* 301 and corresponded to the ESI negative fragmentation of the quercetin aglycone. The identification of compound 30 was also confirmed by NMR and tandem mass spectrometry data in literature (de Almeida et al., 2019b; Y. Wang et al., 2020).

Kaempferol triglycoside was eluted at Rt 22.41 min and reported in Table II.3 as compound 32 (Figure II.7f). The MS^2 tandem mass spectrum evidenced two main fragments at *m/z* 575, identified as [M−Hexose−H2O−H]$^-$ ion and 285 ([M−3Hexose−H]$^-$), that showed a MS^3 fragmentation pattern compatible with the kaempferol aglycon. This compound had already been already identified in *Coffea arabica* leaves and identified through NMR analysis(de Almeida et al., 2019b). The most intense peak in the ESI negative chromatogram was identified as compound 6 (rutin, quercetin rutinoside); the fragmentation of this widely distributed flavonoid is largely described in literature. The most intense fragments are related to the loss of the rutinose moiety (Glu-Rha), producing the aglycon fragment at *m/z* 301 ([M−Glu−Rha−H]$^-$). The *m/z* 301 base peak showed a consequent fragmentation consistent with the quercetin aglycon reported in literature (Justesen & Arrigoni, 2001).

The last flavonoid eluted was compound 35 with a Rt of 25.50 min and a [M−H]$^-$ ion at *m/z* 593 (Figure II.7g), generating a MS^2 fragmentation spectrum with the only presence of the ion at *m/z* 295; the consequent MS^3 fragmentation produced a spectrum compatible with the

kaempferol aglycon. The absence of intermediate neutral losses suggested the identification of the compound 35 as kaempferol rhamnoglucoside (Khallouki et al., 2018).

II.3.2.4 Lignans

Lignans are spread throughout the plant kingdom and high concentrations of these compounds have been measured in various matrices (Angeloni et al., 2020). Compounds 31a and 31b were eluted at Rt 21.75 and 28.52 min, respectively; both compounds show a $[M-H]^-$ ion at *m/z* 451. The fragments generated both in MS^2 and MS^3 fragmentation are identical, suggesting that the two compounds are isomers of the same molecule. The MS^2 fragmentation showed only one fragment at *m/z* 341; this fragment is generated from the loss of a catechol unit with a neutral loss of 110 Da. The following fragmentation of the *m/z* 341 produced three main fragments at *m/z* 231, 219 and 217, respectively. The ion at *m/z* 231 was generated by a second neutral loss of catechol (110 Da). Comparing the tandem mass spectrometry information with data previously published (Dantas et al., 2021; Resende et al., 2011), the compounds 31a and 31b were identified as cinchonain I isomers (Figure II.8).

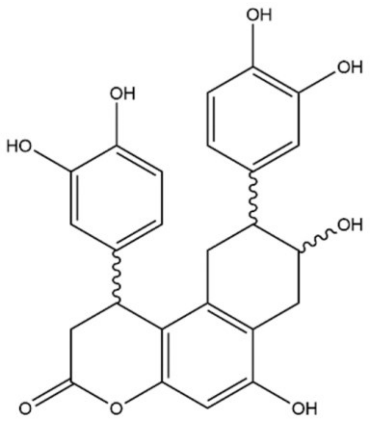

Figure II.8: Structure of the identified lignans (compounds 31a and 31b) cinchonain I isomers.

II.3.2.5 Procyanidins

Procyanidins are polyphenols abundant in a wide distribution of plant species with a multitude of chemo-preventive bioactive effects. The compound 21 eluted at Rt 11.22 min was identified as procyanidin B showing a $[M-H]^-$ ion at *m/z* 577 (Figure II.9a). The molecule was subjected to CID (collision induced dissociation) to obtain the fragments at *m/z* 425, 407 and 289. The 152 Da neutral loss that generated the fragment at *m/z* 425 is generated from a retro-Dies–Alder fragmentation that is typical of procyanidins, while the ion at *m/z* 289 is generated from the cleavage of the covalent bond between the two monomeric units of procyanidins (Rockenbach et al., 2012; Sun & Miller, 2003). Compound 21 was then identified through comparison with databases and Rt and fragmentation of the relative standard.

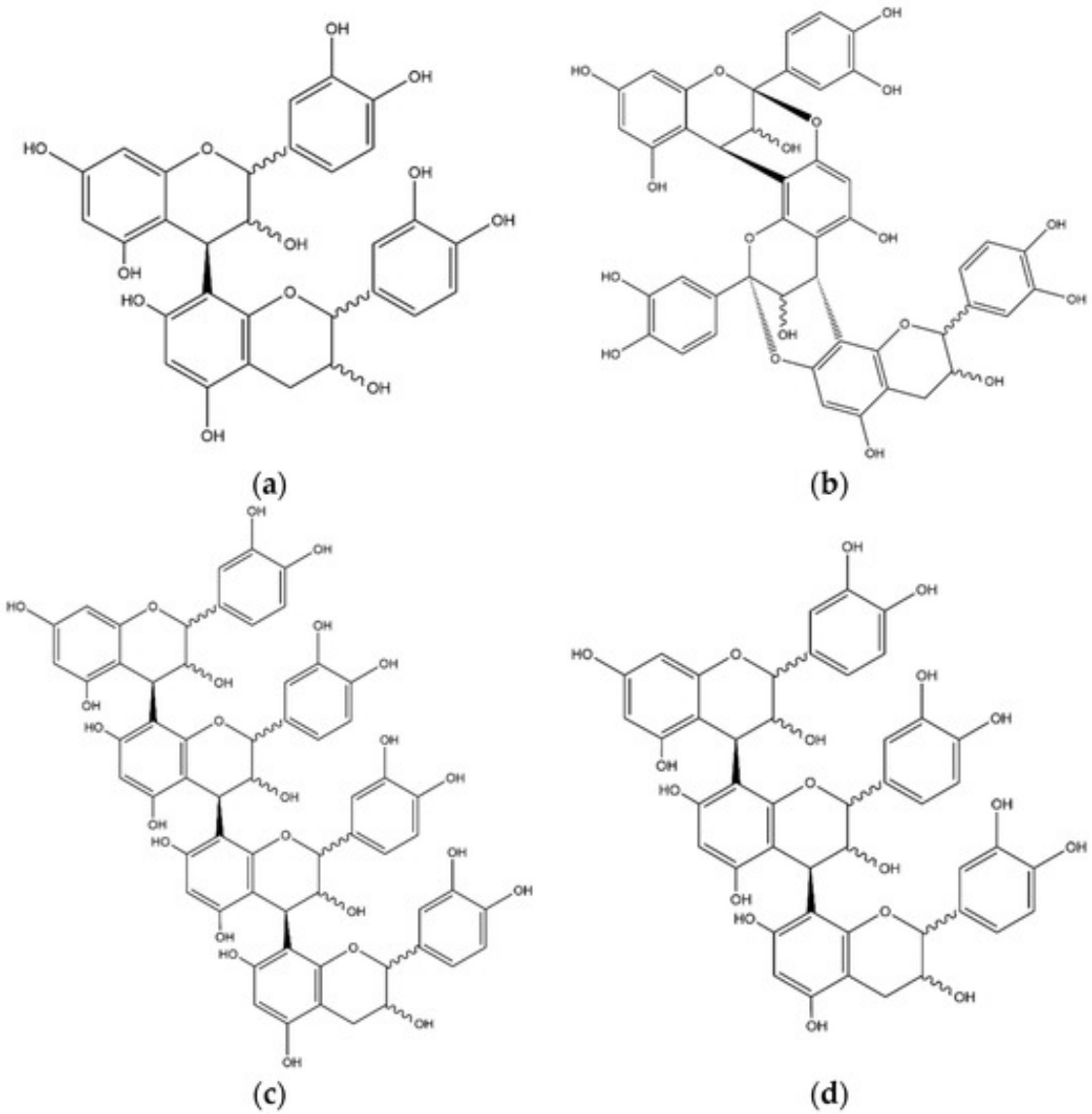

Figure II.9: Structure of the identified procyanidins: (a) procyanidin B, (b) procyanidin dimer A-type, (c) procyanidin tetramer B-type, (d) procyanidin C.

The following elution at Rt 16.19 was attributed to the deprotonated molecule with *m/z* 863, corresponding to compound 24. This compound shown a fragmentation pattern similar to compound 21 and was characterized from the neutral loss of 152, typical of the procyanidins molecules, consisting in a retro Dies–Alder fragmentation mechanism. Comparing the fragmentation of this compound with the literature (Jungfer et al., 2012) and databases, compound 24 was identified as procyanidin trimer A-type (Figure II.9b).

Compound 25 was eluted at Rt 17.10 with a base peak at *m/z* 576; this compound was fragmented, producing the most abundant fragment at *m/z* 550 (neutral loss 76 Da), together with the ions at *m/z* 491, 289 and 451. The low intensity of the MS2 signal did not allow MS^3 fragmentation, but the peculiar loss of 76 Da was used to tentatively identify compound 25 as a procyanidin tetramer doubly charged ion $[M-2H]^{2-}$ (Figure II.9c), as reported in literature (Martini et al., 2017). The procyanidin eluted at Rt 18.95 produced a $[M-H]^-$ ion at *m/z* 865 and generated MS^2 fragments at *m/z* 739, 695 and 577, and the following fragmentation of the MS^2 base peak (*m/z* 695) produced fragments at *m/z* 543, 451, 405 and 289. The fragments of MS^3 are comparable with smaller procyanidins showing the catechin/epicatechin monomer at *m/z* 289. The comparison of the fragmentation pattern allowed the identification of compound 27 as procyanidin C (Figure II.9d), as reported in literature (Rue et al., 2018).

II.3.3 HPLC-ESI(+)-MS^n Profiling of *Coffea arabica* Leaf Extract

The acquisition of the positive ionization chromatogram was necessary to study different classes of compounds contained in the extract, together with the same species already characterized in the previous paragraph. The obtained chromatogram is reported in Figure II.10.

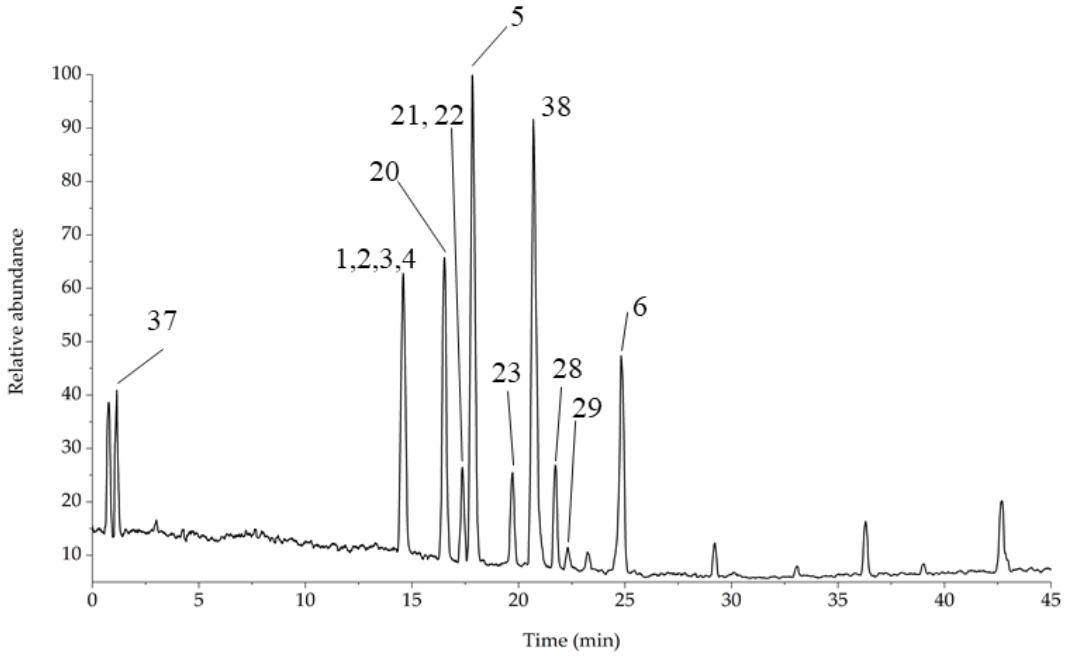

Figure II.10: HPLC-ESI(+) chromatogram of coffee leaves extract. The identified compounds are numbered as also reported Table II.3.

In Figure II.10, fourteen compounds are identified, twelve of which were already identified through the analysis of the ESI negative ionization chromatogram. Only compounds 38 and 39 were absent in the previous chromatogram and were classified as alkaloids. The high noise visible in the baseline is caused from the 100% aqueous mobile phase composition used in the first section of the chromatographic gradient; the use of fully aqueous mobile phases has a deleterious effect on ionization yield and ESI spray stability, but was necessary to load the highly polar compound 38 on the column stationary phase. Compound 38 showed a very short Rt of 1.11 min, emphasizing the very high polarity of this molecule. The protonated molecule shows a $[M+H]^+$ ion at *m/z* 138. The fragmentation of the *m/z* 138 ion generated only one fragment at *m/z* 121 with a mass shift of 17 Da, suggesting an ammonia loss. Comparing the Rt values and the fragmentation with the relative standard, compound 38 was identified as trigonelline (Figure II.11a). The second alkaloid (compound 39) was identified as caffeine; the presence of this alkaloid in coffee leaves is very well known in common knowledge. The fragmentation of caffein produced the MS^2 ion at *m/z* 138 and the following MS^3 product ion at

m/z 121. The identification of compound 38 was performed through direct comparison with the relative standard (Figure II.11b).

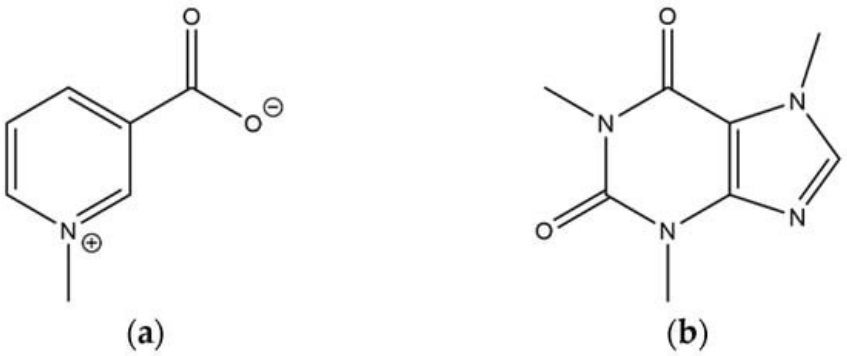

Figure II.11: Structure of the identified alkaloids: (a) trigonelline, (b) caffeine.

II.3.4 HPLC-MS Quantitation of *Coffea arabica L.* leaves extract components

The main components of the *Coffea arabica* L. leaf extracts were quantified in both positive and negative mode to quantify mono-caffeoylquinic acids, mangiferin and isomangiferin, dicaffeoylquinic acids and alkaloids. The single ion monitoring (SIM) method was used for the quantitation of all caffeoylquinic derivatives, mangiferin and alkaloids, selecting ions with the values of *m/z* shown in Table II.1. All molecules, except alkaloids, were quantified in negative mode. Table II.4 shows the quantitative values obtained for selected bioactive molecules in the *Coffea arabica* leaves extracts. Among the chlorogenic acids, the isomer esterified in position 5 (5-CGA) is the most abundant (16.27 ± 1.66 g/kg DW), while the other two isomers (3-CGA and 4-CGA) were found at lower concentrations, 8% and 0.2% of the 5-CGA content, respectively. As for dicaffeoylquinic acids, the three isomers have comparable concentrations, with the 4,5-dCQA isomer having a concentration of 0.91 ± 0.05 g/kg DW, while the lower concentration was found for the 3,5-dCQA isomer (0.58 ± 0.02 g/kg DW). Mangiferin was revealed at a concentration of 4.43 ± 0.14 g/kg DW, while its isomer reveled a concentration about eight times lower (0.52 ± 0.03 g/kg DW). For caffeine and trigonelline, the measured amounts were 7.94 ± 0.42 and 4.47 ± 0.12 g/kg DW, respectively.

Table II.4: Concentration of major bioactive compounds found in *C. arabica L.* leaves extracts.

No.	Compound	g/kg DW	%RSD
1	3-CGA	1.28 ± 0.12	9.2
3	4-CGA	0.89 ± 0.07	8.0
4	5-CGA	16.27 ± 1.66	10.2
34	3,5-dCQA	0.58 ± 0.02	3.4
33	3,4-dCQA	0.63 ± 0.05	7.6
36	4,5-dCQA	0.91 ± 0.05	5.3
5	Mangiferin	4.43 ± 0.14	3.3
22	Isomangiferin	0.52 ± 0.03	5.8
39	Caffeine	7.94 ± 0.42	5.3
38	Trigonelline	4.47 ± 0.13	2.9

The concentration data resulted comparable to those already reported in literature, although the concentration of 5-CGA usually appears to be higher (He et al., 2012; Monteiro et al., 2019; Rodríguez-Gómez et al., 2018). A suggested explanation could be related to the critical variability of many factors, such as fluctuations in environmental and pedoclimatic parameters and agronomic treatments.

II.4 Conclusions

A combined NMR and HPLC-MS approach was developed with the aim to separate, identify and quantify bioactive components in plant matrices belonging to the *Coffea arabica* L. family, Castillo variety. The combined use of spectroscopic and spectrometric techniques allowed the identification of thirty-nine compounds in total (seventeen using ^{1}H NMR and twenty-two using HPLC-MS). The identified molecules belong to various classes such as xanthones, flavonoids, chlorogenic acids, and alkaloids. These molecules are important components of the pool of natural compounds responsible for the main beneficial effects of coffee leaves, as regards antioxidant activity. The results emphasize how coffee leaves represent an important source of bioactive compounds as functional foods. The major metabolites were also quantified using suitable internal standards using ESI positive mode for alkaloids and the negative mode for the other classes of compounds. The combined use of two powerful techniques, chromatography coupled with tandem mass spectrometry and NMR spectroscopy, allowed a sound characterization of the secondary metabolites.

Chapter III

Morus

III.1 Introduction

The genus *Morus*, commonly known as "mulberry," constitutes a group of flowering plants within the Moraceae family and includes several species of deciduous trees. Among these species, *Morus alba*, *Morus nigra*, and *Morus rubra* are the most relevant from a botanical and use/food use perspectives. These plants have a wide geographical distribution, as they grow spontaneously in various regions worldwide, including India, China, Japan, North Africa, and Southern Europe. Their adaptability to a wide range of climatic conditions contributes to their presence in multiple geographic areas. In addition to their ornamental value, mulberries are known for their fruits, which are spherical drupes measuring above 2-3 cm, great sources of anthocyanins and alkaloids, conferring distinctive nutraceutical properties.

Mulberry leaves represent an important component of these plants and have traditionally been used as food for silkworms (*Bombyx mori* L.) and in traditional Chinese medicine. These leaves contain a wide range of bioactive substances, including organic acids, sugars, and various phenolic compounds, such as hydroxycinnamic acids, flavonoids, and anthocyanins. These components have attracted significant interest in the biological, pharmacological, and structural fields due to their antioxidant, anti-inflammatory, and antihypertensive properties (Rohela et al., 2020).

The use of mulberry leaves has witnessed a significant increase in recent decades, particularly in the form of teas and infusions, due to their potential applications in the prevention of liver and kidney diseases, joint disorders, and the treatment of type 2 diabetes, thanks to their effective hypoglycemic action. This action is often attributed to the presence of alkaloids, including 1-deoxynojirimycin (DNJ), a potent inhibitor of glucosidases (C. Chen et al., 2021; Yuan & Zhao, 2017).

DNJ is an amino sugar derived from lysine and represents one of the main bioactive compounds in mulberry leaves. It was identified in 1976 in the root bark of *Morus* plants, hence its alternative name "moranoline." The DNJ is known for its bioactive properties, which include the inhibition of α-glucosidases and the ability of reducing postprandial blood glucose, counteracting fat accumulation and reducing aging. In recent years, it has been growing the interest for its potential clinical applications (Marchetti et al., 2021; Ramappa et al., 2020).

III.2 Materials and methods

All reagents and solvents for chromatographic analyses were purchased from Sigma-Aldrich (Milan) and were used without further purification. Reagents and standards: ammonium formate (> 99% purity; Thermo Scientific), 1-Deoxynojirimycin (DNJ; > 98.5% purity; CarboSynth), voglibose (VOG; > 98% purity; TCI Europe), ethanol (EtOH, LC-MS grade 99.9%), acetonitrile (CH_3CN, ACN, LC-MS grade), formic acid (HCOOH, LC-MS grade 98.5%), ultrapure water (18.2 MΩ·cm, Rephile Direct-Pure purifier).

III.2.1 Plant Material Collection, Pre-treatment and Extraction

Morus alba L. and *Morus nigra L* leaves were collected in a hilly area at an elevation of approximately 322 m asl (Figure III.1). Once collected, they underwent a lyophilization process to enable the preservation of bioactive compounds over time. Initially, the leaves were frozen using liquid nitrogen and subsequently lyophilized (-48 ± 2 °C, 450 ± 50 μBar) until all moisture was completely removed. After the lyophilization process, the samples were cold ground in a knife mill using liquid nitrogen (Pulverisette 11, Fritsch) and sieved to obtain particle sizes <500 μm. The resulting powder was stored at -20 ± 1 °C prior to subsequent analyses. Freeze drying process was used instead of other preservation methods for its superior performance in storing metabolites content (Chan et al., 2009).

Figure III.1: Leaves of *Morus alba L.* (left) and *Morus nigra L.* (right) collected and analyzed.

Aliquots of 0.200 g of lyophilized samples, were treated with 5 mL of a solvent mixture consisting of EtOH/H_2O (50:50, v/v) acidified with 0.1% formic acid. The extraction process was assisted by ultrasonic sonication using an ultrasonic bath (10 min, 20 ± 1 °C; nominal power 120 W; ultrasound frequency 35 kHz; Branson Ultrasonics Corporation, Danbury, CT, USA). The suspension was then centrifuged (5 min, 4000 rpm; Thermo Electron Corporation PK 110 centrifuge), and the supernatant was separated from the solid residue and transferred to a polypropylene vial. The extraction procedure was repeated twice more, using 5 mL of the solvent mixture on the solid residue, and the extracted portions were combined (total volume, 15 mL). The total extract was then dried under a stream of nitrogen for approximately 24 h.

III.2.2 HPLC-MS method set-up

The mulberry leaf extract was reconstituted in a mixture of acetonitrile and water with ammonium formate as modifier (ACN:H_2O 80:20 % v/v, 100 mM ammonium formate). The analyses were performed using an HPLC instrument (Thermo Fisher Scientific UltiMate 3000) coupled with a linear ion trap mass spectrometer (Thermo Fisher Scientific LTQ XL) equipped with an electrospray ionization (ESI) ion source. Spectra and chromatograms were acquired and processed using Xcalibur software (Thermo Fisher Scientific, Waltham, MA, USA). The column used was an amino column (Luna NH_2; 150 x 4.6 mm, 5 µm, Phenomenex), and the mobile phase consisted of two components: A) H_2O and 100 mM ammonium formate, acidified to pH 3 with formic acid; B) Acetonitrile. The elution of analytes occurred in isocratic elution with the mobile phase containing 75% phase B and 25% phase A. The injection volume was set at 3 µL, with a mobile phase flow rate of 1.5 mL/min. During the analyses, the column temperature was thermostatted at 40 ± 1 °C, and the total analysis time for each chromatographic run was 10 min. Amino phase was chosen for its capacity of operate in HILIC chromatography and for its interactions with iminosugars (Nuengchamnong et al., 2007; Piao et al., 2018).

For MS detection, the eluent flow was split after the column using a 3-way fitting to deliver 0.2 mL/min into the ESI source. The ionization parameters were optimized using direct injection of a DNJ (Figure III.2b) standard dissolved in a mobile phase with the same composition as the isocratic mode. The ionization parameters included a spray voltage of 5000 V, sheath gas pressure of 35 AU, auxiliary gas pressure of 10 AU, and capillary temperature of 200 °C.

To minimize quantification random errors associated with ESI ionization efficiency, an internal standard was used, having chemical properties as similar as possible to the analyte and without interfering with analyte signal detection. Voglibose (VOG, Figure III.2a) was used in this study

due to its similar chemical structure and comparable chemical reactivity to DNJ, the selected internal standard also exhibited a different Selected Reaction Monitoring (SRM) fragmentation profile, making it easily distinguishable. Test samples and standards were analyzed to optimize and validate the method.

The quantification of DNJ was performed in SRM mode using the specific fragmentation 164 *m/z* → 146 *m/z* with a normalized collision energy of 30 nCE, using helium as the collision gas. The SRM mode was also used for the quantification of the internal standard, voglibose (VOG) using the fragmentation 268 *m/z* → 206 *m/z* with a collision energy of 40 nCE.

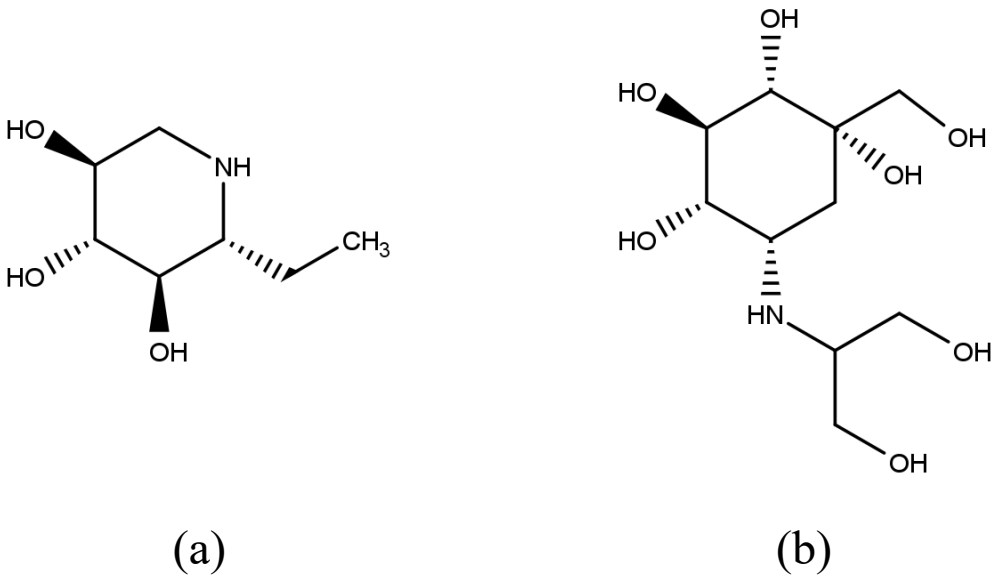

Figure III.2: Structures of 1-Deoxynojirimycin (a) and Voglibose (b).

The limits of detection (LoD) and quantification (LoQ) were also determined, and to calculate LoD, six injections of blank reagent enriched with low analyte concentrations were performed in HPLC-MS (Vial & Jardy, 1999).

The linearity range was then evaluated through a linear regression analysis, using as indicators the R^2 value and the residuals plot. The R^2 value serve as indicator for linearity, values under 0.9980 were associated with low linearity performances of the method or operator/instrumental failures. (Wei et al., 2020)

Then accuracy and precision were determined (Ferenczi-Fodor et al., 2001). Both factors were evaluated by injecting multiple times different analyte concentrations, usually along the linearity range. Each concentration level was injected at least three times to have an average value for the calculation of recovery of the analyte. Recovery is a ratio between the calculated amount of analyte and the theoretical amount. In complex matrices as in this case for *Morus*

leaves, a low concentration sample was spiked with a known amount of analyte and the unspiked sample was measured for background correction. The standard error associated with the replicates of the measures was used as an indicator for method precision. The method validation results are reported in Results and discussion section (Araujo, 2009)

III.2.3 Experimental design

Using the Design-Expert software (Stat-Ease, Inc.), it is possible to explore a multi-level factorial design, which is highly useful for simple treatment comparisons. The design provides an effective resource for screening critical factors in process optimization. Experimental design is a valuable and powerful statistical tool that allows the investigation of few critical factors and their potential interactions with the outcome of the optimized process (Giacomino et al., 2011). The parameters investigated during the process optimization were: sonication time, ultrasonic bath temperature, pH of the extraction solvent, ratio between extraction solvent and solute, and ethanol percentage in extracting mixture (Table III.1).

Table III.1: Parameters used for investigation and optimization through experimental design.

Parameter	Unit	Min Value	Central Value	Max Value
Sonic. Time	min	2	6	10
Temperature	°C	20	30	40
pH	pH units	3	5	7
Solvent/Solute ratio	(mg/mL)	40	170	300
Ethanol percentage	%	20	45	70

The selected variables are those having the maximum significant impact on the extraction of selected compound, while the ranges under consideration are those generally used in comparable processes (Kumar et al., 2021). Subsequently, 37 samples were randomized for extraction with randomized parameters according to the values set in Table III.1. For each combination of these process settings, the software calculates the set of parameters that generate the optimal extraction yield. Indeed, the study aims to maximize the yield by seeking conditions that enable an effective and reliable extraction.

III.3 Results and discussion

III.3.1 1-DNJ extraction and Experimental Design

Once the extraction runs were performed, the following yields were obtained, as shown in Table III.2.

Table III.2: Parameters and yield of randomized extraction runs.

Std N°	Run N°	Sonic_time (min)	Temp (°C)	pH	Sol_solv (mg/mL)	%EtOH (%)	Yield (mg/g DW)
1	6	2	20	3	40	20	0.73
5	7	2	20	7	40	20	1.02
9	28	2	20	3	300	20	0.32
13	13	2	20	7	300	20	0.41
17	16	2	20	3	40	70	0.51
21	24	2	20	7	40	70	0.64
25	29	2	20	3	300	70	0.34
29	15	2	20	7	300	70	0.22
2	20	10	20	3	40	20	0.83
6	3	10	20	7	40	20	0.80
10	8	10	20	3	300	20	0.28
14	35	10	20	7	300	20	0.32
18	12	10	20	3	40	70	0.56
22	33	10	20	7	40	70	0.48
26	1	10	20	3	300	70	0.27
30	34	10	20	7	300	70	0.25
33	14	6	30	5	170	45	0.39
34	9	6	30	5	170	45	0.58
35	31	6	30	5	170	45	0.31
36	27	6	30	5	170	45	0.30
37	37	6	30	5	170	45	0.33
3	5	2	40	3	40	20	0.91
7	17	2	40	7	40	20	0.75
11	22	2	40	3	300	20	0.31
15	32	2	40	7	300	20	0.26
19	30	2	40	3	40	70	0.39
23	18	2	40	7	40	70	0.60
27	2	2	40	3	300	70	0.20
31	25	2	40	7	300	70	0.26
4	11	10	40	3	40	20	0.87
8	4	10	40	7	40	20	0.69
12	10	10	40	3	300	20	0.32
16	19	10	40	7	300	20	0.30
20	26	10	40	3	40	70	0.68
24	23	10	40	7	40	70	0.70
28	21	10	40	3	300	70	0.23
32	36	10	40	7	300	70	0.33

In Table III.2, the "Standard" column contains the list of samples in their order of insertion into the matrix, while the "Run" column indicates the order of experiment execution. This approach is essential to avoid errors arising from the consecutive execution of the same parameters, introducing experiment randomization helps mitigate most of the issues related to systematic errors. Within the results, it becomes evident that the maximum extraction yield is attributed to sample number 5 (Std. 5, Run 7). Additionally, a preliminary observation reveals that the standards yielding high values are those operating at a neutral pH and under mild temperature and ultrasonic bath conditions. To select which parameters to include in the model, it is necessary to observe the Half-Normal Plot, reported in Figure III.3.

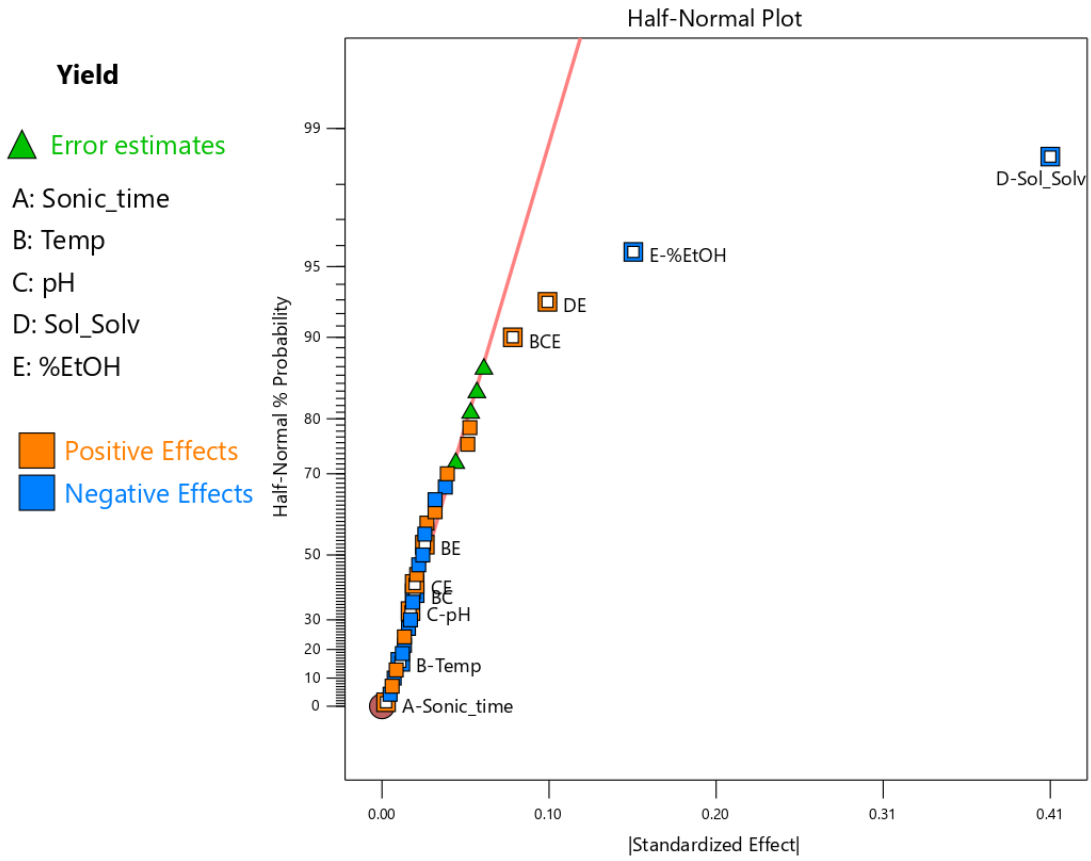

Figure III.3: Half-Normal plot of extraction parameters used for DoE model.

The graph is characterized by a red error line, which represents the 50% of the least significant effects. It is an important visual guide to monitor in variable selection for inclusion in the model: variables that do not significantly contribute align closely to the zero line. On the contrary, parameters that have a greater influence on the extraction are shifted further to the right. Notably, the solute/solvent percentage is at a considerable distance from the line, followed by the EtOH percentage. These two terms can be considered significant factors. The two remaining

values that deviate from the line correspond to various linear combinations of multiple factors (DE: Sol_Solv and %EtOH; BCE: Temp, pH and %EtOH). On the other hand, those shifted to the left represent effects with a lesser impact on the extraction yield. For completeness of information, variables that individually did not influence the model but exert significant actions when combined with others were also included. The colour around the variables also indicates the direction of the effect on the model, as the Half-Normal Plot visualizes the effects of variables in absolute value. Variables with negative correlation are highlighted in blue, while those with positive correlation are highlighted in orange. If no effect deviates from the red error line, it means that it is not significant, and this can be observed considering the ultrasonic bath temperature parameter. Exploring further the statistical significance of the selected effect magnitudes, it is possible to visualize the significance of the parameters, as represented on an ordered bar diagram, called Pareto chart (Figure III.4).

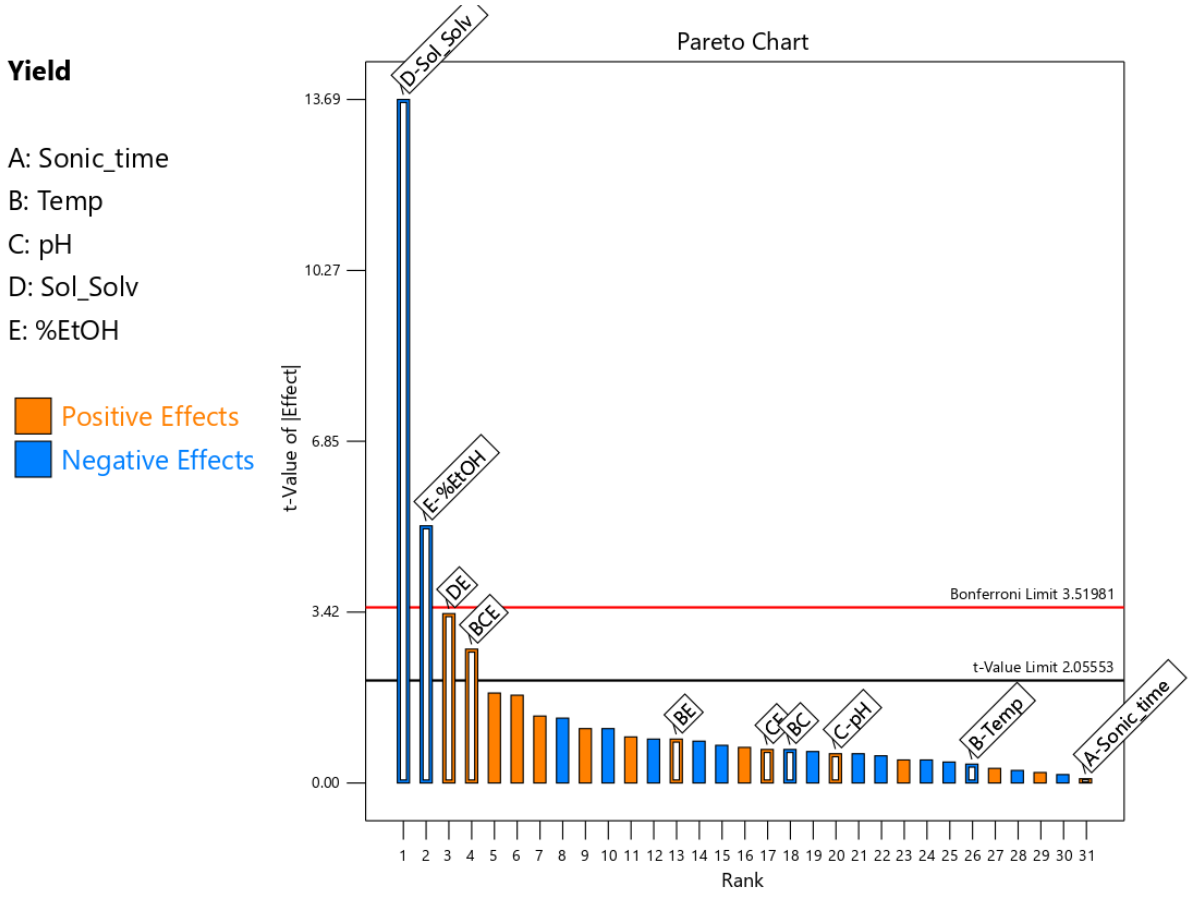

Figure III.4: Pareto diagram for extraction parameters used for DoE model.

This plot represents a dimensionless statistic in which is possible to observe a rescaling of effects in terms of standard deviations. The representation is particularly useful, especially when encountering problematic factor levels, missing data, and similar random errors. In these

cases, the t-value scale provides a more accurate measure of relative effects. The plot gives important and simple information to understand the values that have the greatest influence on the extraction yield.

Once the parameters for the factorial study have been selected, it is necessary to examine them in detail through the analysis of variance (ANOVA, TableIII.3).

Table III.3: Variance analysis results obtained for DoE model.

Source	Sum of Squares	df	Mean Square	F-value	p-value	
Model	1.67	9	0.186	27.13	< 0.0001	significant
B-Temp	0.001	1	0.001	0.1477	0.7039	
C-pH	0.0024	1	0.0024	0.3574	0.5552	
D-Sol_Solv	1.34	1	1.34	194.96	< 0.0001	significant
E-%EtOH	0.1891	1	0.1891	27.58	< 0.0001	significant
BC	0.0032	1	0.0032	0.4667	0.5005	
BE	0.0055	1	0.0055	0.804	0.3781	
CE	0.0032	1	0.0032	0.4667	0.5005	
DE	0.082	1	0.082	11.96	0.0019	significant
BCE	0.0512	1	0.0512	7.47	0.0111	significant
Curvature	0.0534	1	0.0534	7.79	0.0097	
Residual	0.1783	26	0.0069			
Lack of Fit	0.1244	22	0.0057	0.4197	0.9175	not significant
Pure Error	0.0539	4	0.0135			
Cor Total	1.91	36				

The F-value of the model is 27.13, which indicates that the developed model is significant. Notably, there is only a 0.01% probability that such a large F-value could occur due to noise or random errors. P-values less than 0.05 indicate that four terms in the model are significant. D, E, DE and BCE are parameters that can be considered significant, justifying their inclusion in the model. On the contrary, values greater than 0.05 indicate that the model terms are not significant. The F-value, with a lack of fit of 0.42, implies that this lack of fit is not significant compared to pure error: the model fitting has a 91.75% probability of effectiveness. Furthermore, it can be observed that the lack of significance of the lack of fit is an excellent result as it confirms that the model fits various conditions. Table III.4 shows the fitting statistics, which are descriptive statistics used as a secondary check of the model's utility.

Table III.4: DoE model descriptive statistics.

Std Deviation	0.0828	**R^2**	0.9038
Mean	0.4781	**Adjusted R^2**	0.8705
C.V. %	17.32	**Predicted R^2**	0.8125
		Adequate Precision	14.8681

The predicted R^2 of 0.8125 reasonably agrees with the adjusted R^2 of 0.8705, the difference being less than 0.2. This is an excellent result because it demonstrates that the model is fitting the data and can be reliably used for data interpolation. Adequate precision measures the signal-to-noise ratio, a ratio greater than 4 is usually desirable. This model reports a ratio of 14.868, indicating an adequate and sufficiently strong signal for optimization purposes. The Coefficient of Variation (CV%) index is used to assess the capability of a process, and it is preferable to derive a value from the model that is as low as possible. The acceptable values for the CV% in an experimental design model can widely vary, depending on the specific context, and the nature of the experiment.

In diagnostic plots, externally studentized residuals are included by default, unlike internally and raw studentized residuals, which may be available as optional. Unless in extremely rare cases where all runs in a project are identical, the standard errors of the residuals differ because each raw residual belongs to different populations (one for each different standard error). Therefore, raw residuals should not be used to test regression assumptions; instead, studentization of residuals should be employed, wherein all the different normal distributions are mapped into a single standard normal distribution.

Studentized residuals are a way to standardize the residuals by dividing them by their estimated standard deviation. The purpose of studentization is to express the residuals in a common scale and make them directly comparable, allowing for the detection of data points that deviate significantly from the model's expectations.

The normal probability plot (Figure III.5) indicates whether the residuals within an experiment follow a normal distribution, that is, whether they adhere to a straight line. Some dispersion is expected even with normal data. As evidenced in the table below, the residuals are sufficiently aligned along the red line, despite some deviations from it.

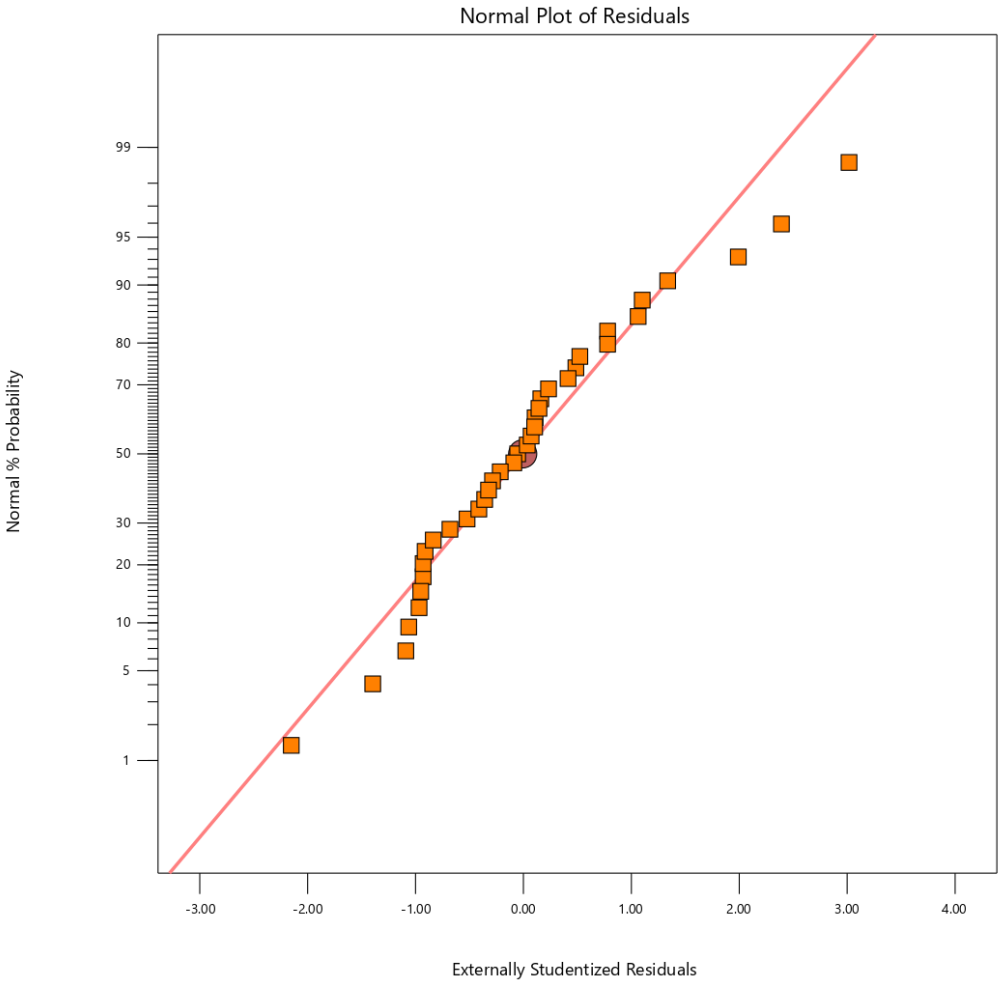

Figure III.5: Residuals normal plot for DoE model.

The diagram presented in Figure III.6 represents the Residuals vs. Predicted plot, which shows the distribution of residuals relative to predicted response values and assesses the hypothesis of constant variance. In the graph (Figure III.6), a random dispersion of residuals is observed (a constant range of residuals in the plot), and they fall between the two boundary lines. There are no significant outlier values; instead, the residuals are arranged in a randomized manner, assessing the presence of constant variance in the model. It is important to note that in the Residuals vs. Run plot (Figure III.7), we also observe random dispersion.

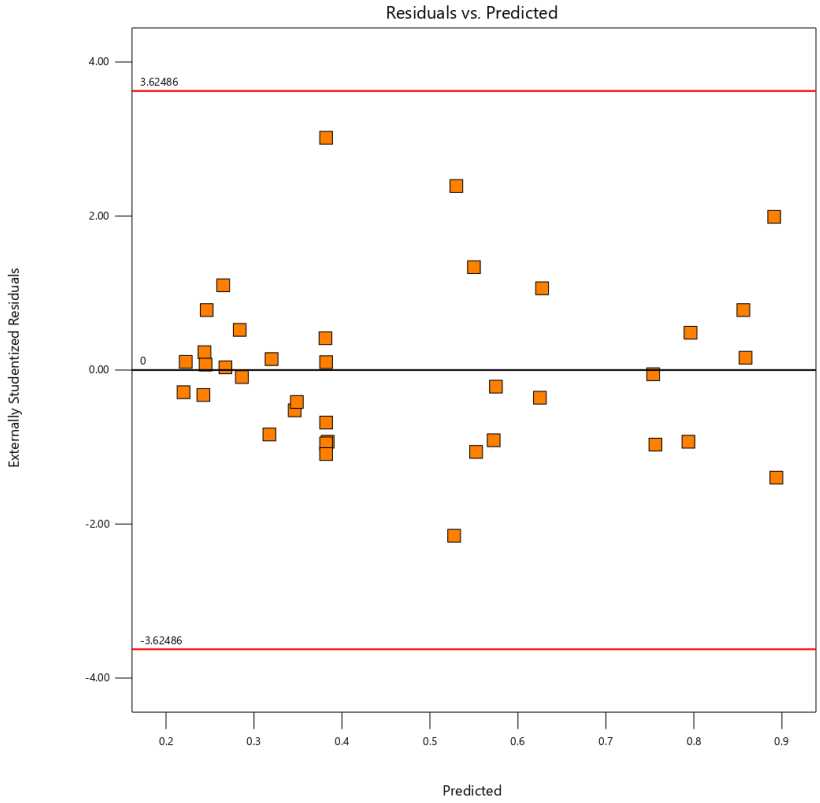

Figure III.6: Residuals vs. predicted plot for DoE model.

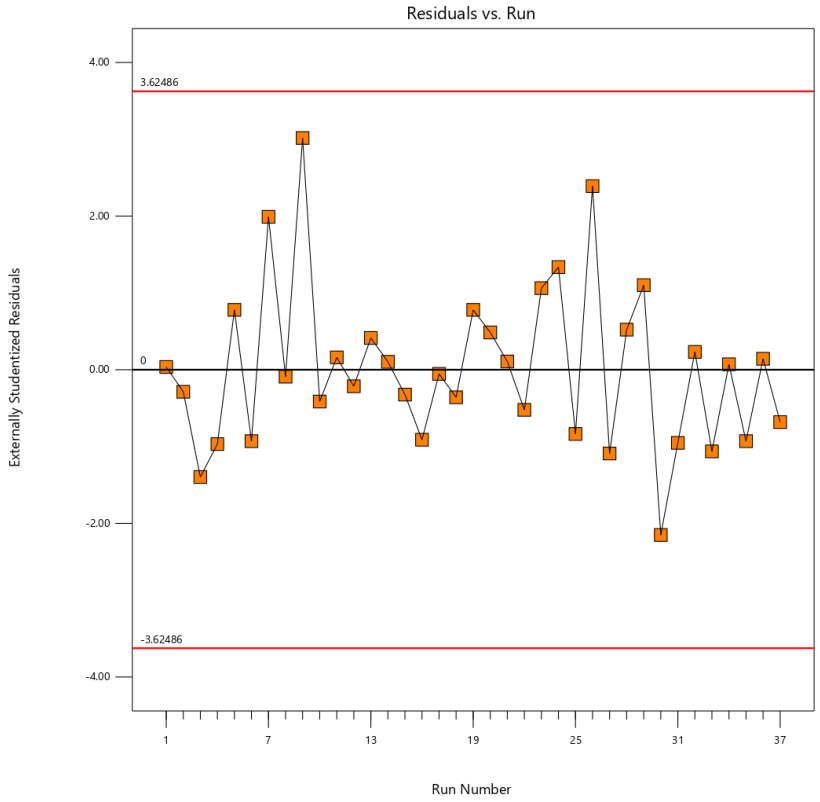

Figure III.7: Residuals vs. run for DoE model.

With this chart, we verify the presence of variables that could influence the response during the experiment: blocking and randomizing the execution of runs provide assurance against trends that could compromise the analysis. In this case as well, the data fall within a range delineated by the two horizontal red boundary lines. The absence of outliers defines that any experiment produced results not included in the model probability.

Through the diagram concerning the model's leverage (Figure III.8), it is possible to obtain a measure of how much each point in the three-dimensional measurement space influences the model's fit. For example, if a point had a leverage of 1.0, the model would fit exactly to the observation at that point, indicating how that point can control the model's prediction outcome. Note that all points lie on the same line, with only 5 runs lying outside of it. Overall, it can be observed that there are no anomalous leverage phenomena that would alter the predictive power of the model.

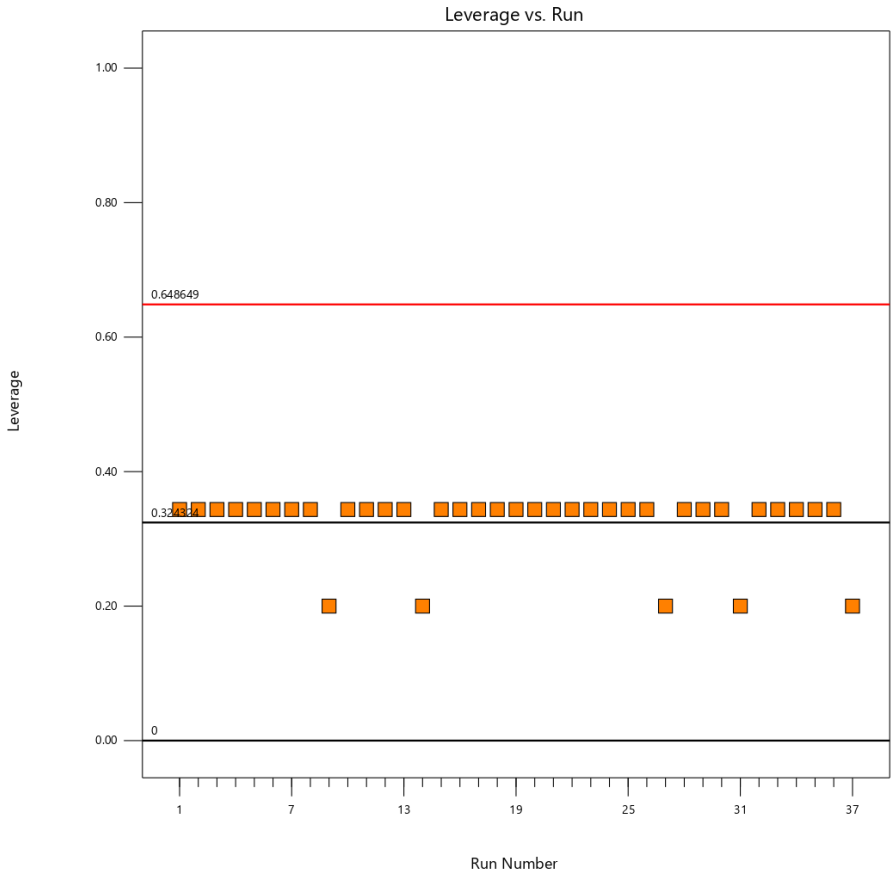

Figure III.8: Leverage vs. run plot for DoE model.

The 3D Surface chart illustrates the trends of the variables considered in the model, generating a surface that quantitatively indicates the extraction yield. Along the three axes shown in Figure III.9, it is possible to observe the variables solute-to-solvent ratio and ethanol percentage on the x and z axes, respectively. The extraction yield is represented along the y-axis. By calculating

the corresponding extraction yield for each point of combination on the graph generated by the x and z axes, a flat surface can be generated, representing the extraction yield for that specific combination of solute-to-solvent ratio and ethanol percentage. Other factors considered as non-significant were set to values that are more favourable to laboratory activities to align the model prediction to the real laboratory conditions. The temperature of 20°C does not require aggressive extraction conditions and can be easily used even for equipment that does not allow for ultrasonic bath temperature control. The pH value was set to the neutral value of 7, requiring no modification to the pH of the extraction solution, thereby accelerating its preparation and minimizing potential pH measurement errors. The sonication time was set to two minutes to speed up the extraction procedures as much as possible and avoid overheating of the ultrasonic bath itself.

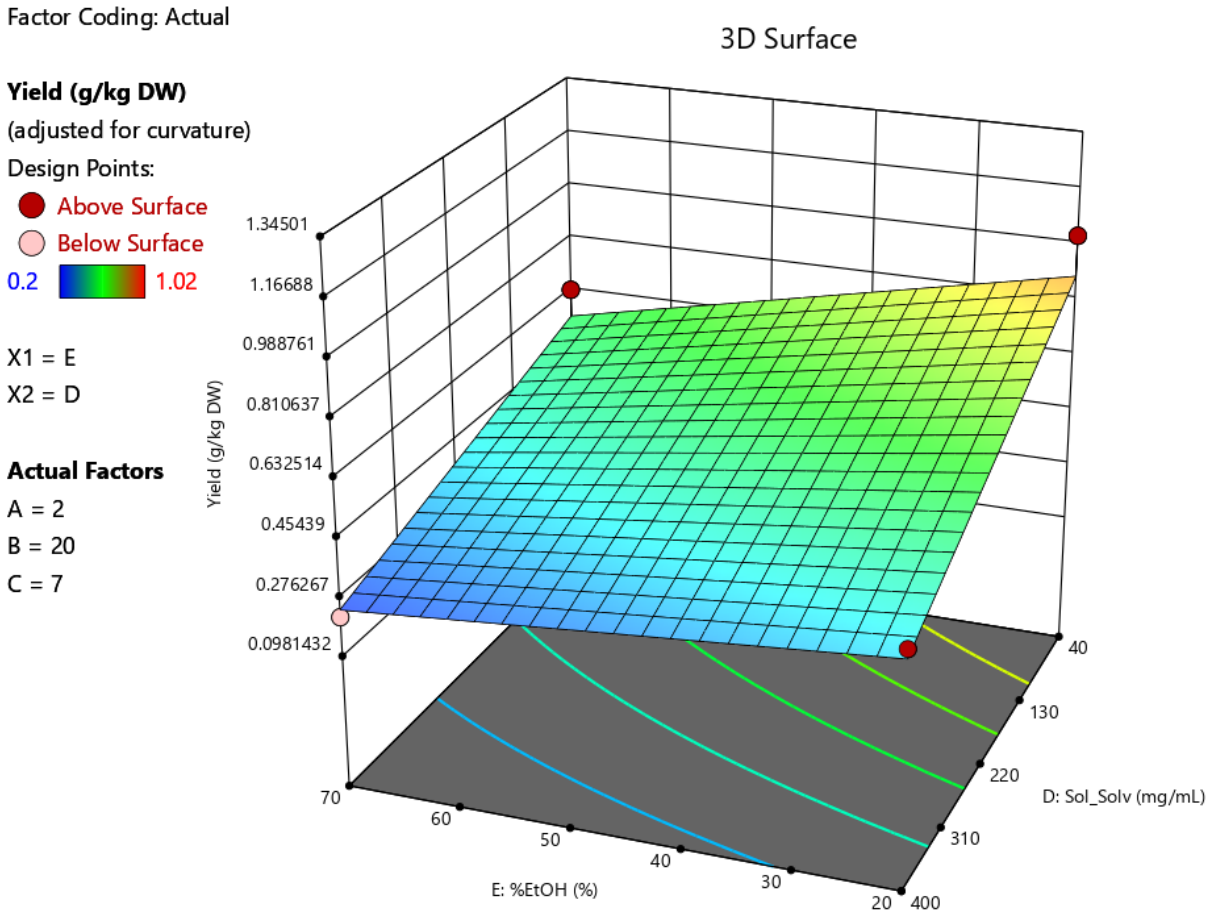

Figure III.9: Yield 3D surface obtained for DoE model.

Observing the effect of the variable related to the ethanol percentage, it can be noted that lower concentrations of ethanol significantly increase the extraction yield. This effect can be attributed to the strong polarity of the target molecule, which exhibits chemical and physical characteristics very similar to those of simple sugars. A similar consideration can be made regarding the solute-to-solvent ratio, as increasing the ratio leads to a lower extraction yield. This is often reported in the literature (L. Wang & Weller, 2006), consistent with the findings in this thesis. From the set of results obtained, it is possible to observe that the optimal parameters for the extraction of DNJ from mulberry leaves are those listed in Table III.5.

Table III.5: Optimal extraction conditions for 1-DNJ in *Morus* leaves.

% EtOH (%)	Ratio Sol/Solv (mg/mL)	pH	Sonication (min)	Temperature (°C)
20	40	7	2	20

III.3.2 HPLC-MS method set up and validation

Several methods for DNJ determination are available in the literature, and many other quantitative techniques are constantly being developed. However, regardless of these advancements, some analytical challenges must be considered. Firstly, due to its high hydrophilicity and small molecular weight, DNJ exhibits weak interactions with the stationary phase of conventional reverse-phase columns, making it poorly retained using reverse-phase approaches. Additionally, because the molecule lacks a UV-Vis chromophore, direct UV-Vis detection is not applicable, as is the case for many other aminoglycosides. Pre-column derivatization is often employed, but this involves sample manipulation, which can introduce impurities or degradation products (L. Wang & Weller, 2006). On the other hand, derivatization is not required when using detectors like evaporative light scattering detection (HPLC–ELSD) and tandem mass spectrometry (HPLC–MS/MS). Kimura et al. (Kimura et al., 2004) successfully employed an ELSD detector, which is a universal detector for non-volatile analytes. However, its main drawbacks are low sensitivity and the extended analysis time required to complete the analysis.

Hydrophilic interaction chromatography (HILIC) coupled with mass spectrometry has proven to be a promising technique for DNJ quantification and is the most cost-effective method, as it has shown low limits of detection and quantification (LoD and LoQ) and a short retention time. The mass parameters of the detector used in this thesis work (linear ion trap) were optimized

through electrospray ionization in positive mode, while the analyte was detected using the selected reaction monitoring (SRM) technique, exploiting the fragments generated from the protonated molecule. Under the experimental conditions of this study, the retention time (Rt) for 1-Deoxynojirimycin is 3.50 min, as reported in Figure III.10 below.

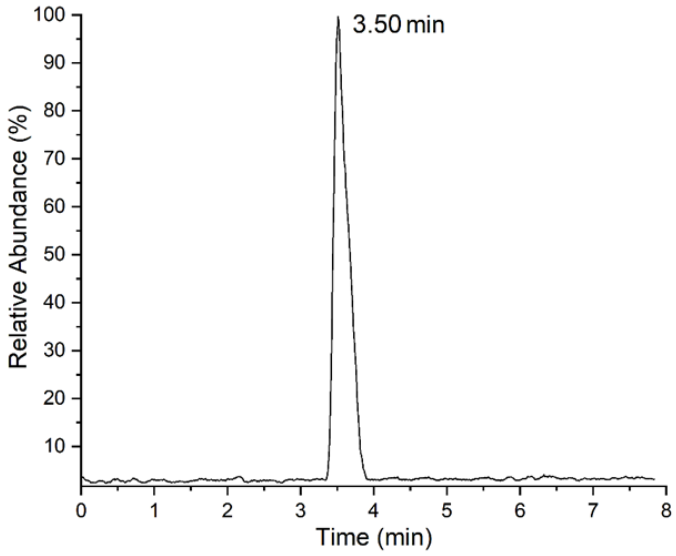

Figure III.10: *Typical DNJ Full Scan ESI chromatogram.*

Figure III.11 displays the mass spectrum in Full Scan ESI (+) mode of DNJ. The protonated molecule $[M+H]^+$ with *m/z* 164 is shown as the base peak of the spectrum. The fragmented molecule in MS^2 spectra shown a loss of a water molecule, with the peak at a 146 *m/z*.

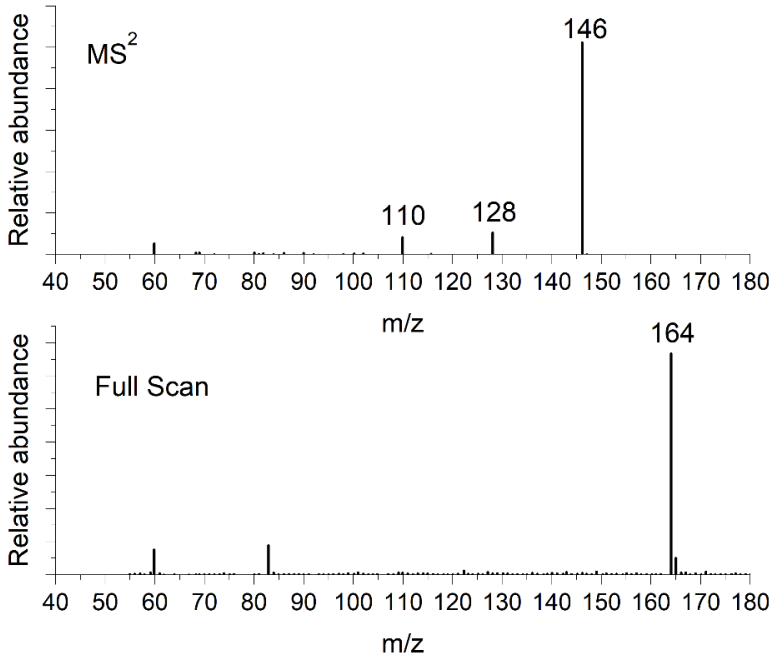

Figure III.11: *ESI-MS spectra for Full Scan and MS^2 fragmentation of DNJ.*

The analytical method was validated through four steps: quantitation and detection limits, linearity range, precision and accuracy.

III.3.2.1 LoD and LoQ

For determination of LoQ, six injections of a blank solution spiked with 0.75 ppm of DNJ and 5 ppm of voglibose (VOG; IS) were performed. Signal to Noise value was calculated using the baseline noise on the blank run before the samples in the same region of the chromatogram. The time region selected for noise calculation was 5 times the width at 50% of the height of the analyte peak as reported in *European Pharmacopoeia* (chapter 2.2.46).

Table III.6: Experimental results for LoQ evaluation**.**

Injection	DNJ ppm	Area DNJ	VOG ppm	Area VOG	Area ratio	S/N
1	0.75	11482	5	37981	0.302	62
2		15387		38326	0.401	49
3		15305		37654	0.406	47
4		13631		37631	0.362	61
5		12335		37829	0.326	48
6		12088		38117	0.317	74

The values obtained for S/N of DNJ were used to establish the values for LoD and LoQ set at 0.5 ppm for LoQ and 0.3 ppm for LoD, the solutions were injected three times for LoD and six times for LoQ obtaining the results reported in Table III.7

Table III.7: LoD and LoQ results.

Injection	DNJ ppm	Area DNJ	VOG ppm	Area VOG	S/N
1 LoD	0.3	5363	5	38507	17
2 LoD		5381		38116	15
3 LoD		5139		38208	19
1 LoQ	0.5	8842		38013	32
2 LoQ		8959		37192	34
3 LoQ		8987		37509	35
4 LoQ		8914		37118	37
5 LoQ		9006		38250	39
6 LoQ		8903		36731	34

III.3.2.2 Linearity range

The values obtained from the LoD and LoQ determination were used to establish the measurement range within which the method provides results with an acceptable level of uncertainty. To determine the measurement range, blank and test samples for calibration were analyzed at ten different concentrations, equidistantly distributed along the range of interest. The measured concentration (y-axis) and the concentration of the test samples (x-axis) were plotted as reported in Figure III.12. The graph was examined to identify the approximate linearity range and the upper and lower limits of the measurement range. The parameters of the appropriate regression type were calculated, and the residuals (the difference between the observed value and the value predicted by the regression line for each x-value) were plotted. Linearity was confirmed if the residuals were randomly distributed around zero. This phase is necessary to evaluate whether the proposed instrumental range and calibration procedure are suitable for the purpose.

The residual plot in Figure III.13 is in concordance with the method linearity, there is no evidence of significant data trends that deviate from linearity. The lowest three concentrations have a lower residual value that could be associated with the interference of baseline fluctuations that increase the error associated with these levels. In Table III.8 the parameters obtained for method linearity are reported.

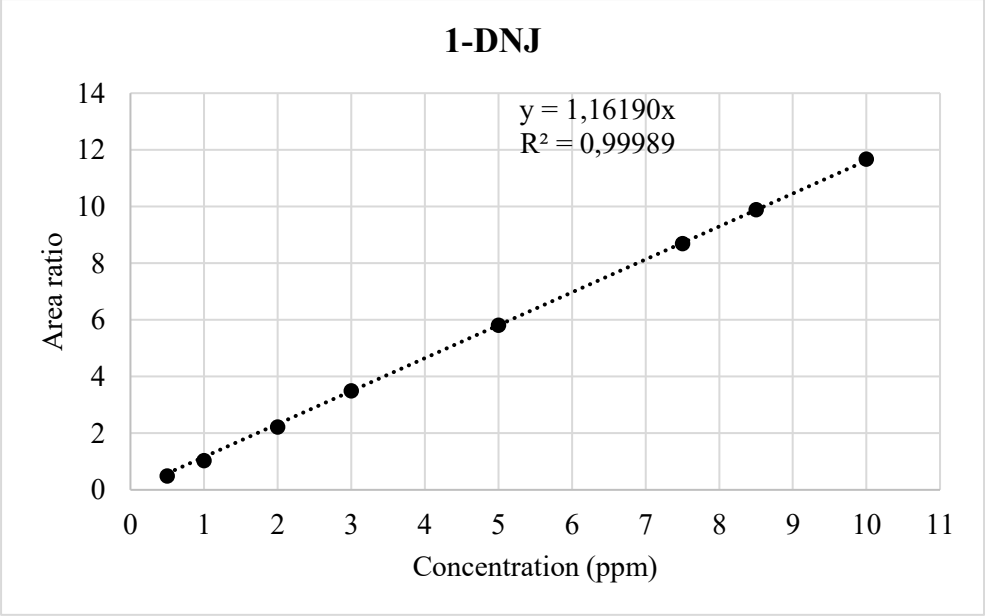

Figure III.12: Calibration curve obtained for DNJ.

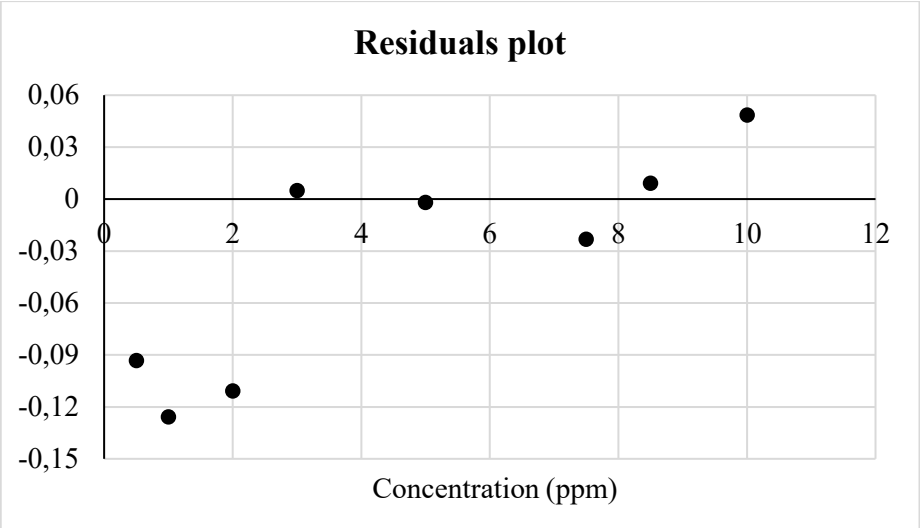

Figure III.13: Residuals plot obtained for DNJ calibration curve.

Table III.8: Linearity and sensitivity parameters obtained for DNJ.

IS	$[M-H]^+$ (*m/z*)	SRM (*m/z*)	Equation	R^2	Range (ppm)	LOD // LOQ (mg/g DW)
Voglibose	164	164→146	y = 1.1619x	0.99989	0.5 - 10 ppm	0.0164 // 0.0273

III.3.2.3 Accuracy and repeatability

To calculate the method accuracy, test samples and corresponding fortified aliquots with the analyte of interest at various concentrations are analysed. Afterwards, the relative percentage recovery of the added concentration at various concentrations is calculated.

A *Morus* leaves sample was extracted in triplicate and used as background for DNJ value. The same sample was spiked at three different levels of 1-DNJ using a 10 ppm solution of reference standard. The amount of DNJ was then measured and recovery % was calculated with the formula:

$$Recovery\% = \frac{DNJ\ in\ spiked\ samples - Avg.DNJ\ in\ Background\ samples}{Theoretical\ spiked\ DNJ\ amount} \cdot 100$$

It is useful to calculate a precision limit starting from the standard deviation of the quantitation amounts, to allow the operator to decide if there is a significant difference, at a specified level of confidence, between duplicate analysis results of the sample obtained under specified conditions. The same analyst and instrumentation, the same laboratory, a brief period of time, and 9 replicates are prepared for each material, and then the standard deviation (s) of the results is determined.

The precision of the method was evaluated on the three injections at three different levels used for accuracy measurements and on the background samples, the results are reported in Table III.9. For every level of concentration, the % RSD between three different extracts was calculated.

Table III.9: Values obtained for accuracy and precision of DNJ quantitation.

Sample	DNJ Spiked	DNJ (ppm)	Std. Dev.	RSD %	Recovery %	Average Recovery %
Backg. 1		1.185			-	
Backg. 2	0 ppm	1.138	0.024	2.072	-	
Backg. 3		1.171			-	
ACC 3-1		2.219			105.4	
ACC 3-2	1 ppm	2.191	0.036	3.555	102.6	102.1
ACC 3-3		2.147			98.2	
ACC 2-1		5.201			100.9	
ACC 2-2	4 ppm	5.061	0.070	1.779	97.4	99.0
ACC 2-3		5.117			98.8	
ACC 1-1		9.351			102.3	
ACC 1-2	8 ppm	9.035	0.185	2.322	98.4	99.7
ACC 1-3		9.026			98.3	

The results obtained for the DNJ accuracy are consistent for all the range of concentrations, proving that the method is accurate with recoveries in the range 98 – 105 %. Precision was evaluated with RSD% values at four different concentrations of DNJ. The RSD % values were always under 3.6% showing that the method is precise. Precision was also consistent at any concentration level allowing the method to be used with low errors in the total of the linearity interval.

III.3.2.4 Intermediate precision

Intermediate precision was evaluated repeating the accuracy analysis on a different day using the same instrumental setup. Four different concentration levels were prepared in triplicate and the RSD% was also calculated between the two sessions to estimate the error of the interday measurements. Table III.10 shows that the interday performance does not significantly differ from that of the analyses conducted on the same day.

Table III.10: Values obtained for intermediate precision of DNJ quantitation.

Sample	DNJ Spiked	DNJ (ppm)	Std. Dev.	RSD %	Recovery %	Average Recovery %	Total RSD %
Backg. 1		1.183			-		
Backg. 2	0 ppm	1.269	0.043	3.507	-	-	-
Backg. 3		1.227			-		
ACC 3-1		2.179			95.3		
ACC 3-2	1 ppm	2.258	0.040	4.050	103.2	99.7	3.644
ACC 3-3		2.233			100.7		
ACC 2-1		5.169			98.6		
ACC 2-2	4 ppm	5.257	0.072	1.767	100.8	100.5	1.785
ACC 2-3		5.312			102.1		
ACC 1-1		9.089			98.3		
ACC 1-2	8 ppm	9.610	0.029	3.515	104.8	100.7	2.744
ACC 1-3		9.148			99.0		

The percentage recoveries range from approximately 95.3% to 105.4%. This similarity is confirmed by the RSD% values of the result combination, for each level of concentration the RSD% never exceeds the 4%. The method is accurate and comparable to other MS/MS methods found in the literature that utilize triple quadrupole detectors (QqQ) (Marchetti et al., 2021). The values of standard deviations and consequently RSD% are consistent regardless of the time gap between measurements or the concentration of the various spikes applied to the samples to be extracted. These characteristics together provide the method with excellent accuracy and precision qualities, comparable to recently published methods that, however, use chromatographic columns with stationary phases different from those proposed in this study (Han et al., 2018).

The data were obtained from the analysis of dried leaves and are expressed as DNJ mg/g dry weight (DW). The concentration of DNJ found in the *Alba* species is significantly higher than

that measured in the *Nigra* species, namely, 1.20 mg/g and 0.48 mg/g, respectively. The relative standard deviation values (RSD%) are aligned with low percentages, reflecting low variability in the measured concentration within the samples. These DNJ concentration values are consistent with what has been previously reported in the literature. As previously reported in the studies by Hu et al. (Hu et al., 2013), the DNJ content in mature leaves of 132 cultivars of *Morus* from 9 Chinese species can vary significantly. The concentration found in mature leaves ranged from 0.13 to 1.47 mg/g DW (Hu et al., 2013), with the M. *alba* species being the most represented as reported in Table III.11 and Figure III.14. An essential factor that influences the measurable quantities of DNJ in mulberry leaves is the wide variety of cultivars and their different yields depending on agronomic practices and environmental factors.

Table III.11: DNJ contents measured in varieties of *Morus.*

Cultivar	DNJ (mg/g DW)	Dev.Std. (mg/g)	RSD %
M. Alba	1.20	0.046	3.85
M. Nigra	0.48	0.014	2.98

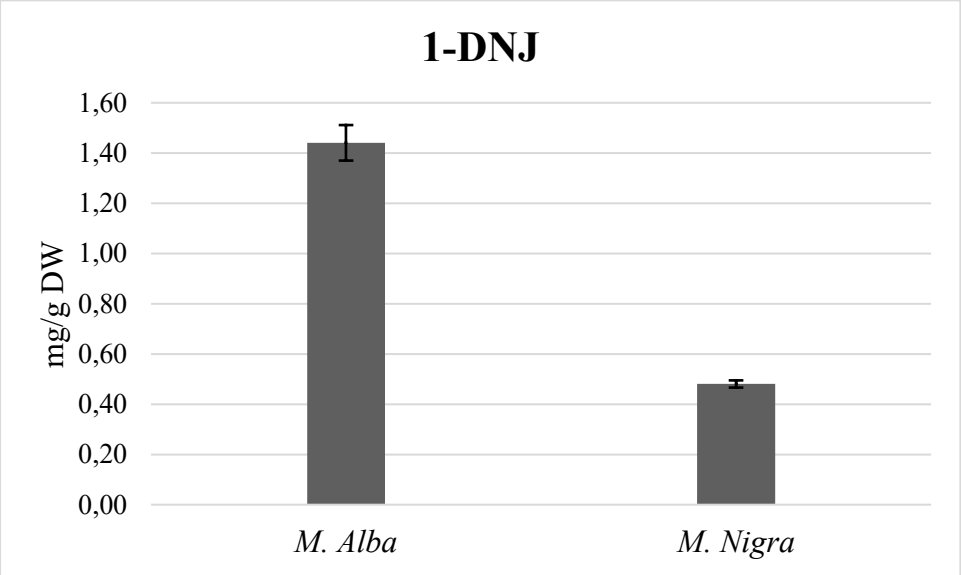

Figure III.14: Plot of DNJ concentrations in *Morus nigra* and *Morus Alba*.

As previously demonstrated in the literature, environmental conditions play a decisive role in regulating the concentration of bioactive substances in *Morus* species (Hu et al., 2013; Kimura et al., 2004). Amino sugar levels typically begin to increase in the spring months and then gradually decrease until September, with a concentration peak around June and July (Han et al., 2018).

III.4 Conclusions

In this chapter, *Morus* samples were quantitatively analysed using HPLC-MS after freeze-drying stabilization and hydroalcoholic extraction. The target molecule was identified through MS fragmentation analysis and quantified using SRM mode.

Furthermore, the Design-Expert software was used to investigate the parameters that most influence the extraction of DNJ from these matrices, for optimizing the process. The chemometric approach of experimental design was used to rigorously assess the method variables. After selecting an appropriate internal standard, Voglibose, LoD and LoQ values were estimated, together with the method's linearity range. By spiking the samples at three different concentrations, the method accuracy and precision were also evaluated. Finally, the method was tested for intermediate precision with result aligned to the intraday precision.

The HPLC-MS method for quantitative determination of DNJ extracted from *Morus nigra* and *Morus alba* leaves was developed and validated, demonstrating high specificity and good sensitivity. The combination of these factors classified it as reliable and reproducible.

The obtained results demonstrate that the extraction yield of 1-deoxynojirimycin is highest under mild extraction conditions in terms of ultrasonic bath, temperature and process time. It has also been observed that acidic pH condition in the extraction mixture is not necessary, as the extraction efficiency is higher at neutral pH, and that a low percentage of EtOH in the extraction mixture is sufficient to achieve high yields of the analyte.

Chapter IV

Glycoalkaloids

IV.1 Introduction

Belonging to the *Plantae* kingdom, *Solanales* order, and *Solanaceae* family, *Solanum* encompasses economically vital plants, like tomatoes and potatoes, as well as lesser-known cultivated species. *Solanum*, the largest genus of angiosperms with about 1500 species globally, played a key role in traditional medicine. The *Solanaceae* family comprises 3000–4000 species across approximately 90 *genera*, exhibiting diversity in perennial trees and annual herbaceous species across terrestrial habitats ranging from deserts to rainforests (Knapp et al., 2004). The *Solanaceae* species have played crucial roles in human civilization for millennia, serving as sources of food and medicine, and more recently, as ornamental plants. Noteworthy, *Solanaceae* include peppers, eggplants, tomatoes, potatoes, and tobacco, all of which produce bioactive components, with both beneficial and potentially toxic properties, such as alkaloids and glycoalkaloids (Friedman, 2006). Model plants, including tomatoes, tobacco, and petunias, were central to classical and molecular genetics. While potatoes, eggplants, and peppers played crucial roles in addressing agricultural challenges like disease resistance and improved cultivation (Gebhardt, 2016).

Glycoalkaloids, nitrogenous steroid glycosides, are synthesized by plants belong the *Solanaceae*, *Asclepiadaceae*, and *Liliaceae* families, known for their medicinal, toxicological, and pharmaceutical properties (Nepal & Stine, 2019). These secondary metabolites, found in *Solanaceae* family plants' leaves, as well as in edible parts, serve as a defense against stressors, like insect attacks, exhibiting concentration-dependent toxic effects in human diets. They also possess biological activities, including anti-inflammatory and antimicrobial properties (Abu Bakar Siddique & Brunton, 2019). Selected secondary metabolites, such as tropane alkaloids and steroidal alkaloids, are produced by plants as response to environmental challenges. Glycoalkaloids, like those found in widely consumed crops such as potatoes, tomatoes, and eggplants, play a crucial role in the defense mechanisms of these plants (Wink, 2003). These compounds feature a six-ring heterocyclic steroidal skeleton with nitrogen, consisting of aglyconic and oligosaccharide components (Figure IV.1). Aglycons can be grouped into five categories based on their structure, influencing the chemical character of the compound. Nitrogen can be linked in various ways, impacting the biological activity of glycoalkaloids. Overall, glycoalkaloids are multifaceted compounds with diverse roles in plant defense and human health. If properly extracted, glycoalkaloids could serve as effective insecticides, antimicrobials, and antifungals. The configuration and sugar content influence their activity. The synergism of major glycoalkaloids, α-solanine and α-chaconine, enhances membrane-disruptive activity.(Sánchez-Maldonado et al., 2016). Tomato glycoalkaloids protect plants

from insects and fungal pathogens, acting on cell membranes. Bioactive compounds in tomatoes exhibit various beneficial effects, including antioxidant, anti-inflammatory, cardiovascular, and immunostimulant effects(Marcolongo et al., 2020). α-tomatine also shows antiviral, antifungal, and antibiotic effects. However, further research is needed to understand the mechanism and potential harm to normal cells for establishing glycoalkaloids clinical use.

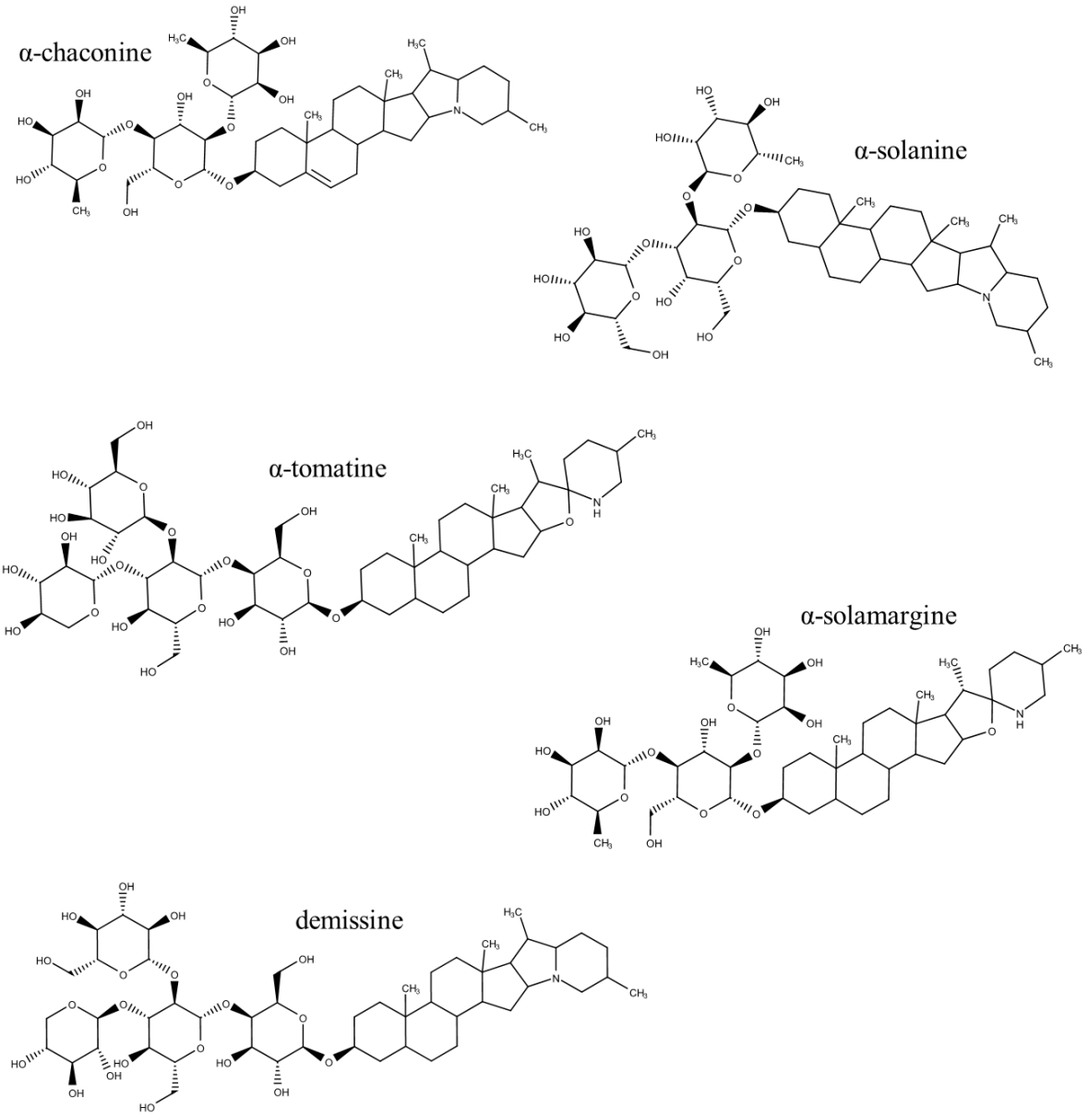

Figure IV.1: Structures of glycoalkaloids found in Solanaceae plants.

IV.2 Materials and methods

IV.2.1 Reagents and standards

All reagents and solvents listed below for chromatographic analyses were purchased from Sigma-Aldrich (Milan). All standards used were purchased from Extrasynthese (Lyon, France). Reagents and standards: Peimine (≥98%, Sigma Aldrich, Milan), α-chaconine, α-solamargine, Solanidine, α-solanine, Solasodine, α-solasonine, tomatidine, α-tomatine (≥98%, Extrasynthese, Lyon, France). Solvents: Methanol (MeOH, LC-MS grade 99.9%), Ethanol (EtOH, LC-MS grade 99.9%), acetic acid (CH_3COOH, LC-MS grade 98%), Acetonitrile (CH_3CN, ACN, LC-MS grade), formic acid (HCOOH, LC-MS grade 98.5%), ultrapure water (18 MΩ·cm) produced by a purifier (Rephile Direct-Pure).

IV.2.2 Samples treatment and extraction

The plant products just after collection underwent a lyophilization process to guarantee a long-term preservation of bioactive components. Specifically, the products were lyophilized using the VirTis BenchTop Pro after liquid nitrogen freezing, to maintain the integrity of the leaves and prevent/reduce leaf oxidation processes. Then, the lyophilized samples were cold ground using a knife mill (Pulverisette 11, Fritsch) and sieved to achieve a particle size < 500 µm. The processed samples were stored at a temperature of -20 ± 1 °C until subsequent use/analysis. The extraction protocol was optimized based on a previously published and studied procedure, with minor modifications (Milner et al., 2011). Briefly, a total of 0.500 g of lyophilized sample was added to 10 mL of a solvent mixture consisting of 70:30 (% v/v) of EtOH/H_2O (1% CH_3COOH, v/v), followed by ultrasound-assisted extraction (10 min, 21 ± 2 °C; nominal power 120 W; sound frequency 35 kHz; Branson® ultrasonic bath). The suspension was centrifuged (5 min, 4000 rpm; Thermo Electron Corporation PK 110 centrifuge), and the supernatant was separated from the solid residue and transferred to a polyethylene container. The extraction procedure was repeated twice using 10 mL of solvent mixture on the residual solid phase. The extracts were combined, resulting in a total volume of 30 mL, and subsequently dried overnight under a stream of ultrapure nitrogen. The dried extracts were stored in polyethylene tubes at -20 ± 1 °C before further analyses.

IV.2.3 HPLC Analysis

The analysis was conducted using an HPLC instrument (Thermo Scientific UltiMate 3000) coupled with a mass spectrometer (Thermo-Scientific LTQ XL) and operated by the Xcalibur software (Thermo-Scientific). The column employed was a C18 Polar Phenomenex Kinetex 5 µm, 100 Å, 150 x 2.1 mm, with a Phenomenex C18 Polar pre-column, 4 x 2.0 mm, thermostated at 35 °C. The mobile phase consisted of (A) H_2O/formic acid (0.1%, v/v) and (B) ACN/formic acid (0.1%, v/v), eluted according to the gradient reported in Table IV.1. Standards and samples were analyzed in triplicate, injecting a volume of 3 µL, with a flow rate of 0.4 mL/min for chromatographic runs of 40 min.

Table IV.1: HPLC final gradient developed for the analysis of the glycoalkaloids.

Time (min)	%A	%B	Curve
0.0	80	20	5
1.0	80	20	5
23.0	50	50	8
25.0	5	95	5
29.0	5	95	5
30.0	80	20	5
40.0	80	20	5

The ionization technique was Electrospray Ionization (ESI), coupled with a mass spectrometer equipped with a linear ion trap analyzer (LIT). Spectra were acquired in positive ion mode, optimizing the following parameters through direct injection of standards diluted in MeOH (1 mg/L) along with a 25% B mobile phase flow using a three-way splitter to simulate the chromatographic elution conditions of the analyte most accurately. The ESI parameters used were as follows: spray voltage, 5000 V; sheath gas pressure, 35 AU; auxiliary gas pressure, 10 AU; capillary temperature, 200 °C.

During the determination, the standards of the major glycoalkaloids categories were selected to analyze all the major diffused *Solanaceae* plants. After the gradient development, the chromatographic method was able to separate all the standards. The standards are reported in Table IV.2 with the m/z of their respective protonated molecules and retention times.

To perform quantitative measurements, the same amount of internal standard (IS) was added to all standards used for the calibration curves and samples analysis. The internal standard was

obtained by appropriate dilution of a 10 mg/L Peimine solution in MeOH. Peimine was selected as the internal standard due to its similarity to the aglycones of glycoalkaloids commonly used as internal standards as shown in Figure IV.2. However, in rare cases, small concentrations of aglycones may be observed within the extracts, potentially influencing the internal standard content in individual analyses (Caprioli et al., 2014). Peimine is produced only by plants belonging to the lily family (*Liliaceae*), making it an excellent internal standard for the quantification of glycoalkaloids in species belonging to the Solanaceae family (Fig.IV.3).

Table IV.2: Retention times and m/z values for the glycoalkaloids standards selected for the method development.

Standard	**Rt (min)**	**Mass**	**$[M+H]^+$**
Peimine	4.77	431.7	432.5
α-solasonine	12.04	884.1	884.7
α-solanine	12.61	868.1	868.8
α-chaconine	13.37	852.1	852.8
Solamargine	13.84	868.1	868.7
α-tomatine	14.87	1034.2	1034.8
Solanidine	22.32	397.6	398.5
Solasodine	23.72	413.6	414.5
Tomatidine	23.94	415.8	416.5

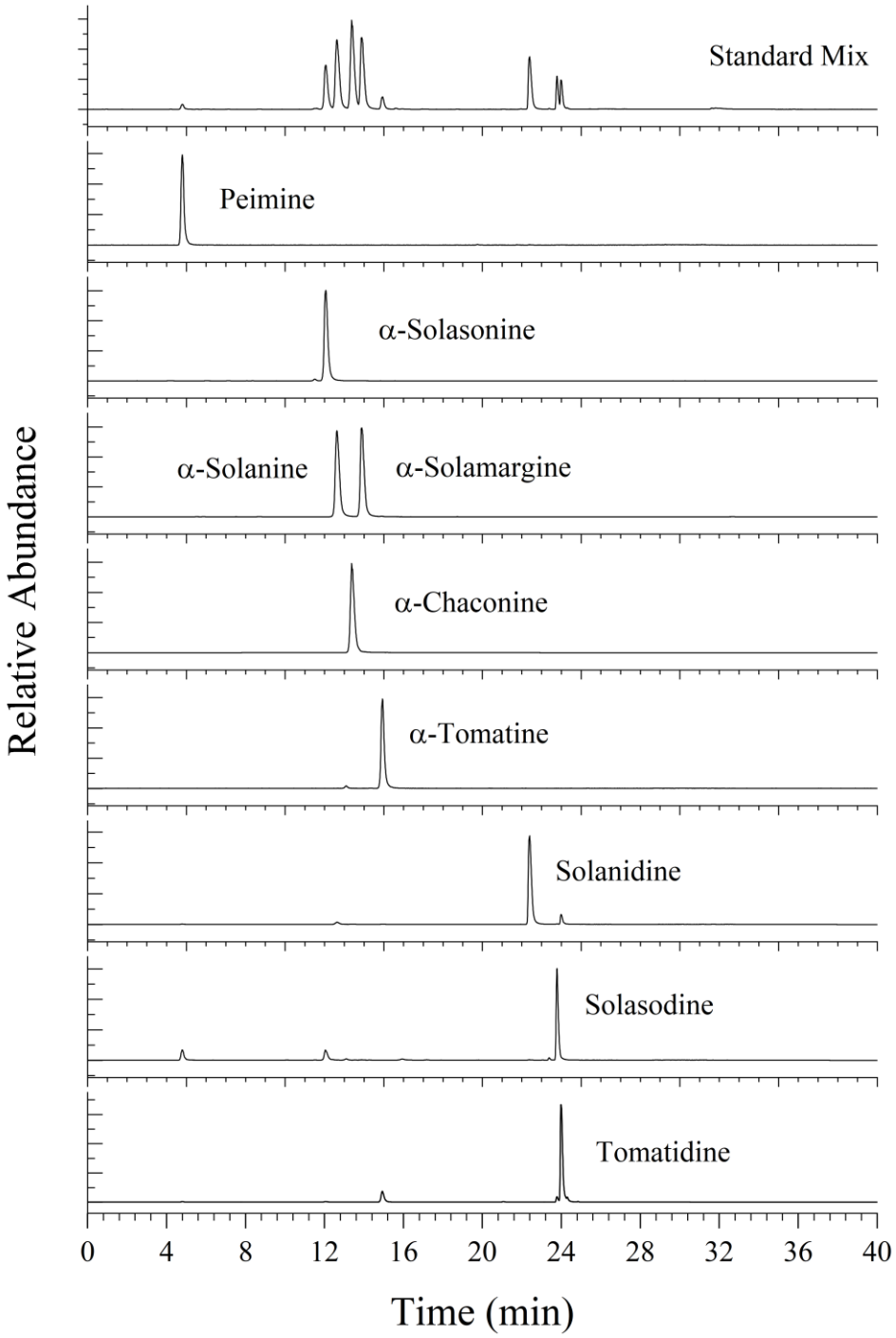

Figure IV.2: Stacked mass chromatograms of the glycoalkaloids standard mix and the extracted mass chromatograms of the selected standards.

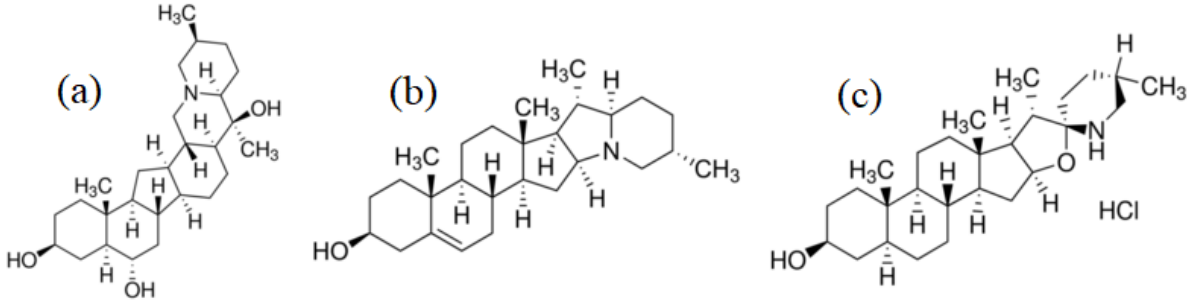

Figure IV.3: Structures of the selected internal standard peimine (a), solanidine (b), tomatidine (c).

The calibration curves were generated by plotting the concentration of the solutions against the normalized peak areas of the chromatogram peaks, corresponding to the signals of various glycoalkaloids relative to the peak area of Peimine (IS). Table IV.3 and Figure IV.4 show the calibration curves used for the analytical determination of glycoalkaloids. Quantitative analysis was conducted in SIM (Selected Ion Monitoring) mode.

Table IV.3: Parameters of the calibration curves obtained for the glycoalkaloids standards.

Analyte	Equation	R^2	Range
α-solanine	y=2.9383x	1.0000	0.025 – 2.5 µg/mL
α-chaconine	y=3.5944x	1.0000	0.025 – 2.5 µg/mL
α-tomatine	y=0.3453x	0.9981	0.05 – 10 µg/mL
α-solasonine	y=1.6941x	0.9999	0.025 – 10 µg/mL

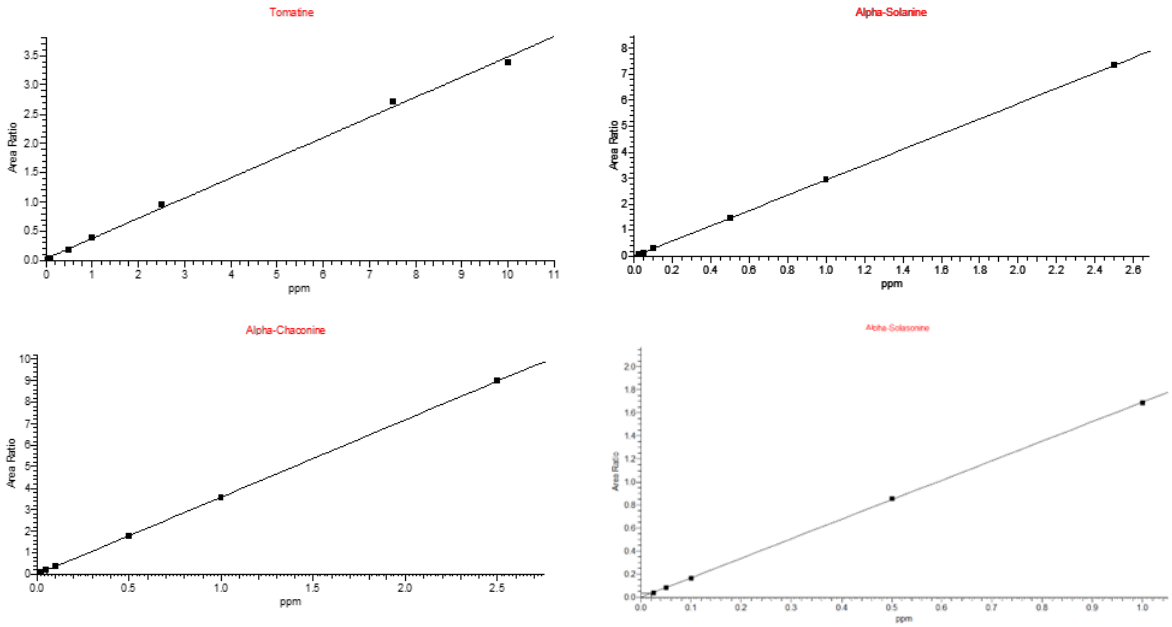

Figure IV.4: Calibration curves obtained for the glycoalkaloids standards.

IV.2.4 Qualitative MS method

LTQ mass spectrometers are recognized for their high sensitivity and versatility. This type of mass analyzer plays a crucial role in data-dependent mass spectrometry (DDA) applications. In a DDA experiment, the instrument autonomously selects and fragments precursor ions, employing Collision-Induced Dissociation (CID) within the Linear Trap Quadrupole (LTQ) configuration. The MS/MS capability of the LTQ enhances the depth of structural information obtained from the analysis. This tandem mass spectrometry approach allows for the investigation of both precursor and product ions, providing comprehensive insights into the composition and structure of the analyzed molecules. DDA with LTQ mass spectrometers proves particularly valuable in the analysis of complex samples, such as those encountered in proteomics. This tailored data processing approach is essential in extracting meaningful information from the complex datasets generated during DDA experiments. LTQ mass spectrometers, with their advanced DDA capabilities, stand as indispensable tools in analytical research, facilitating in-depth analysis of complex samples and contributing to advancements in fields like proteomics and metabolomics (Lim et al., 2007; Mullard et al., 2015). To identify the analytes in the extracts, the MS^n spectra produced by the fragmented molecules within the ion trap are compared with the spectra of characteristic fragments obtained from standards and those reported in the literature. The main feature of this method is the instrument's ability to fragment a specific ion within the trap. The first-order MS spectrum provides information regarding the ionized mass of the compound under analysis ($[M+H]^+$) and corresponds to the peak with the highest relative abundance (base peak). The second order MS^2 spectrum allows visualization of the fragments originating from the precursor ion (identified in the MS spectrum) obtained through Collision-Induced Dissociation (CID) with helium within the ion trap. The third order MS^3 spectrum displays the fragments of the two most abundant ions identified in the MS^2 spectrum. The obtained fragments are then compared with those tabulated from literature articles. In cases where the values coincide, it is possible to attribute the most probable structure to the analyzed compound. The use of the MS^n method is crucial, as it not only identifies the most probable structure but also, in some cases, can discriminate isobaric ions, thereby enhancing the efficiency of the analysis. The tandem mass spectrometry method utilized is detailed in Table IV.4.

Table IV.4: Data dependent acquisition method for qualitative spectrometric study of the leaves extracts.

Data dependent scan Top 1 MS^3			
Scan type	**nCE (collision energy)**	**Scan interval (m/z)**	*Data Dependent Acquisition*
Full MS	-	100-1200	Full Scan
MS^2	45	100-1200	Select the most intense fragment in full MS
MS^3	60	100-1200	1^{st} & 2^{nd} most intense fragments in MS^2

IV.3 Results and discussion

The percentage moisture content (%) of the samples was determined by the difference in weight before and after the lyophilization process. The determination of this parameter is fundamental for an accurate measure of the dry weight (DW) concentration of the analytes. The moisture content in the leaves of the plant matrices is reported in Table IV.5.

Table IV.5: Water content of the potato (Pat) and tomato (Pom) leaves samples (values are ± 3%).

Potato leaves	Water content (%)	Tomato leaves	Water content (%)
Pat 1	89.4	Pom 1	89.2
Pat 2	87.9	Pom 2	88.7
Pat 3	88.5	Pom 3	89.3

An average moisture content of 88.6% is obtained in potato leaves, while tomato leaves exhibit a moisture content of 89.1%.

IV.3.1 Qualitative HPLC-MS

As previously mentioned, glycoalkaloids are important due to their medicinal, pharmaceutical, and defense properties against insects and bacteria. However, these compounds can also have toxic effects on human consumption depending on their concentration in foods and therefore their quantitation is very important.

An analytical procedure was optimized using reverse-phase HPLC-ESI-MS. Such procedures are particularly valuable when analytes include molecules with similar structures and/or isomers at equal m/z ratios, or in the case of samples derived from highly complex matrices. In such instances, optimizing selective techniques such as Single Ion Monitoring (SIM) or MS/MS (tandem MS) protocols like Selected Reaction Monitoring (SRM) are particularly suitable and advantageous in terms of analysis time, selectivity, sensitivity, accuracy, precision, and repeatability of the analytical method. In this study, analyses were performed in SIM mode on all detected analytes to identify these compounds present in higher quantities through qualitative analysis of extracts from tomato and potato plant leaves.

IV.3.1.1 Tomato

The compounds in the chromatogram shown in Figure IV.5 were detected in tomato leaves extracts. The three identified analytes were subjected to tandem mass spectrometry (MS^n) using helium as collision gas within the ion trap. The study of fragmentation patterns allowed the identification of the following analytes as listed in Table IV.6.

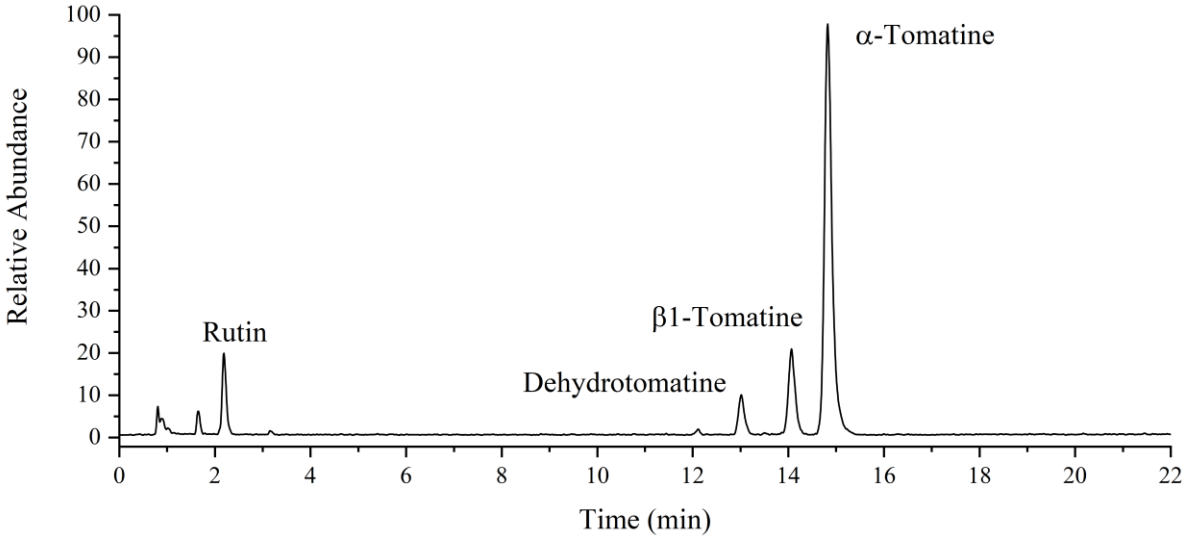

Figure IV.5: Full scan mass chromatogram of tomato leaves extract.

Table IV.6: Identified glycoalkaloids in tomato leaves extract.

Name	Rt (min)	$[M+H]^+$	Fragment ions
Dehydrotomatine	13.01	1032.7	576.6, 414.6
β1-tomatine	14.07	902.7	578.6, 416.6
α-tomatine	14.82	1034.7	578.5, 416.5

Observing the MS full scan chromatogram of the tomato leaf extract, the first analyte eluting at a retention time of 13.01 minutes is dehydrotomatine. The discovery of dehydrotomatine (Milner et al., 2011; Pan et al., 2016), along with the demonstration of its presence in all parts of the tomato plant (Shin et al., 2016), led to analytical studies aimed at elucidating the exact structure of dehydrotomatine (Caprioli et al., 2014). Dehydrotomatine, in combination with α-tomatine, represents the commercially available tomatine mixture and is identified as a secondary metabolite present in tomatoes, leaves, fruits, and other parts of the plant. The ESI positive ion mass spectrum of dehydrotomatine is shown in Figure IV.6.

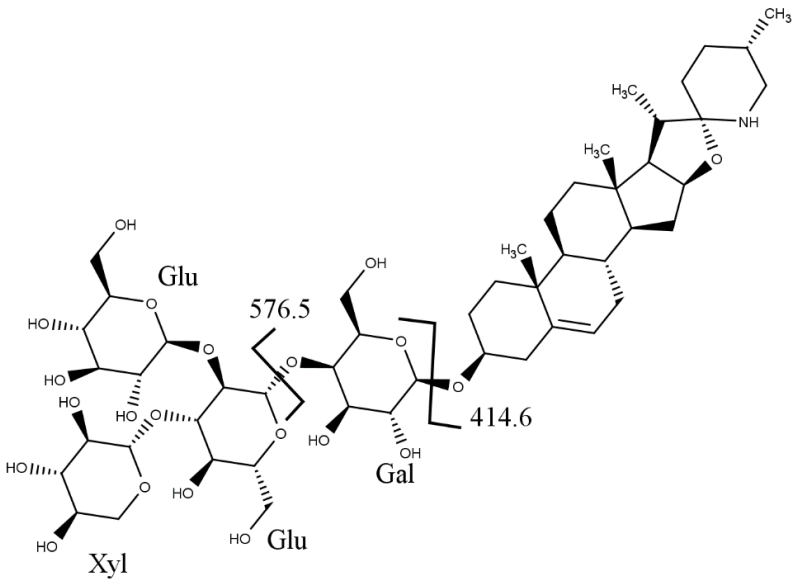

Figure IV.6: Structure and major fragmentation pathway for dehydrotomatine.

The protonated molecule $[M+H]^+$ is found at m/z 1032.7, as shown in Figure IV.7. Fragment ions corresponding to $[Tomatidenol+Gal+H]^+$ at m/z 576.7 and $[Tomatidenol+H]^+$ at m/z 414.6 were also detected. These ions correspond to the loss of Xyl-Glu-Glu and the entire glycosidic part (lycotetraose), respectively. The glycosidic portion of the molecule known as lycotetraose is composed of four sugar molecules, respectively glucose, galactose and xylose. This fragmentation results aligns with tomato glycoalkaloid analyses reported in the literature using the same analytical technique (Cataldi et al., 2005).

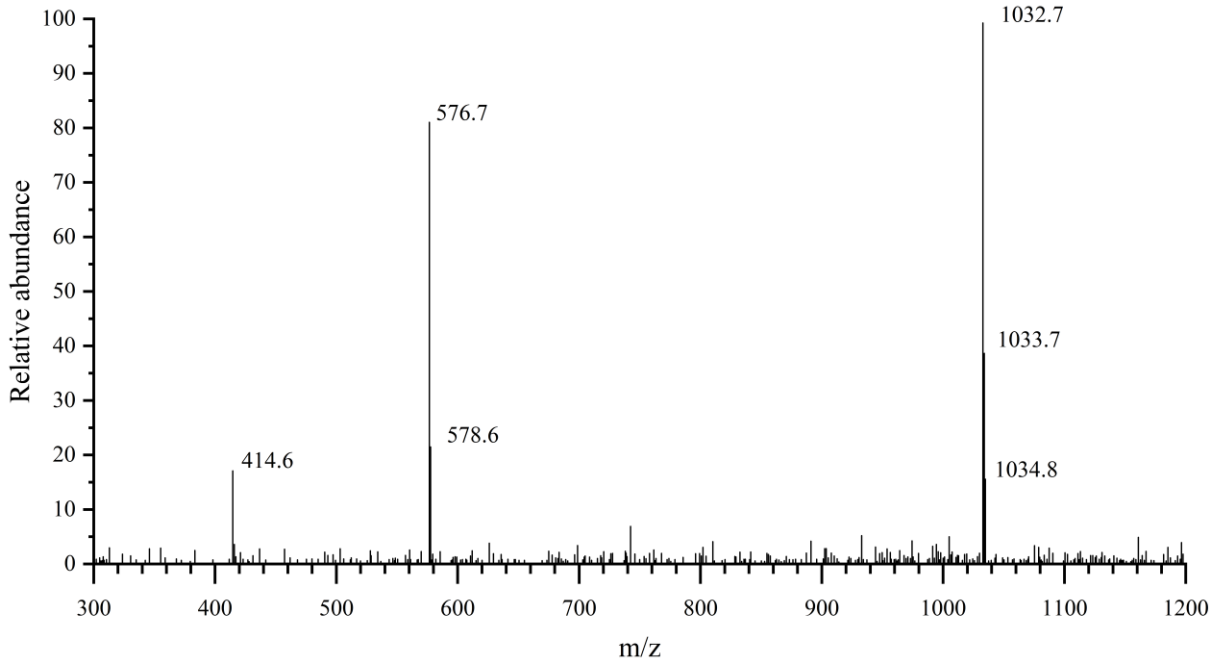

Figure IV.7: Mass spectrum extracted for dehydrotomatine.

Subsequently, at a retention time of 14.07 minutes, the detected analyte is β1-tomatine. The ESI positive ion mass spectrum, as shown in Figure IV.8, highlights the presence of the protonated molecule $[M+H]^+$ at m/z 902.7 and ions corresponding to $[Tomatidine+Gal+H]^+$ at m/z 578.6 and $[Tomatidine+H]^+$ at m/z 416.6. These ions correspond to the loss of Glu-(Glu) and the entire glycosidic part (lycotriose).

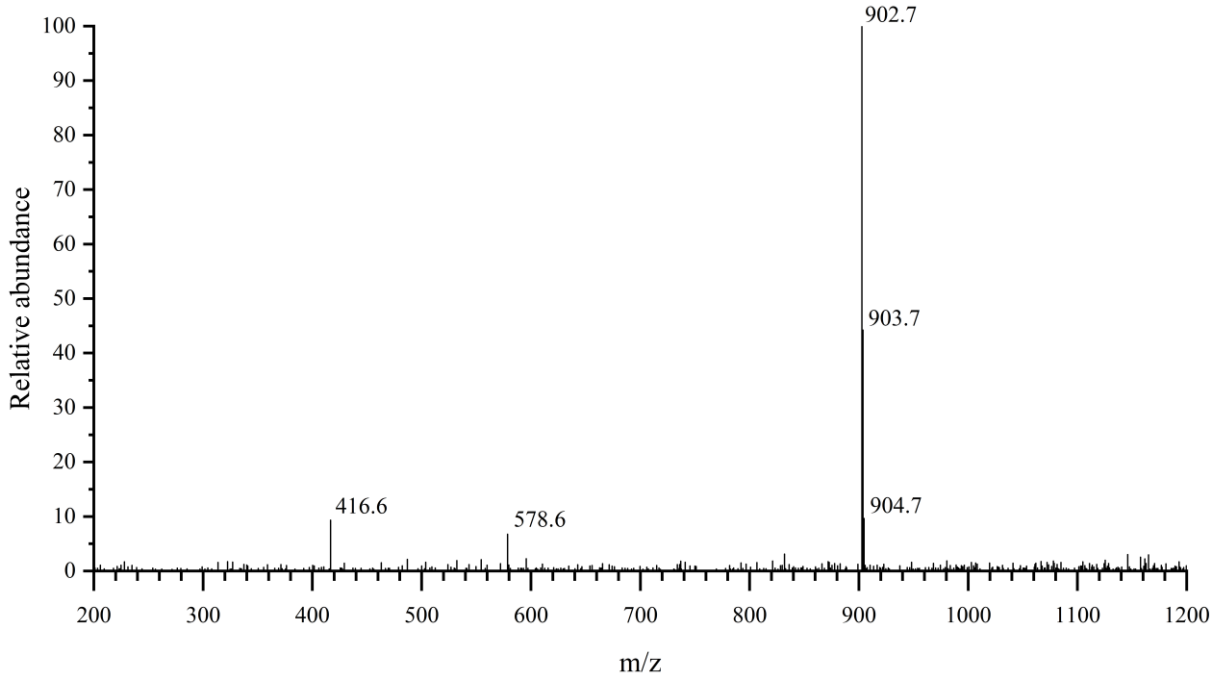

Figure IV.8: Mass spectrum extracted for β1-tomatine.

The information contained in the tandem mass spectra for this molecule were sufficient to hypothesize the fragmentation pathway reported in Figure 9.

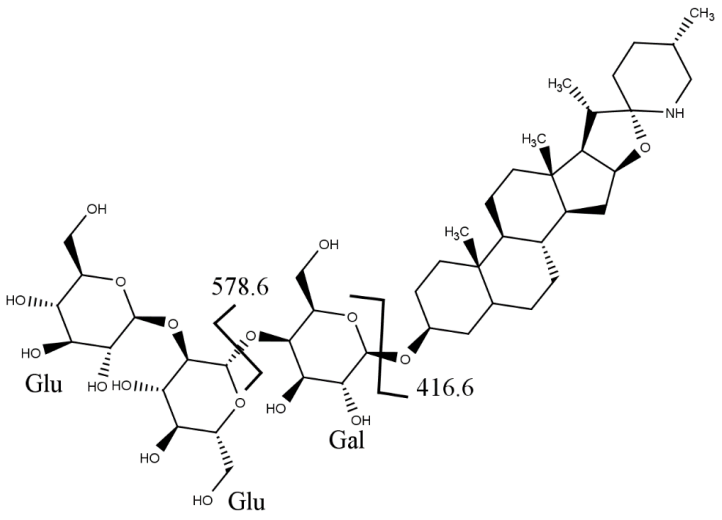

Figure IV.9: Structure and major fragmentation pathway for β1-tomatine.

This protonated molecule, through a comparison with literature articles(Friedman, 2006; Kozukue et al., 2008), was identified as a derivative of tomatine. β1-tomatine represents the product of the biological hydrolysis processes of tomatine: The glycosidic portion of tomatine is hydrolysable in acidic solutions, producing β1-, β2-, γ-, and δ-tomatine as reported in Figure IV.10.

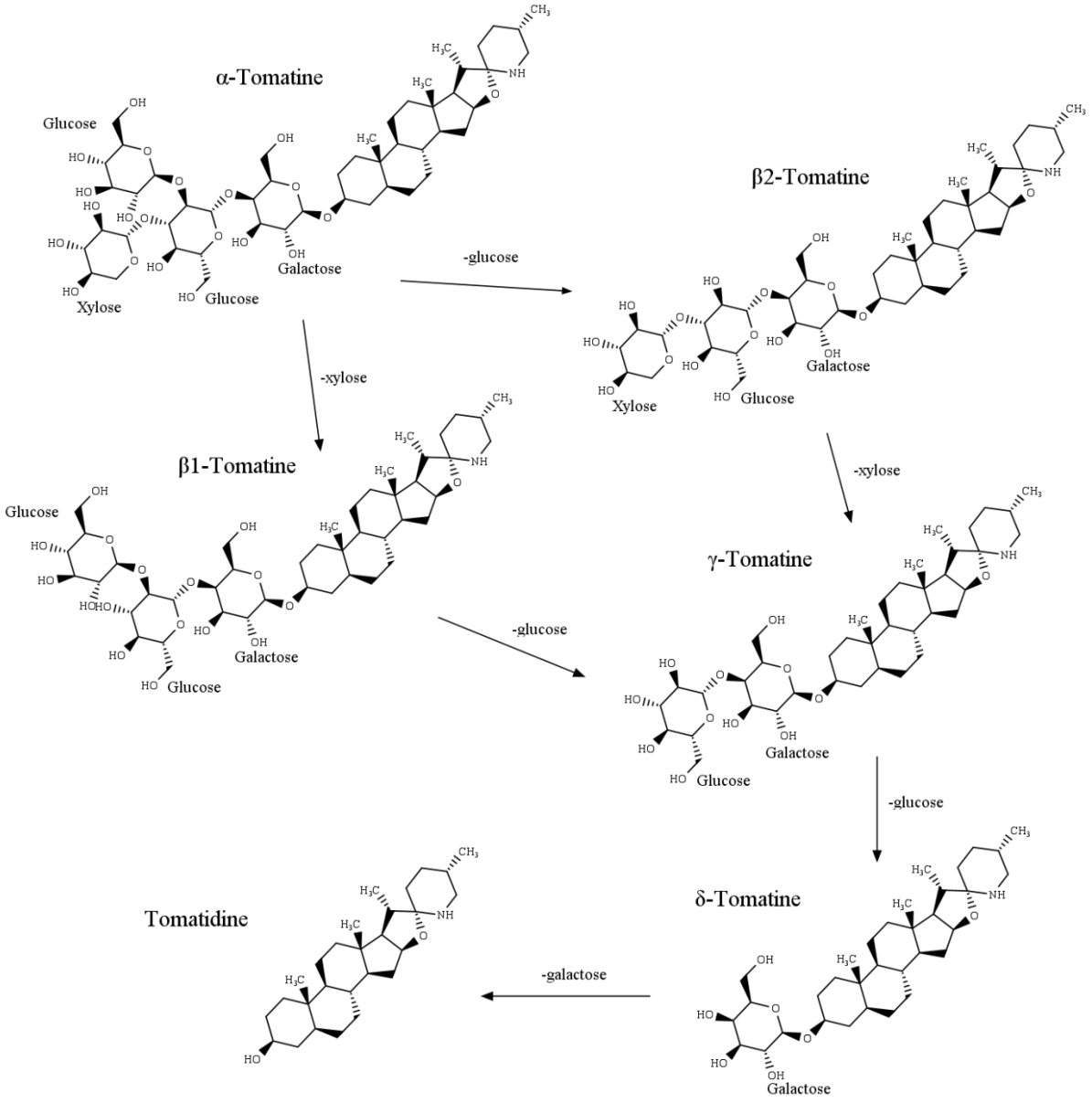

Figure IV.10: Metabolomic degradation pathway of α-tomatine.

The ESI positive ion mass spectrum of the α-tomatine molecule is shown in Figure IV.11.

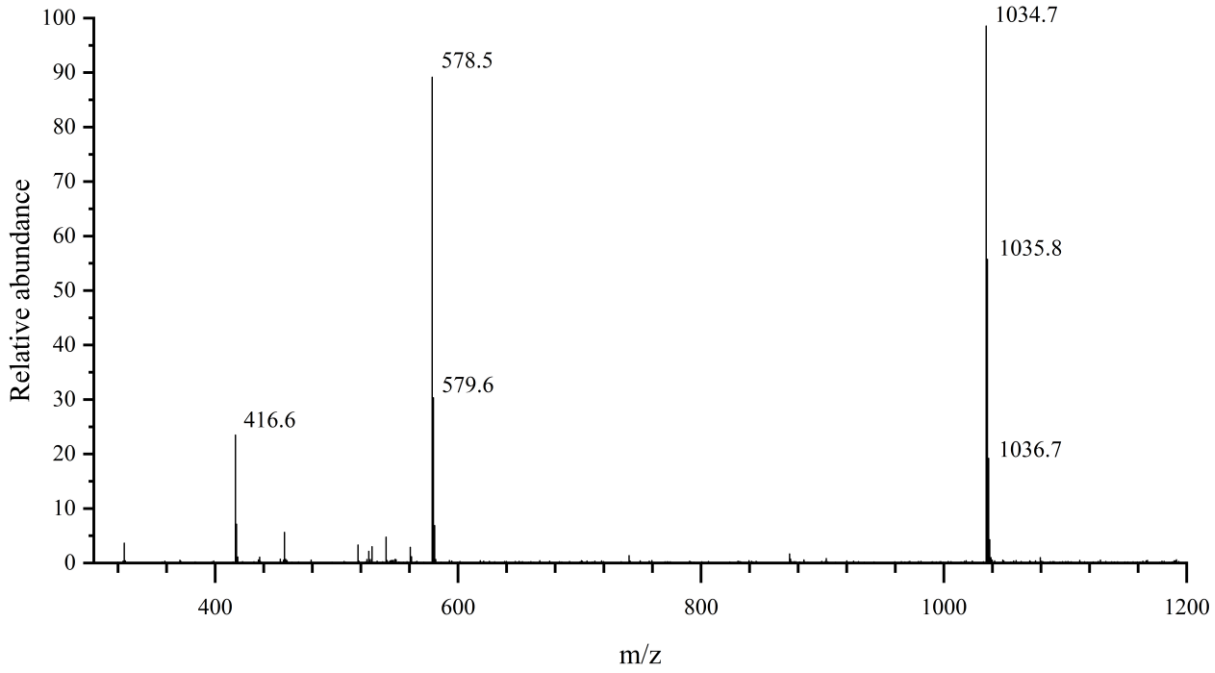

Figure IV.11: Mass spectrum extracted for α-tomatine.

In addition to the protonated molecule $[M+H]^+$ (m/z 1034.7), relatively abundant ion fragments at m/z 578.5 and 416.5 were also detected. Observing the molecular structure, it is evident that the secondary amine of tomatidine is easily protonated during the ESI ionization process. The ions at m/z 578.5 and 416.5 correspond to $[Tomatidine+Gal+H]^+$ and $[Tomatidine+H]^+$, primarily formed by eliminating the Xyl-Glc-Glc- moiety and the entire glycosidic chain (lycotetraose), respectively. This analysis aligns with previous studies in the literature (Bianco et al., 2002). The fragmentation pathway of tomatine was reported in Figure IV.12.

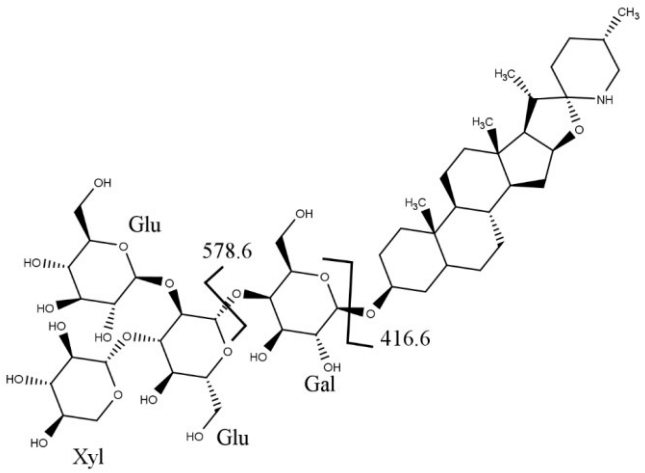

Figure IV.12: Structure and major fragmentation pathway for α-tomatine.

Regarding α-tomatine and β1-tomatine, it is noteworthy that both glycoalkaloids are glycosidic derivatives of the aglycone tomatidine (molecular weight 415.6). α-tomatine contains the glycosidic group lycotetraose composed of Xylose, two units of Glucose, and one unit of Galactose. β1-tomatine has only two units of Glucose and one unit of Galactose. Unlike α-tomatine, the glycoalkaloid dehydrotomatine, derived from the aglycone tomatidenol, shares the same glycosidic component.

According to the literature, beneficial effects of α-tomatine and dehydrotomatine, as well as their hydrolysis products in the human diet, have been reported, including lowering cholesterol and triglycerides, enhancing the immune system, chemotherapy for cancer, and protection against fungi, bacteria, viruses, and virulent protozoa (Friedman, 2006).

IV.3.1.2 Potato leaves

The qualitative analysis of potato leaf extracts was conducted similarly to those obtained from tomato leaves. Existing literature suggests that the analytes α-solanine and α-chaconine are present in higher quantities. Indeed, the chromatogram in Figure IV.13 illustrates that this extract is rich in analytes present in much lower concentrations compared to the two major components. The employed technique allowed also the identification of analytes present in lower concentrations.

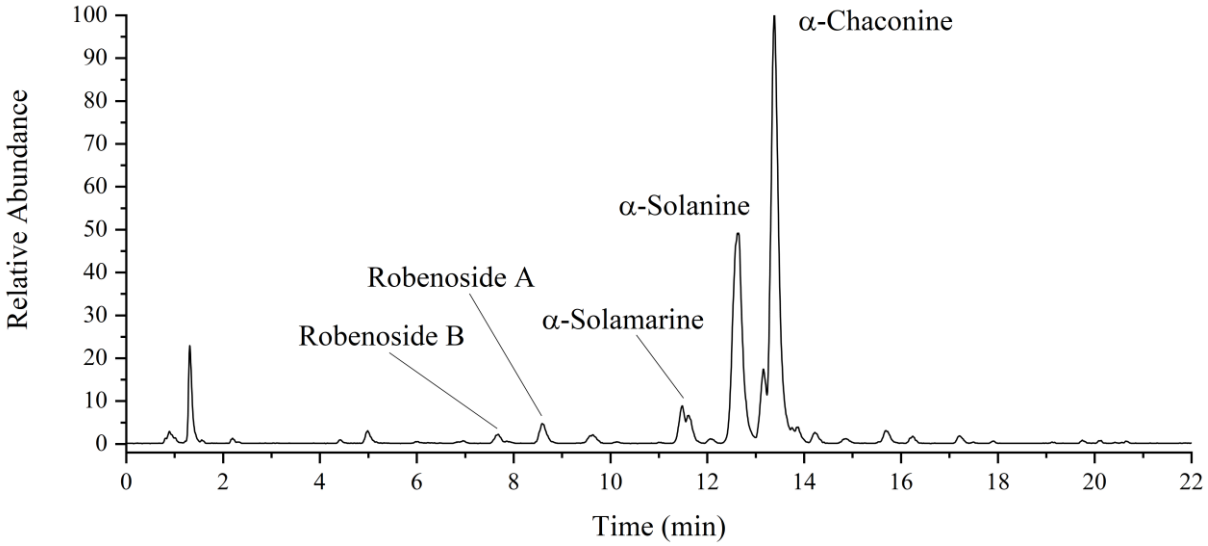

Figure IV.13: Full scan mass chromatogram of potato leaves extract.

Studies on wild and cultivated potato species suggest the heritability of the following glycoalkaloids: α-chaconine, α-solanine, demissine, α-tomatine, dehydrotomatine, α- and β-solamarine, solamargine, solasonine, and soladulcine, along with other known and unknown glycoalkaloids(Osman et al., 1978; Shakya & Navarre, 2008). The use of fragmentation patterns facilitated the identification of these analytes in the studied samples, as detailed in Table IV.7.

Table IV.7: Identified glycoalkaloids in potato leaves extract.

Nome	Rt (min)	$[M+H]^+$	Fragment ions
α-solanine	12.62	868.8	850.7; 722.7; 706.6; 398.5
α-chaconine	13.39	862.7	708.8, 398.6
α- solamarine	11.49	884.7	738.8; 722.4; 430.4; 414.5
Robenoside A	8.65	884.1	866.7; 738.7; 430.5.
			866.7; 720.6; 412.4
Robenoside B	7.73	900.7	882.7; 754.7; 738.6; 430.5
			882.7; 736.6; 412.4

The mass spectrum of the positive ion electrospray ionization (ESI) of the peak identified as chaconine in Figure 14 reveals the protonated molecule $[M+H]^+$ at m/z 852.7, along with ions corresponding to $[Solanidine+Glu+H]^+$ at m/z 708.8 and $[Solanidine+H]^+$ at m/z 398.6. These ions signify the loss of Rha-Rha- and the entire glycosidic moiety (chacotrioside).

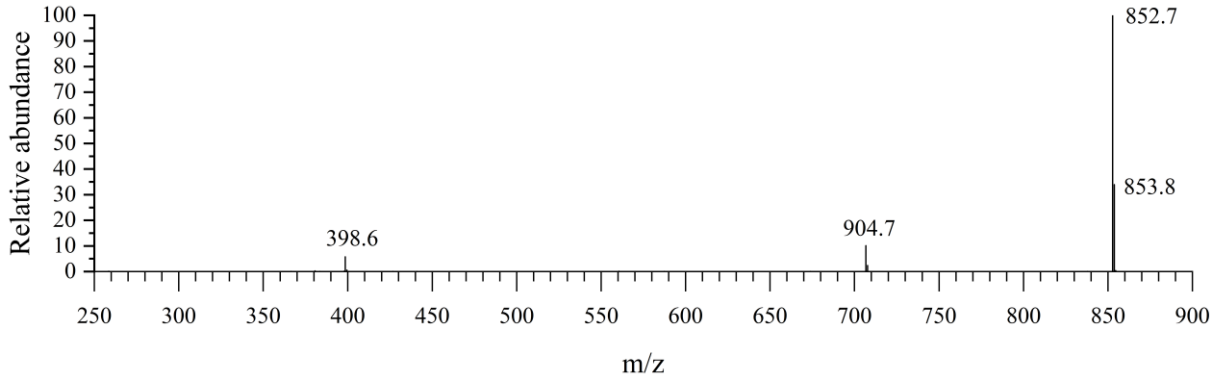

Figure IV.14: Mass spectrum extracted for chaconine.

These results are aligned with literature findings, confirming the higher concentrations of α-chaconine in Solanum Tuberosum, utilizing the same analytical method (Cahill et al., 2010), the fragmentation pathway proposed is reported in Figure IV.14.

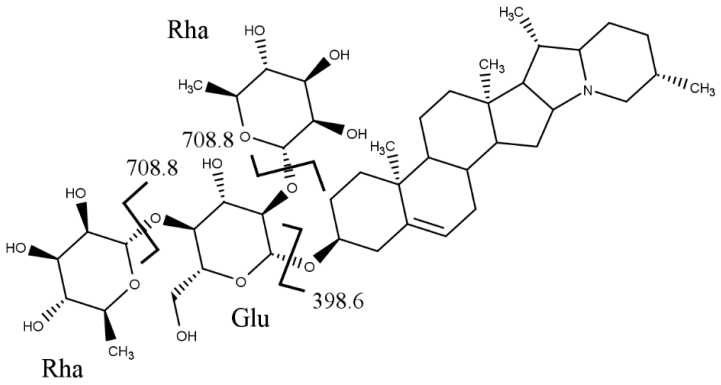

Figure IV.15: Structure and major fragmentation pathway for chaconine.

The compound eluted at Rt 12.62 min was identified as α-solanine and its structure is reported on Figure IV.15.

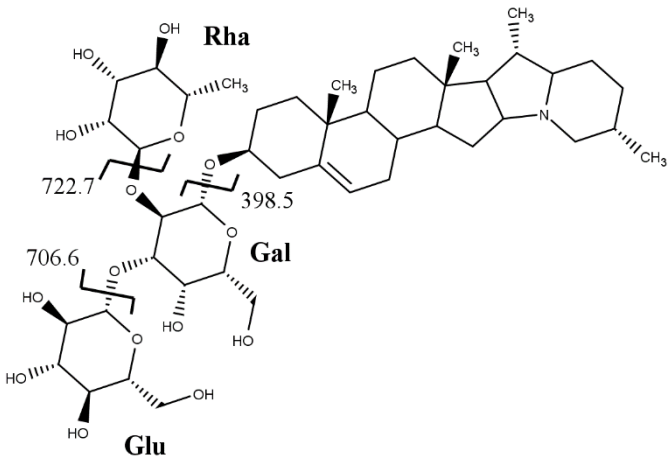

Figure IV.16: Structure and major fragmentation pathway for solanine.

The mass spectrum of the positive ion ESI of solanine reported in Figure IV.17 highlights as base peak the protonated molecule $[M+H]^+$ at m/z 868.8. Subsequent fragmentation of the protonated molecule produces ions such as $[Solanidine+Gal+Glu+Rha+H]^+$ at m/z 850.7 due to a water neutral loss, $[Solanidine+Gal+Glu+H]^+$ at m/z 722.7, $[Solanidine+Gal+H]^+$ at m/z 706.6, and $[Solanidine+H]^+$ at m/z 398.5. These ions correspond to the loss of Rhamnose, the consecutive loss of Glucose, and finally, the entire glycosidic moiety (solatrioside) as reported in Figure IV.16. This analysis is consistent with literature data on glycoalkaloid distribution in *Solanum Tuberosum*, confirming the higher concentrations of α-solanine and α-chaconine identified using the same analytical technique.(Cahill et al., 2010)

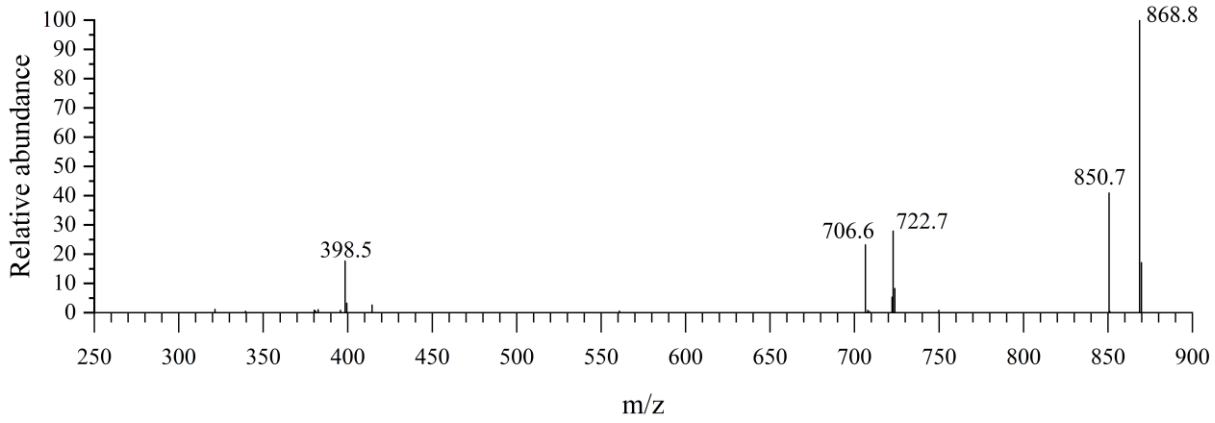

Figure IV.17: Mass spectrum extracted for solanine.

The positive ion ESI mass spectrum of the compound eluted at Rt 11.49 min was identified as α-solamarine, the structure of the glycoalkaloid is reported in Figure IV.17. The tandem mass spectrum shown in Figure IV.18 indicates the presence of the protonated molecule $[M+H]^+$ at m/z 884.7. The corresponding ions after fragmentation include $[Solasodine+Glu+Gal+H]^+$ at m/z 738.8, $[Solasodine+Gal+H]^+$ at m/z 722.4, $[Solasodine+O+H]^+$ at m/z 430.4, and $[Solasodine+H]^+$ at m/z 414.5. These ions are produced by the loss of deoxymannose (dMan), the loss of Glucose, the successive loss of the entire glycosidic moiety with the presence of a hydroxyl group, and finally, the loss of the entire glycosidic moiety (solatrioside). This analysis identified the protonated molecule as α-solamarine, a glycoalkaloid uncommon in most *Solanum* species but demonstrated in literature to be present in potato leaves of the Kennebec cultivar, confirming our analysis.(Distl & Wink, 2009; Shih & Kuć, 1974)

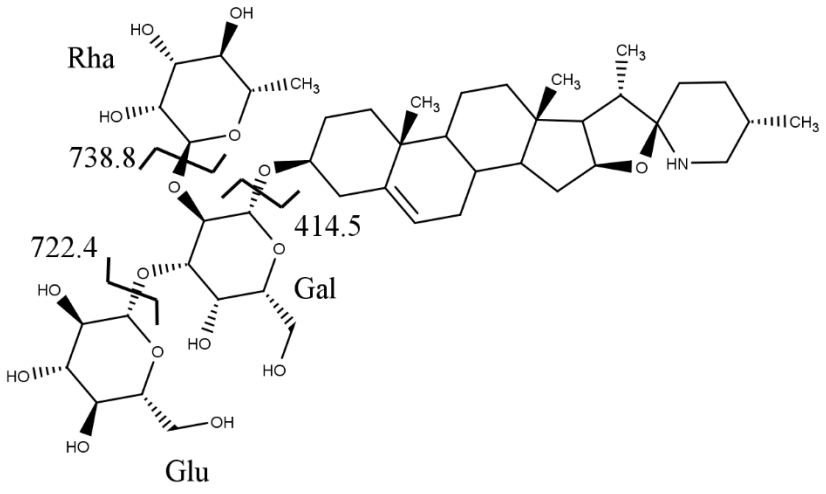

Figure IV.18: Structure and major fragmentation pathway for α-solamarine.

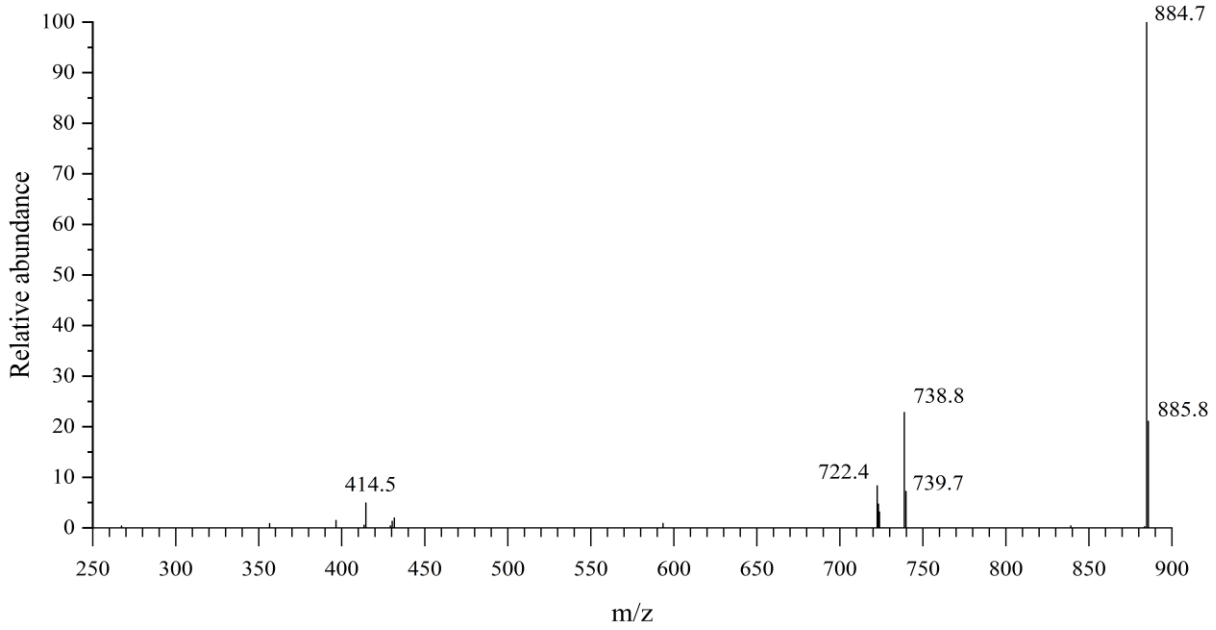

Figure IV.19: Mass spectrum extracted for α-solamarine.

The positive ion ESI mass spectrum of the glycoalkaloid with Rt 8.65 min (Fig. 19) displays the protonated molecule $[M+H]^+$ at m/z 884.7. Through MS^2 analysis, the protonated molecule has a high probability of losing the hydroxyl group attached to the aglycone, evidenced by the peak at m/z 866.7 corresponding to [Solasodine-H_2O+H]$^+$. Further peaks include the loss of Rhamnose at m/z 738.7, the loss of Glucose at m/z 720.6, the loss of the entire glycosidic moiety (cacotrioside) at m/z 430.5. MS^3 analysis (precursor ion 866.7 m/z) reveals the permanent loss of the hydroxyl group attached to the aglycone, with peaks at m/z 866.7 corresponding to [M-H_2O+H]$^+$ and m/z 720.6 corresponding to the loss of Rhamnose from the free aglycone, namely [M-Rha-H_2O+H]$^+$ (Fig. IV.21). The final loss corresponds to the entire glycosidic moiety (cacotrioside) at m/z 412.4, confirming that the molecule possesses a side chain directly attached to the aglycone portion, characteristic of the glycoalkaloid Robenoside A.(Wanyonyi et al., n.d.; Wu et al., 2013) The proposed major fragmentation pathway is shown in Figure IV.20.

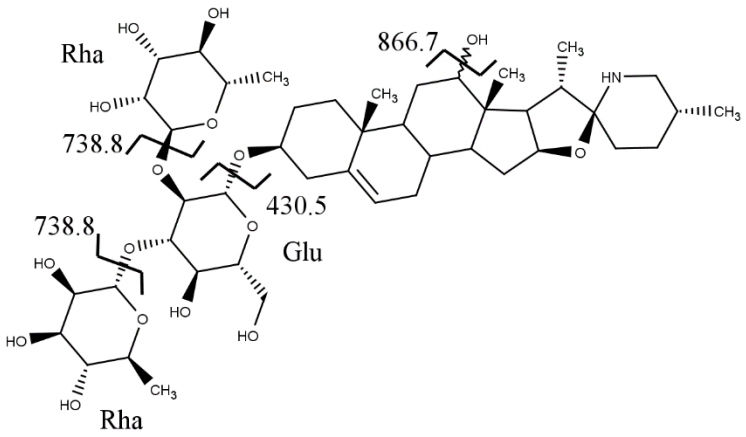

Figure IV.20: Structure and major fragmentation pathway for Robenoside A.

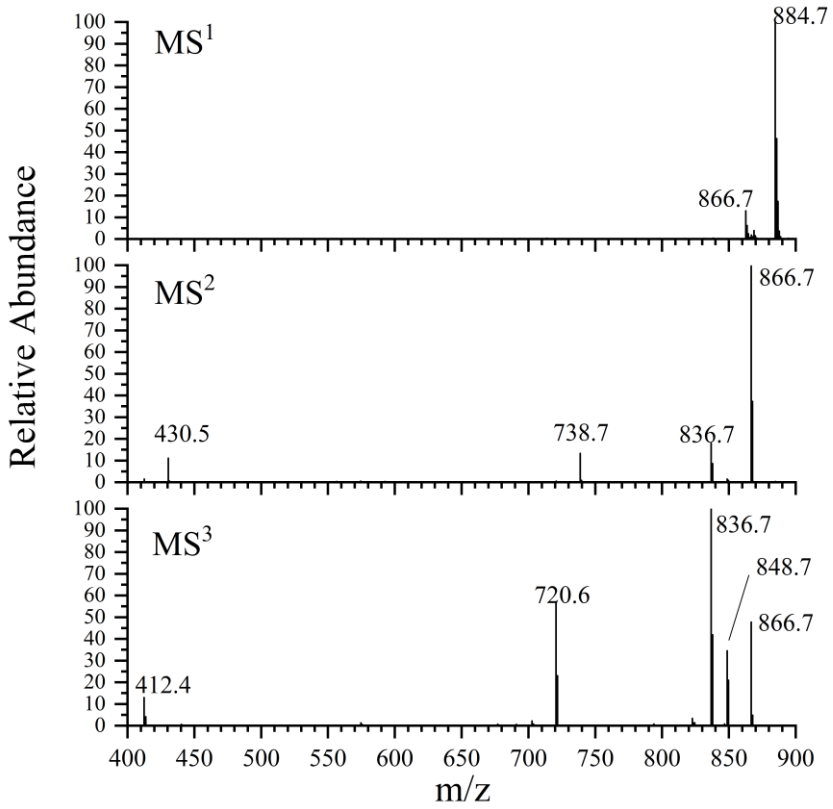

Figure IV.21: Tandem mass spectrum of glycoalkaloid identified as Robenoside A.

The positive ion ESI mass spectrum of the compound identified as Robenoside B with Rt 7.73 is reported in Figure IV.22.

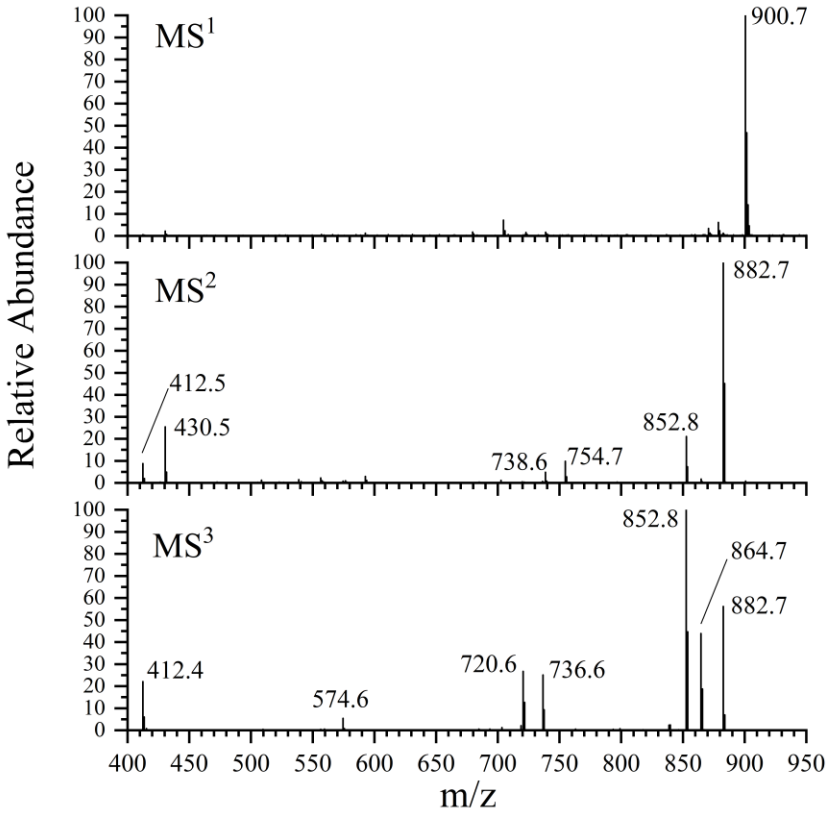

Figure IV.22: Tandem mass spectrum of glycoalkaloid identified as Robenoside B.

The spectrum shows the protonated molecule $[M+H]^+$ at m/z 900.7. Through MS^2 analysis, the protonated molecule is likely to lose the hydroxyl group attached to the aglycone, as seen in the peak at m/z 882.7 corresponding to $[M-H_2O+H]^+$. There is a small probability of losing Rhamnose at m/z 754.7, Glucose at m/z 738.6, and the entire glycosidic moiety (solatrioside) at m/z 430.5. MS^3 analysis reveals the peaks at m/z 882.7 corresponding to $[M-H_2O+H]^+$ and m/z 736.6 corresponding to the loss of Rhamnose from the free aglycone, $[M-Rha-H_2O+H]^+$. Additionally, there is a peak at m/z 720.6 corresponding to the loss of Glucose, $[M-Glu-H_2O+H]^+$, a peak at m/z 574.6 corresponding to $[M-Glu-Rha-H_2O+H]^+$, and finally, a peak at m/z 412.4 corresponding to the loss of the entire glycosidic moiety (solatrioside). The proposed fragmentation pathway of the molecule is reported in Figure IV.23.

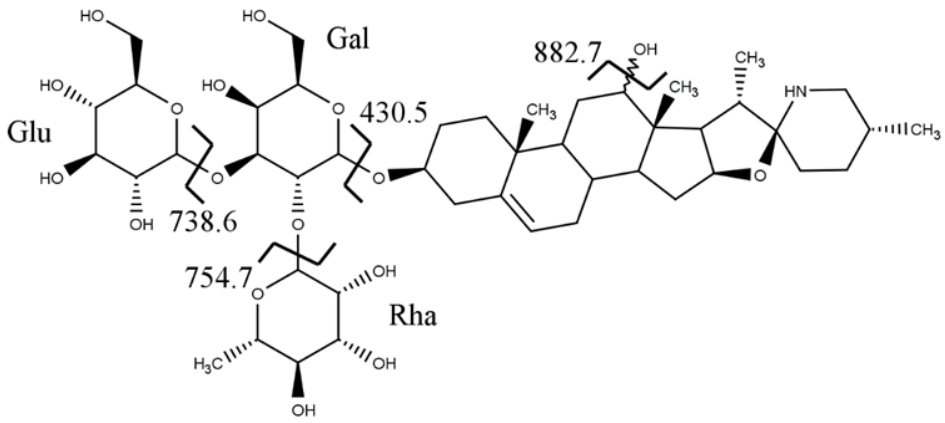

Figure IV.23: Structure and major fragmentation pathway for Robenoside B.

The identification of these two glycoalkaloids as Robenoside A and B was achieved by comparing the analysis with varieties of *Solanum melongena* L and *Solanum lycocarpum* (Wanyonyi et al., n.d.; Wu et al., 2013)

The LC-MS analysis conducted with this methodology detected glycoalkaloid concentrations in tomato leaves, such as α-tomatine, dehydrotomatine, and β-tomatine.

The measured concentrations reported in literature are very different in contents of tomatine and dehydrotomatine, this particular behavior is addressable to a high varietal influence on the production of glycoalkaloids as reported in literature (Juvik & Stevens, 1982). The presence of β1-tomatine is quite uncommon in literature and as previously stated could be potentially addressed to biological degradation processes. (Quidde et al., 1998). The detection of these analytes aligns with literature confirming the presence of primarily α-tomatine and in various parts of tomato plants(Tam et al., 2021). The quantitative analysis results are summarized in Table IV.8 and Figure IV.24.

Table IV.8: Quantitation of tomato glycoalkaloids extracted from tomato leaves.

Analyte	**Extract Concentration**	**DW**	**H_2O**	**FW**	**mg/g DW**	**SD**
	mg/L	g	%	g	average	
α-tomatine	2.988	0.5	89.2	4.64	13.40	0.11
β-tomatine	0.572	0.5	89.2	4.64	2.59	0.11
Dehydrotomatine	0.209	0.5	89.2	4.64	0.94	0.05

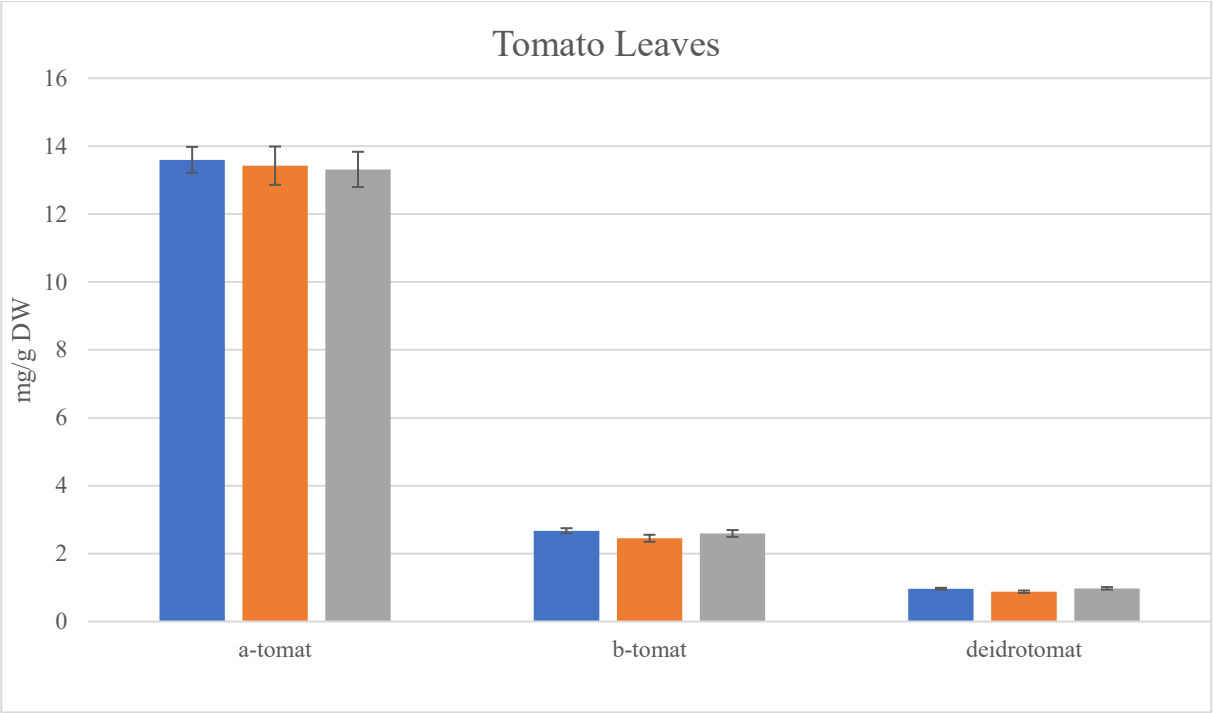

Figure IV.24: Quantified glycoalkaloids in tomato leaves.

The quantitative analysis on tomato leaves extracts revealed that tomatine is the most abundant glycoalkaloid, followed by β1-tomatine and dehydrotomatine. The same LC-MS analysis was performed on potato leaf extracts (Fig. IV.25 and Tab. IV.9), revealing concentrations of glycoalkaloids such as α-chaconine, α-solanine, α-solamarine, Robenoside B, and Robenoside A. The identification of these analytes is consistent with literature (Brown et al., 1999; Friedman & Dao, n.d.) with high concentrations of the two major constituents, chaconine and solanine.

Table IV.9: Quantitation of potato glycoalkaloids.

Analyte	Extract Concentration	DW	H_2O	FW	mg/g DW	SD
	mg/L	g	%	g	average	
α-chaconine	0.768	0.5	88.7	4.42	6.92	0.41
α-solanine	0.571	0.5	88.7	4.42	5.14	0.36
α-solamarine	0.141	0.5	89.2	4.42	1.27	0.08
Robenoside B	0.040	0.5	89.2	4.42	0.36	0.05
Robenoside A	0.078	0.5	89.2	4.42	0.70	0.03

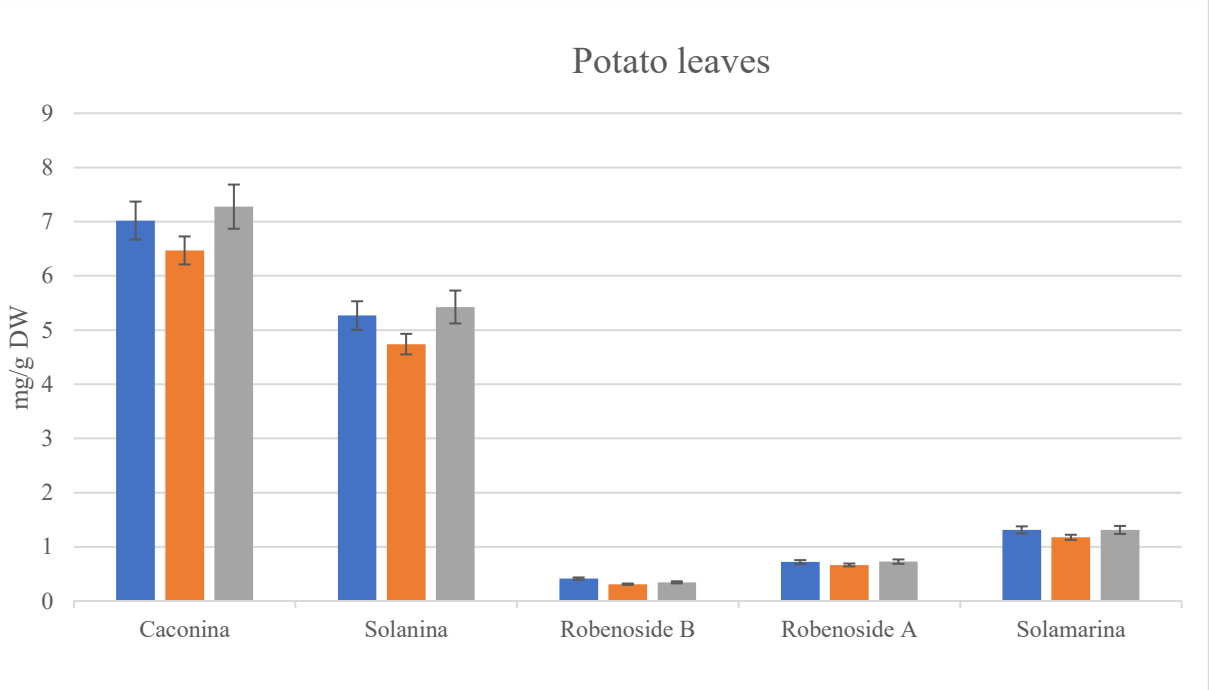

Figure IV.25: Quantified glycoalkaloids in potato leaves.

IV.4 Conclusions

A new chromatographic method was optimized for the identification and quantification of various glycoalkaloids in two plant matrices, namely tomato leaves and potato leaves. The leaves were harvested, lyophilized, and extracted using a previously developed procedure involving hydroalcoholic and acidified solutions ($EtOH/H_2O$ 70/30%, v/v with 1% CH_3COOH). For compound identification, a tandem mass spectrometry method using a data dependent approach was developed. This method leverages the progressive fragmentation of the analyzed molecules to reconstruct their structure. The identified structures were validated through cross-checks with literature and databases (mzCloud and MassBank). The content of various extracted glycoalkaloids was determined through HPLC-MS analysis in Selected Ion Monitoring (SIM) mode, using Peimine as an internal standard and calibration curves obtained from various standards. The analysis of glycoalkaloid content in potato leaves confirmed that α-chaconine and α-solanine are present in higher quantities compared to other analytes in the same class, showing average contents of 6.9±0.4 mg/g DW for α-chaconine and 5.1±0.4 mg/g DW for α-solanine. Other glycoalkaloids found in potato leaves were quantified using solasonine as an external standard. Tomato leaves revealed the presence of α-tomatine, β-tomatine, and dehydrotomatine, all three species quantified using tomatine as an external standard. The measured average concentrations for α-tomatine and dehydrotomatine are respectively 13.4±0.1 mg/g DW for α-tomatine and 0.94±0.05 mg/g DW for dehydrotomatine. The presence of β-tomatine (2.6±0.1 mg/g DW) in tomato leaves, although not commonly reported, is likely due to glycosidic group hydrolysis during plant vegetative processes.

The method developed applies to various matrices for qualitative and quantitative determination of glycoalkaloid concentrations. The standards used are representative of the major compound categories present in the Solanaceae family.

Chapter V

Liposomes

V.1 Introduction

Liposomes, lipidic particles were discovered by A. Bangham in the 1960s, these structures vary from nanometers to micrometers in diameter. Comprising one or more lipid bilayers encapsulating aqueous compartments, these vesicles exhibit an amphipathic nature, allowing them to encapsulate both lipophilic and hydrophilic molecules(Akbarzadeh et al., 2013). The lipid membrane serves as a protective barrier, rendering liposomes highly compatible with cellular membranes(Bozzuto & Molinari, 2015). Liposomes, which are widely used in the cosmetic and pharmaceutical industries are classified according to their size, including multi-lamellar vesicles (MLV), multivesicular vesicles (MVV), large unilamellar vesicles (LUV), and small unilamellar vesicles (SUV)(Maja et al., 2020; Sharma & Sharma, 1997). Cationic liposomes, with positively charged lipids such as DOTAP or DDAB, show significant promise as carriers for molecules such as RNA and DNA, with their behavior in biological systems intricately linked to physicochemical properties(Campbell et al., 2001; Sharma & Sharma, 1997). *Coffea arabica* leaves, equally as coffee beans, present a wealth of compounds with noteworthy properties. Indigenous to southwestern Ethiopia, *Coffea arabica* plants thrive in tropical and subtropical climates(Lashermes et al., 1999; Patay et al., 2016). The dried leaves find utility as a traditional tea substitute in various countries(Ngamsuk et al., 2019b). These leaves feature a rich composition, including caffeine, flavonoids such as quercetin and rutin, chlorogenic acids, and mangiferin.(de Almeida et al., 2019a) While the leaves contribute to antioxidant and anti-inflammatory effects, flavonoids play a key role in potential disease prevention. Within *Coffea arabica* leaves, flavonoids emerge as an important compound category from over 9000 classified flavonoids, ubiquitous in the plant kingdom. Specific flavonoids, like quercetin and rutin, contribute to overall health benefits. Known for antioxidant capacity and modulating enzymatic functions, flavonoids play a role in potential disease prevention(Terahara, 2015). The complexity lies not just in the diversity of flavonoids but also in their glycosylation patterns, impacting solubility and bioavailability. An additional compound of interest is chlorogenic acid, an important molecule with varied health implications. Chlorogenic acid, found abundantly in coffee beans and leaves, is recognized for its antioxidant properties(Miao & Xiang, 2020; Naveed et al., 2018). It acts as a scavenger for free radicals, contributing to cellular protection and potential health benefits(Niggeweg et al., 2004). Liposomes are biomimetic structures with versatile applications, from pharmaceuticals to cosmetic formulations. These vesicles, with their unique properties, represent an important research topic in various fields. Simultaneously, the leaves of *Coffea arabica* emerge as a source of bioactive compounds with potential health benefits.

V.2 Materials and method

V.2.1 Reagents and standards

The phospholipids employed in the liposome synthesis were purchased from Avanti Polar Lipids (Alabama, U.S.A.): DOTAP (1,2-dioleoyl-3-trimethylammonium propane), DDAB (dimethyl-dioctadecyl-ammonium bromide), and DOPC (1,2-dioleoyl-sn-glycero-3-phosphatidylcholine). The cellulose dialysis membrane (diameter 10 mm, molecular weight cut-off 14 kDa) and all other reagents and solvents used for the analyses were acquired from Sigma-Aldrich (Milan). These included formic acid (HCOOH, LC-MS grade 98.5%), ethanol (EtOH, LC-MS grade 99.9%), methanol (MeOH, LC-MS grade 99.9%), acetonitrile (CH_3CN, ACN, LC-MS grade) from Sigma Aldrich, Milan, Italy, and ultrapure water (18.2 MΩ·cm, Rephile Direct-Pure purifier), as well as MeOD d_4 (Sigma Aldrich, Milan, Italy). Standards for HPLC determinations were purchased from Sigma Aldrich, Milan, Italy, including chlorogenic acid (> 98.0%), mangiferin (> 98.0%), 5CGA (> 95.0%), hydrochloride trigonelline (> 95.0%), and caffeine (> 98.0%). All materials were used without further purification.

V.2.2 Coffee leaves extraction

The samples underwent a lyophilization process aimed at preserving the bioactive components present in them. Additionally, the leaves were kept intact throughout the lyophilization process to minimize the activation of oxidation processes at potential cut points. The lyophilization process was carried out using a VirTis BenchTop Pro freeze dryer from SP Scientific. After lyophilization, the samples were cold pulverized using a knife mill and liquid nitrogen (Pulverisette 11, Fritsch). To achieve as homogeneous a sample as possible, the crushed sample was sieved to a particle size of less than 500 µm. A 0.100 g aliquot of pre-treated *Coffea arabica* leaves was placed in a polypropylene centrifuge tube along with 2 mL of a solvent mixture composed of EtOH/H_2O in ratio 70/30 (v/v). Subsequently, a vortex mixer was used at 2400 rpm for 5 seconds to homogenize the mixture. The sample was sonicated in an ultrasonic bath to optimize the extraction process (10 min, 20 ± 1°C; nominal power 120 W; ultrasound frequency 35 kHz; Branson Ultrasonics Corporation). The obtained extract was centrifuged for 5 minutes at 4000 rpm (Thermo Electron Corporation PK 110 centrifuge), and the supernatant was separated from the solid residue and transferred to a polypropylene vial. The extraction

procedure was repeated two more times, each time using the same amount of solvent with the same percentage composition. The supernatants from the three respective extractions were combined to obtain a total volume of approximately 6 mL. A volume of 5 mL of the final extract was withdrawn, which was then dried using a nitrogen flow overnight. The resulting extract was stored in polyethylene vials at -20 ± 1°C for subsequent analyses.

V.2.3 Liposomes synthesis and purification

V.2.3.1 Synthesis

The liposome synthesis involved the creation of two distinct formulations, namely composed of DOPC-DOTAP and DOPC-DDAB, respectively. For each type of liposome, three samples were synthesized: one containing empty liposomes and other two loaded with a previously obtained coffee leaf extract and a chlorogenic acid solution respectively. In the synthesis of extract loaded liposomes, the phospholipid film was hydrated using 1 mL of a solution of freeze-dried coffee leaf extract reconstituted in deuterated water. While in the synthesis of CGA loaded liposomes a solution of chlorogenic acid in deuterated water was used. The synthesis yielded six distinct samples (Table V.1):

Table V.1: Liposome formulations synthesized in this chapter.

Sample N°	Synthetized Liposome (molar ratio)
1	DOPC/DOTAP (1.0 : 0.5)
2	DOPC/DOTAP (1.0 : 0.5) + Extract
3	DOPC/DOTAP (1.0 : 0.5) + Chlorogenic acid
4	DOPC/DDAB (1.0 : 0.5)
5	DOPC/DDAB (1.0 : 0.5) + Extract
6	DOPC/DDAB (1.0 : 0.5) + Chlorogenic acid

The synthesis method is based on the formation of a lipid film through solvent evaporation, followed by rehydration with deuterated solution to perform following NMR experiments. The phospholipids dissolved in chloroform (10 mg/mL) were introduced into Pyrex tubes according to the molar ratios previously reported in Table 1 and were mixed using a Vortex shaker at 2400 rpm for 30 seconds. The solvent was then evaporated under a nitrogen flow, while the solution

was kept in rotation to obtain a lipid film on the vial surface. The tubes containing the lipid film were kept under vacuum for 12 hours at a temperature of 30 °C to ensure complete solvent evaporation.

Samples 1 and 4 were hydrated with 1 mL each of deuterated water (D_2O 99.9%), while samples 2 and 5 were hydrated with 1 mL each of a suspension of *Coffea arabica* leaf extract in deuterated water. Samples 3 and 6 were hydrated using a solution of chlorogenic acid in D_2O 4 mg/mL Each sample then underwent 9 cycles of "Freeze and Thaw," a procedure involving immersion of the vial in liquid nitrogen until complete freezing, followed by immersion in water at 45°C for rapid thawing and subsequent agitation using a Vortex shaker. Afterwards, each sample underwent 27 cycles of extrusion, performed using a LiposoFast extruder equipped with a fixed-pore-size polycarbonate membrane (100 nm). The purpose of the "Freeze and Thaw" cycles and extrusion is to achieve predominantly unilamellar vesicle systems (SUV)(Traïkia et al., 2000).

V.2.3.2 Purification

The obtained liposomes were purified using the dialysis method. The dialysis preparation procedure involved the immersion of the membranes in deuterated water, where they were agitated for 4 hours, followed by washing with D_2O. The samples (total volume 1 mL) were introduced into the membrane tube, and both ends were sealed with a nylon thread to prevent the leakage of liposomes. The system was immersed in 30 mL of deuterated water to allow the release of excess loaded extract that had remained in solution and obtain purified liposomes. The dialysis was the replaced and the process was repeated for a total time of 12 hours.

V.2.4 Dynamic Light Scattering (DLS)

The samples obtained from the synthesis and subsequent dialysis were analyzed using the dynamic light scattering (DLS) technique without prior dilution. The analysis was performed using a Zetasizer Nano ZS90 instrument (Malvern Instrument Ltd., UK). PMMA cuvettes were employed for conducting the analyses. Data acquisition involved three repeated measurements, and the results were reported as the average of the three measurements ± the standard deviation.

V.2.5 Nuclear magnetic resonance ^{1}H NMR

For NMR analyses, a 450 µL aliquot was drawn from each of the four samples obtained during the liposome synthesis. The coffee leaves extract, on the other hand, was analyzed using MeOD-d_4 as solvent. The instrument used for acquiring ^{1}H nuclear magnetic resonance (NMR) spectra is a Bruker DRX-600 Avance III spectrometer operating at 600.13 MHz. Data processing was performed using TopSpin 3.6 software (Bruker). The processing of the obtained spectra was performed using MestReNova software.

V.2.6 HPLC-MS Analysis

The extract of *Coffea arabica* leaves was reconstituted in a MeOH/H_2O mixture (40:60 v/v), and the analyses were conducted using an HPLC instrument (Thermo Fisher Scientific UltiMate 3000) coupled with a linear ion trap (LIT) mass spectrometer (Thermo Fisher Scientific LTQ XL) equipped with an electrospray ionization (ESI) source. Xcalibur software (Thermo Fisher Scientific) was employed for spectrum acquisition and processing. The column employed was a biphenyl column (Biphenyl Phenomenex Kinetex, 100 x 2.1 mm; particle diameter 2.6 µm; porosity 100 Å) with a biphenyl Security Guard pre-column (4.0 x 2.0 mm, Phenomenex). The column temperature was maintained at 35 ± 1°C. The eluents used were (A) H_2O and (B) MeOH, both acidified with formic acid (0.1%). The elution gradient was optimized based on the subsequent positive or negative ESI process, as described below. Gradient for negative ESI mode: from 0.0 to 15.0 min, 10-15% B (linear); from 15.0 to 25.0 min, 15-50% B (linear); from 25.0 to 35.0 min, 50-95% B (linear). Gradient for positive ESI mode: from 0.0 to 5.0 min, 0% B (isocratic); from 5.0 to 45.0 min, 0-70% B (linear). For each analysis, 3 µL of the sample were injected, and elution followed a flow rate of 0.4 mL/min. Each sample was injected and analyzed in triplicate. The column effluent was split in a 1:1 ratio using a splitter towards the two detectors (LIT-MS and DAD) operating in parallel.

V.2.7 UV Spectroscopy

To obtain UV-Visible spectra, a Perkin Elmer EZ 201 double-beam spectrophotometer was employed, equipped with Pessw 1.2 software (Perkin Elmer, Monza, Italy). The maximum absorption of the analyte (chlorogenic acid) was determined by performing a scan in the range of 210-750 nm, using disposable UV-grade plastic cuvettes. A calibration curve was built by measuring the absorbance of standard solutions at 330 nm. Samples were diluted to obtain a calibration line within the range of 1-10 mg/L in H_2O, and each sample was analyzed in triplicate.

V.2.8 Encapsulation efficiency (EE)

The encapsulation efficiency (EE%) for the extract loaded liposomes was calculated using the chromatographic method reported in paragraph 2.6, using a MS detector. The liposomal system, previously dialyzed, was disrupted by adding an appropriate amount of MeOH necessary to dilute and quantify all the substances present in it. Following the addition of methanol, all samples were filtered before chromatographic analyses using 0.22 μm PTFE syringe filters (Whatman). The encapsulation efficiency values (EE%) were calculated using calibration curves related to the main components of the extract (Table V.2).

Table V.2: Calibration curves produced for the quantitation of the major compounds in coffee leaves extract.

Compound	Equation	R^2
Chlorogenic acid	y=0.00868x	0,9974
Catechin/Epicatechin Procyanidin B Isomangiferin Mangiferin Procyanidin A trimer Rutin glycoside Quercetin glycoside Rutin Kaempferol-3-O-rhamno glucoside	y=0.0793x	0,9982
Trigonelline	y=0.02416x	0,9955
Caffeine	y=0.2176x	0,9986

The quantification for flavonoid compounds was based on the curve constructed using the Mangiferin standard. Consequently, the quantifications are to be considered in terms of Mangiferin equivalents.

The encapsulation efficiency for CGA loaded liposomes was measured using direct UV quantification of chlorogenic acid (CGA) in dialysis water to avoid any possible interference from the liposome sample.

The encapsulation efficiency was quantified using the formula(Bonechi et al., 2019):

$$EE\% = \frac{C_{lipo}}{C_{extr}} * 100 \ ,$$

where C_{lipo} indicates the amount of the compound found in the liposome, and C_{extr} represents the amount of the compound found in the extract.

V.3 Results and discussion

V.3.1 Dynamic light scattering

The Dynamic Light Scattering (DLS) analyses were conducted to determine the size, polydispersity index (PDI), and surface charge of the synthesized liposomes. The DLS technique analyzes Brownian motion and the size of particles associated with it. Typically, DLS deals with measuring particles suspended in a liquid, assessing the rate at which particles diffuse due to Brownian motion. These data are obtained by measuring the fluctuation in the intensity of scattered light when detected by a suitable optical device(Surianarayanan et al., 2016). This type of analysis in systems such as liposomes is particularly relevant. The size of particles and the corresponding PDI are descriptive attributes for lipid nanocarriers, influencing stability, encapsulation efficiency, drug release profile, biodistribution, mucoadhesion, and cellular absorption. Cellular absorption or internalization is one of the most crucial physicochemical criteria to evaluate before in vivo applications. The absorption of small molecules by any cell is mainly dependent on the endocytosis process(Danaei et al., 2018). The polydispersity index (PDI) is used to describe the non-uniformity degree in the size distribution of particles. Values below 0.2 are commonly considered optimal for nanoparticulate materials based on polymers. In drug delivery applications using lipid-based carriers like liposome formulations, a PDI of 0.3 or lower is considered optimal, indicating a homogeneous population of phospholipid vesicles(Danaei et al., 2018). The zeta potential provides information on nanoparticle stability, circulation times, protein interactions, particle permeability into cells, and biocompatibility(Smith et al., 2017). Nanoparticles with a zeta potential between -10 and +10 mV are considered approximately neutral, while those with a zeta potential greater than +30 mV or less than -30 mV are considered strongly cationic or anionic, respectively(Clogston & Patri, 2011). High zeta potential values suggest that nanosystems in solution or suspension repel each other, minimizing the possibility of aggregation and/or flocculation processes.

V.3.1.1 DOTAP-DOPC Liposomes

In this section, the results obtained from the DLS analysis conducted on DOPC-DOTAP liposomes are reported in Table V.3.

Table V.3: DLS experiment results for DOPC-DOTAP empty and loaded liposomes.

	Avg Diameter ± sd (nm)	**Polydispersivity (PDI)**	**ζ-potential ± sd (mV)**
DOPC-DOTAP	112.1±5.0	0.20	74.5±2.1
DOPC-DOTAP + Extract	140.5±1.5	0.51	119±5
DOPC-DOTAP + CGA	134.7±2.2	0.23	53.1±2.1

The empty DOPC-DOTAP liposomes exhibit a mean hydrodynamic diameter of 112.1 ± 5.0 nm, as shown in the size distribution curve depicted in Figure V.1. This size corresponds to liposomal systems categorized as Small Unilamellar Vesicles (SUV) and can be considered as nanosystems. The PDI value indicates that the synthesis method employed results in monodisperse systems.

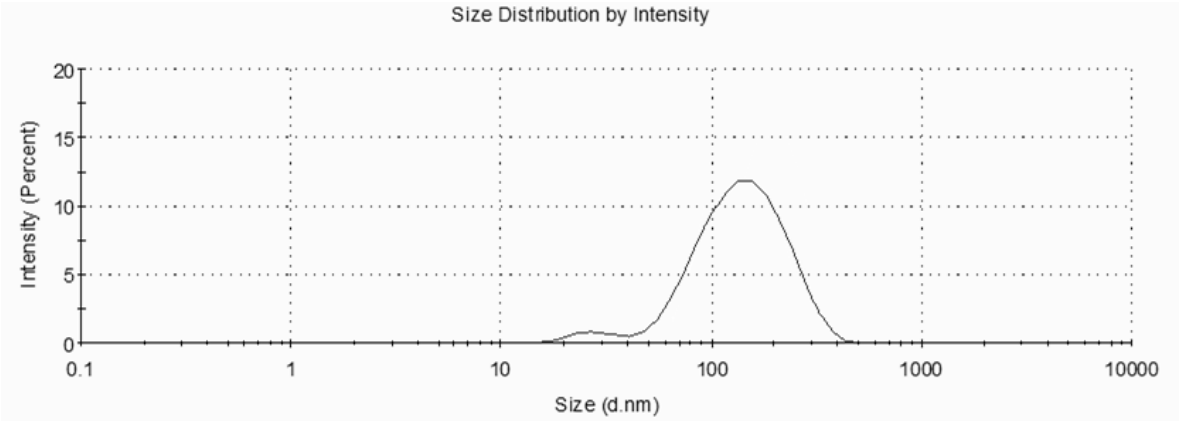

Figure V.1: Size distribution curve obtained for empty DOPC-DOTAP liposomes.

The three measurements have a relative standard deviation of 2.94%, indicating good repeatability in the synthesis of empty DOPC-DOTAP liposomes. Regarding the surface charge, the sample of empty DOPC-DOTAP liposomes exhibits a ζ-potential of 74.5 ± 2.1 mV, describing a strongly cationic system.

The values of the mean sizes and zeta potential of empty DOPC-DOTAP liposomes can be directly compared with those of DOPC-DOTAP liposomes loaded with coffee leaf extract. The obtained data show that loaded DOPC-DOTAP liposomes have a mean hydrodynamic diameter of 140.5 ± 1.5 nm (the distribution curve of the mean diameter is shown in Figure V.2), with a

PDI value of 0.51. Following the loading process, there is an increase in the average size of liposomal systems, making them also more polydisperse. The loading of complex systems, such as plant extracts, leads to an increase in the average size of vesicles influenced by the different distribution of phospholipid molecules compared to those present in the extract itself. This increase is addressable to a major degree of complexity in the interactions that regulate the membrane stability and therefore the vesicle size. The increase in the polydispersity index value confirms that the incorporation of complex matrices influences the homogeneity of liposomal suspensions.

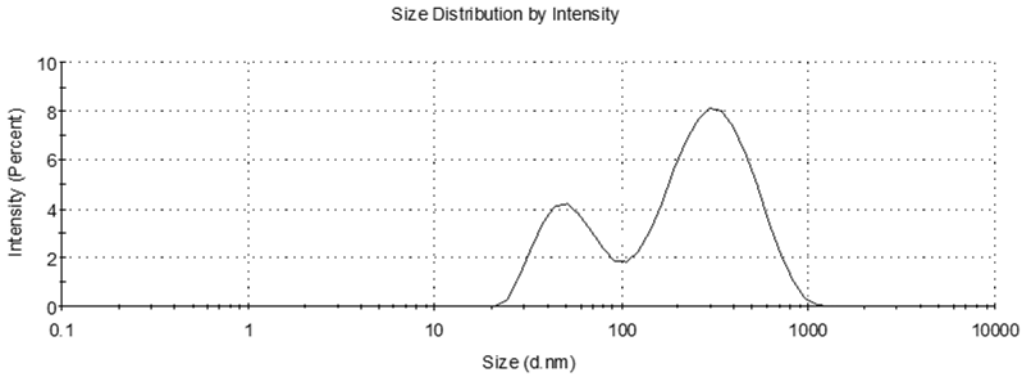

Figure V.2: Size distribution curve obtained for extract loaded DOPC-DOTAP liposomes.

From the plot reported in Figure V.2, the presence of two liposomal systems with different mean diameters is evident: the first at 57 nm, and the second at 335 nm. It can be asserted that the presence of the plant extract leads to a different organization of DOPC and DOTAP lipids during the formation of liposomes. The predominant population of liposomes formed, however, remains that with a larger hydrodynamic diameter compared to empty DOPC-DOTAP systems. The ζ-potential of DOPC-DOTAP liposomes loaded with the plant extract is 119 ± 5 mV. Distribution plot is not reported due to high conductivity of the solution, in these conditions the instrumental apparatus can only measure the single value of potential. The significant increase in surface charge is attributed to the presence of positively charged molecules naturally present in the coffee leaf extract as trigonelline. These chemical species interact with the outer part of the liposomes, increasing the vesicle surface charge. The comparison between the two systems (empty liposomes and those loaded with coffee leaf extract) highlights that DOPC-DOTAP liposomes, after being loaded, undergo a percentage increase in their mean hydrodynamic diameter of 25.33%, while their surface charge undergoes a percentage increase of 59.73%.

Comparing the DLS data of empty DOPC/DOTAP liposomes with DOPC/DOTAP liposomes loaded with chlorogenic acid reveals an increase in the mean hydrodynamic diameter to 134.7 ± 2.2 nm. Figure V.3 illustrates the size distribution curve of DOPC/DOTAP-CGA liposomes. The increase in diameter suggests again, as shown for the extract loaded liposomes, an increase in the system's complexity attributed to interactions between chlorogenic acid and phospholipids.

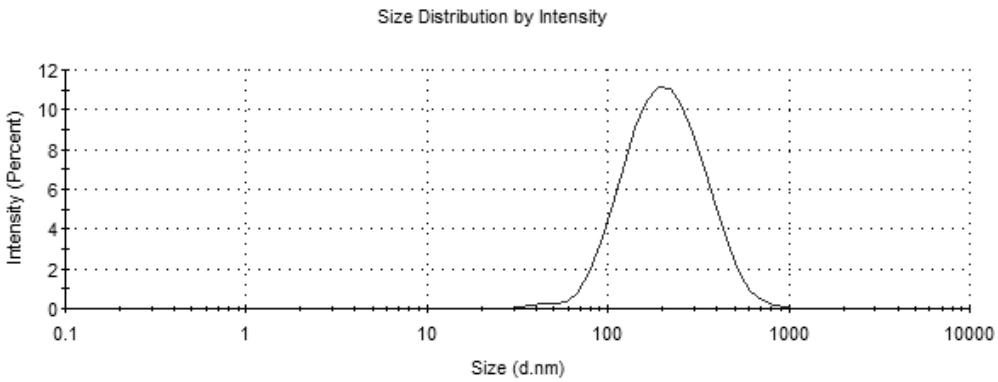

Figure V.3: Size distribution curve obtained for CGA loaded DOPC-DOTAP liposomes.

Following the loading process, the PDI value increased to 0.23, suggesting the presence of monodisperse or poorly polydisperse systems, while the surface charge value decreased to 53.1 ± 2.1 mV as reported in Figure V.4. Both variations, PDI and surface charge, can be attributed to the effects of loading with CGA, as the carboxylic group present in the loaded molecule interacts with the surface charges of the nanosystems, thereby reducing their positive charge.

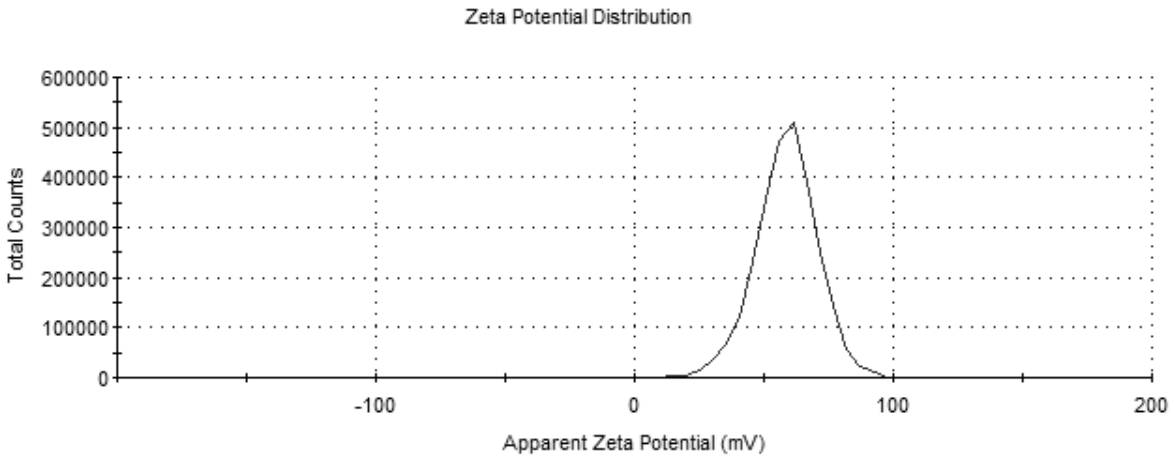

Figure V.4: Zeta potential distribution curve obtained for CGA loaded DOPC-DOTAP liposomes.

V.3.1.2 DOPC-DDAB Liposomes

In this section, the results obtained from the DLS analysis conducted on DOPC-DDAB liposomes are reported (Table V.4).

Table V.4:DLS experiment results for DOPC-DDAB empty and loaded liposomes.

	Avg. diameter ± sd (nm)	**Polydispersity index (PDI)**	**ζ-Potential-± sd (mV)**
DOPC-DDAB	126.8 ± 2.2	0.28	89.4 ± 2.2
DOPC-DDAB + Extract	145.2 ± 1.4	0.48	105 ± 3.0
DOPC-DDAB + CGA	145.7 ± 2.9	0.26	89.4 ± 1.6

The unloaded DOPC-DDAB liposomes exhibit a mean hydrodynamic diameter of 126.8 ± 2.2 nm, as shown in the distribution curve of the mean diameter in Figure V.6. Compared to DOPC-DOTAP liposomes, the difference in the mean hydrodynamic diameter can be explained by analyzing the nature of the liposome components (Fig. V.5). With the incorporation of DDAB, a lipid composed of fully saturated chains is introduced. The spatial arrangement of these chains can influence the canonical formation of liposomes, leading to the creation of liposomal systems with a larger mean hydrodynamic diameter compared to when lipids with monounsaturated chains are used. However, the obtained PDI value demonstrates that the synthesis method employed results in monodisperse systems.

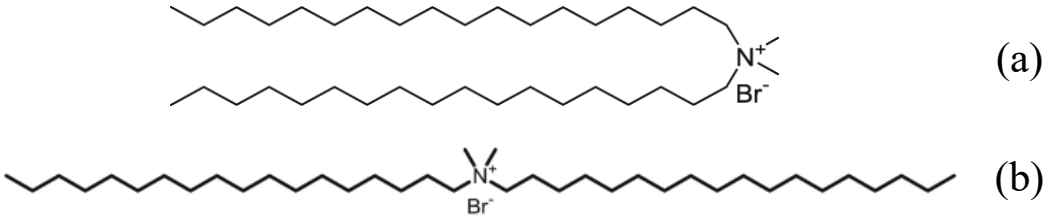

Figure V.5: Structural conformations of DDAB as paired chain (a) or extended chain (b).

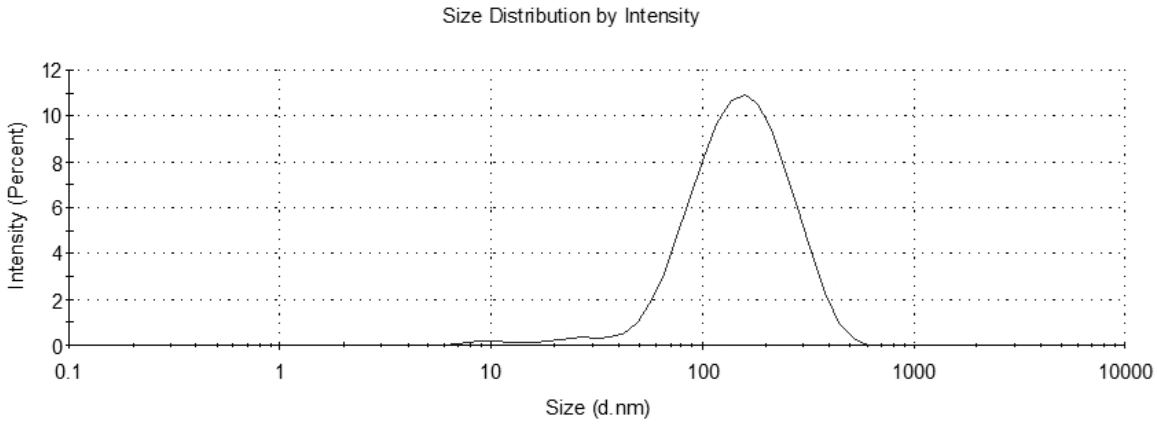

Figure V.6: Size distribution curve obtained for empty DOPC-DDAB liposomes.

The sample of empty DOPC-DDAB liposomes has a ζ-potential of 89.4 ± 2.2 mV. As already observed in DOPC-DOTAP formulation, a strongly cationic system was synthesized. With an increase in positive surface charge of 12.47% respect the empty DOPC-DOTAP liposomes. A comparison between empty and extract-loaded DOPC-DDAB liposomes is possible. The obtained data show that loaded DOPC-DDAB liposomes have a mean hydrodynamic diameter of 145.2 ± 1.4 nm with a PDI value of 0.48 as reported in Figure V.7. Similar to the DOPC-DOTAP systems, in this case as well, loading the extract results in an average increment of liposomal system size, resulting in polydisperse population. DOPC-DDAB liposomes exhibit a behavior analogous to DOPC-DOTAP liposomes; when loaded with plant extracts, these systems undergo an increase in their mean size with a loss of homogeneity in liposomal suspensions.

Figure V.7: Size distribution curve obtained for extract loaded DOPC-DDAB liposomes.

The ζ-potential of DOPC-DDAB liposomes loaded with the plant extract is 105 ± 3 mV. Like DOPC-DOTAP liposomes, there is an analogous behavior; the significant increase in surface

charge is attributed to the presence of positively charged molecules naturally present in the coffee leaf extract. These chemical species interact with the exterior part of the liposomes, resulting in an increase of surface charge. A comparison between loaded and empty DOPC-DDAB systems shows that the mean hydrodynamic diameter undergoes an increase of 12.67%, while similarly, their surface charge experiences a percentage increase of 17.45%.

The formulated DOPC/DDAB liposomes, loaded with chlorogenic acid exhibit a hydrodynamic diameter of 145.7 ± 2.9 nm as reported in Figure V.8.

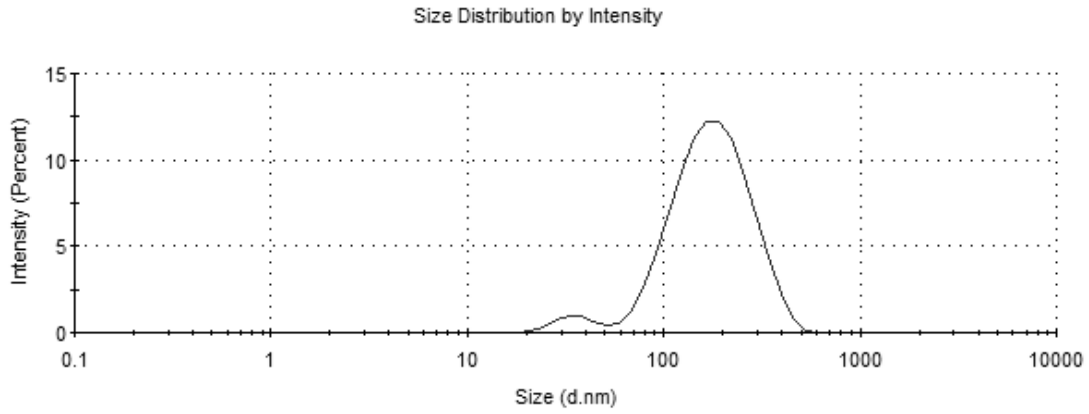

Figure V.8: Size distribution curve obtained for CGA loaded DOPC-DDAB liposomes.

The hydrodynamic diameter of CGA-loaded DOPC/DDAB systems confirms the increment in system complexity as effect of CGA loading, the PDI values close to those of monodisperse systems is observed. The loading of CGA has a different impact on DOPC-DDAB liposomes respectively to the loading of *Coffea arabica* extract. The polydispersity values are increased in comparison to the empty liposomes but the curve that represents the distribution of the average diameter is consistent with the empty liposomes.

Regarding surface charge analysis, empty DOPC/DDAB liposomes loaded with CGA (Fig. V.9) exhibit a value of 61.8 ± 1.6 mV, decreased in comparison to empty liposomes. This trend is similar to liposomes prepared with DOPC-DOTAP and can demonstrate the effective interaction between the liposome system and the loaded CGA molecule.

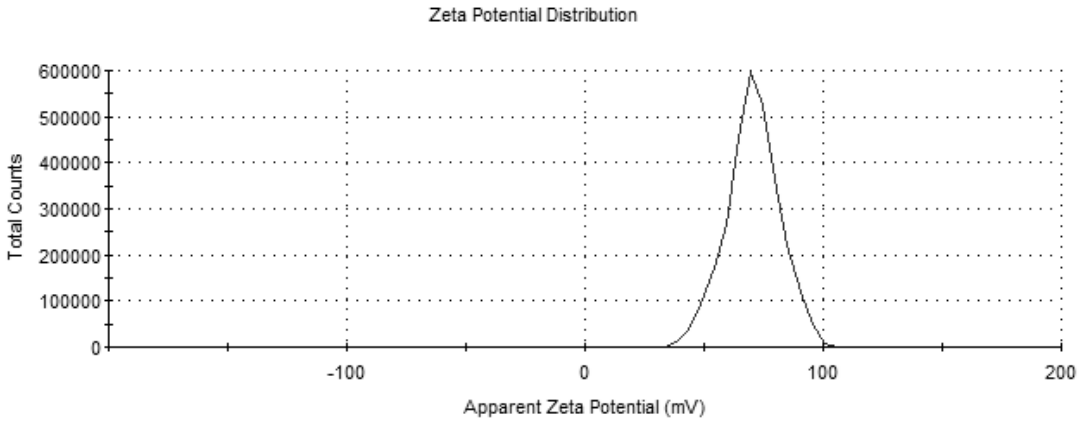

Figure V.9: Zeta potential distribution curve obtained for CGA loaded DOPC-DDAB liposomes.

The presence of populations with different sizes also influences the zeta potential distribution curve, which, nevertheless, presents a highly positive value, consistent with the presence of cationic lipids.

The experimental data suggest that the synthesis of DOPC/DOTAP liposomes occurred, confirming the incorporation of chlorogenic acid and *Coffea* leaves extract into the phospholipid bilayer. The extract, by altering the geometry and interactions of the liposomal systems, allows the formation of larger and more polydisperse vesicles.

DOPC/DDAB liposomes form more polydisperse systems, suggesting the possible formation of large aggregates over time. However, the surface charge confirms CGA's ability to integrate into the phospholipid bilayer, achieving vesicles with lower surface charge. The extract interacts with the vesicles in a similar way of DOPC-DOTAP liposomes, increasing both size and polydispersity index.

In general, it can be observed that the different types of synthesized liposomes respond to the presence of coffee leaf extract and CGA in a similar trend; both systems generally increase in size and increase their PDI after loading process. The surface charge of the systems increases in extract loaded vesicles, the use of chlorogenic acid as loading compound leads to a charge reduction in both lipidic formulations. The increase in ζ-potential is more than three times higher in the DOPC-DOTAP systems than in the DOPC-DDAB systems.

V.3.2 Nuclear Magnetic Resonance ^{1}H NMR

Proton magnetic resonance (^{1}H NMR) allows the monitoring of the correct formation of the synthesized liposomal systems and the subsequent verification of the loading of coffee leaves extract and chlorogenic acid. In the case of amphiphilic molecules forming aggregates, the ^{1}H NMR spectra commonly obtained from the analysis exhibit poor resolution of proton signals, an effect associated with the slow molecular motions of liposomes present in solution. Upon the formation of liposomal systems, the protons of the lipid bilayer experience a higher degree of order, impacting the relaxation time, which, when increased, leads to a loss of signal resolution(Bonechi et al., 2009, 2012). The most interesting information in the study of liposomal systems is obtained by comparing the spectrum of empty liposomal systems with that of systems loaded with coffee leaf extract and the spectrum of the coffee leaves extract itself.
In this section, the ^{1}H NMR spectrum of the extract from *Coffea arabica* leaves is shown (Fig. V.10). The assignment of the proton signals was performed using data available in the literature(Cangeloni et al., 2022).

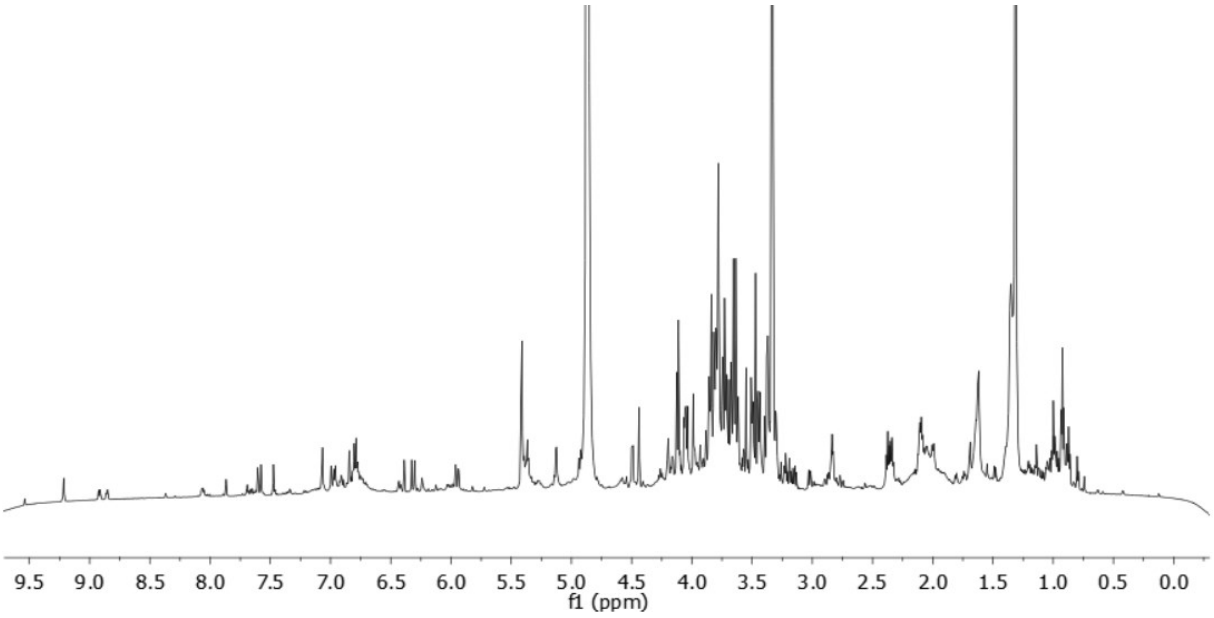

Figure V.10: ^{1}H NMR spectrum of Coffea Arabica extract recorded at 600 MHz and 298K.

To study the encapsulation of chlorogenic acid the ^{1}H NMR spectrum of the pure molecule in deuterated water is reported in Figure V.11 with the peak assignment on the structure reported in Figure V.12(Y. Wang et al., 2011)

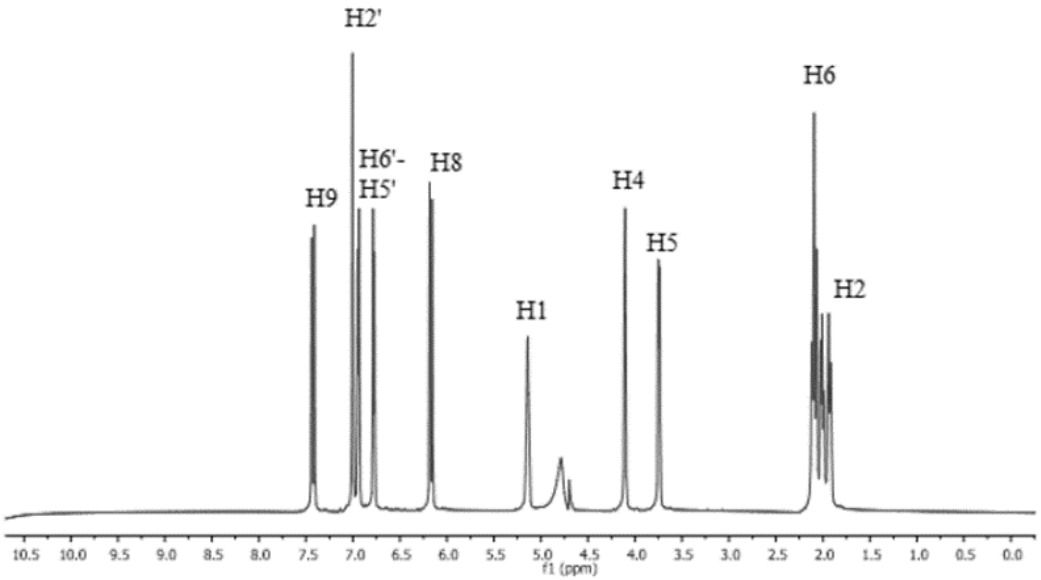

Figure V.11: ^{1}H NMR spectrum of chlorogenic acid recorded at 600 MHz and 298K, the spectrum was acquired using a water presaturation sequence.

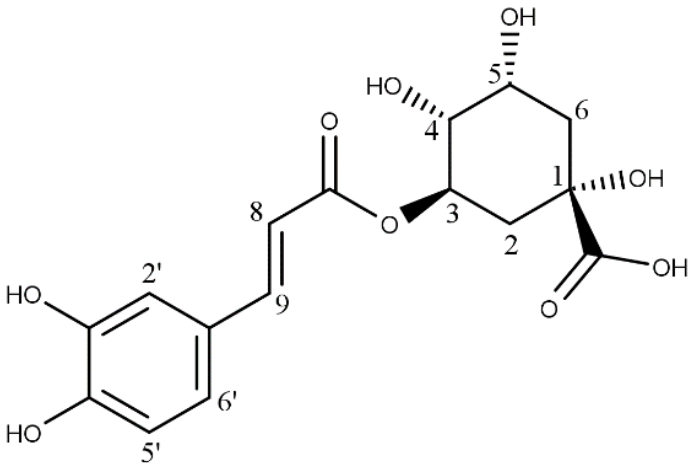

Figure V.12: Structure of chlorogenic acid with assignment of NMR signals.

The proton chemical shift values (ppm) are reported in Table V.5.

Table V.5: Chemical shifts of recorded signals for chlorogenic acid.

Hn	Chemical shift (ppm)
H2	2.02
H6	2.17
H5	3.75
H4	4.10
H1	5.14
H8	6.18
H6’	6.78
H5’	6.95
H2’	7.00
H9	7.49

V.3.2.1 DOPC-DOTAP Liposomes

In Figure V.13 is reported the ^{1}H NMR spectrum of empty DOPC-DOTAP liposomes in D_2O.

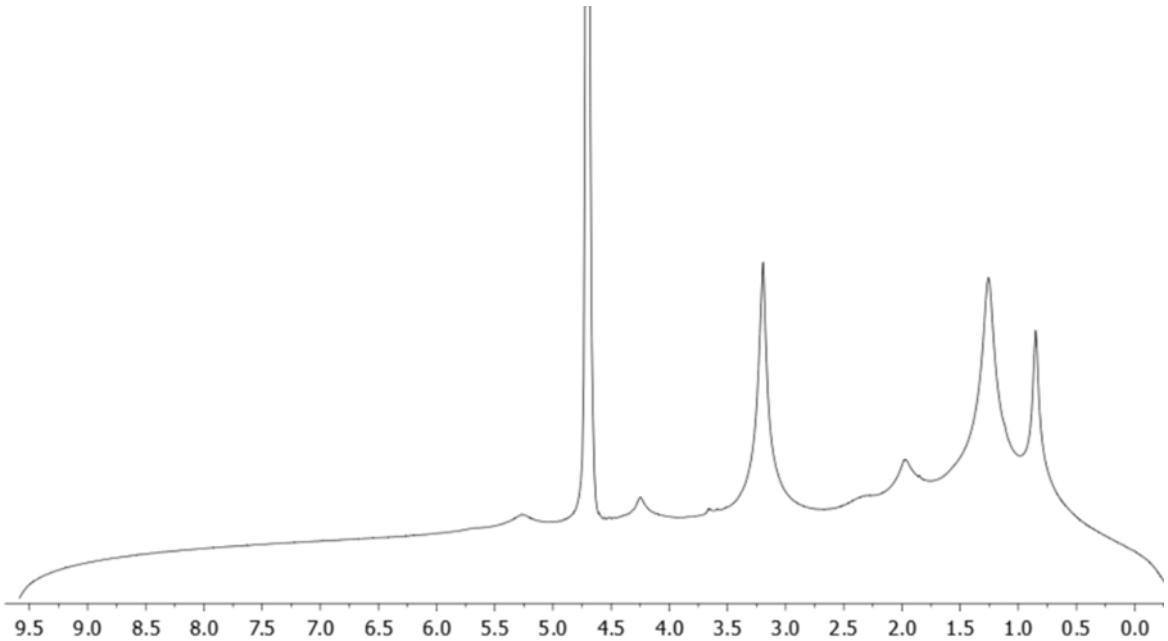

Figure V.13: ^{1}H NMR spectrum of empty DOPC-DOTAP liposomes.

The spectrum reveals the presence of broad peaks with poor resolution of signals, attributed to the formation of liposomal systems. It is also possible to assign the chemical shift values of the protons in the individual lipid structures. The assignment is based on previous data(Troiano et

al., 2015). The assignment of proton peaks is shown in Figure V.14, while the corresponding chemical shift values have been reported in Table V.6. The proton signal at 4.71 ppm is attributed to H_2O.

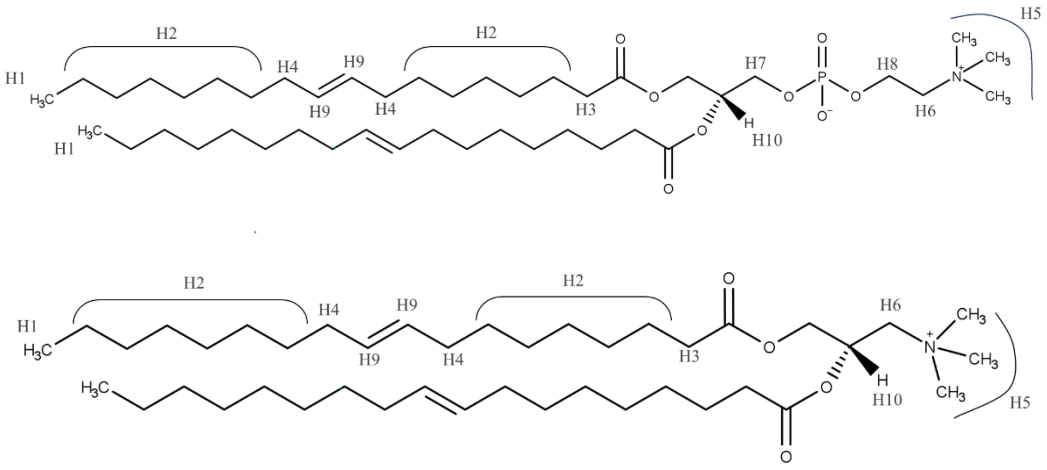

Figure V.14: Structure and assignment of NMR signals for DOPC (a) and DOTAP (b).

Table V.6: Chemical shifts values for DOPC and DOTAP lipids.

Hn	Chemical shift (ppm)
H1	0.85
H2	1.26
H3	2.30
H4	1.97
H5	3.19
H6	3.67
H7, H8	4.25
H9, H10	5.25

Figure V.15 illustrates the overlay of proton spectra of empty DOPC-DOTAP liposomes, loaded DOPC-DOTAP liposomes (after dialysis), and the spectrum of coffee leaf extract. This overlay allows the analysis of conformational changes in the liposomal system following the loading of the extract.

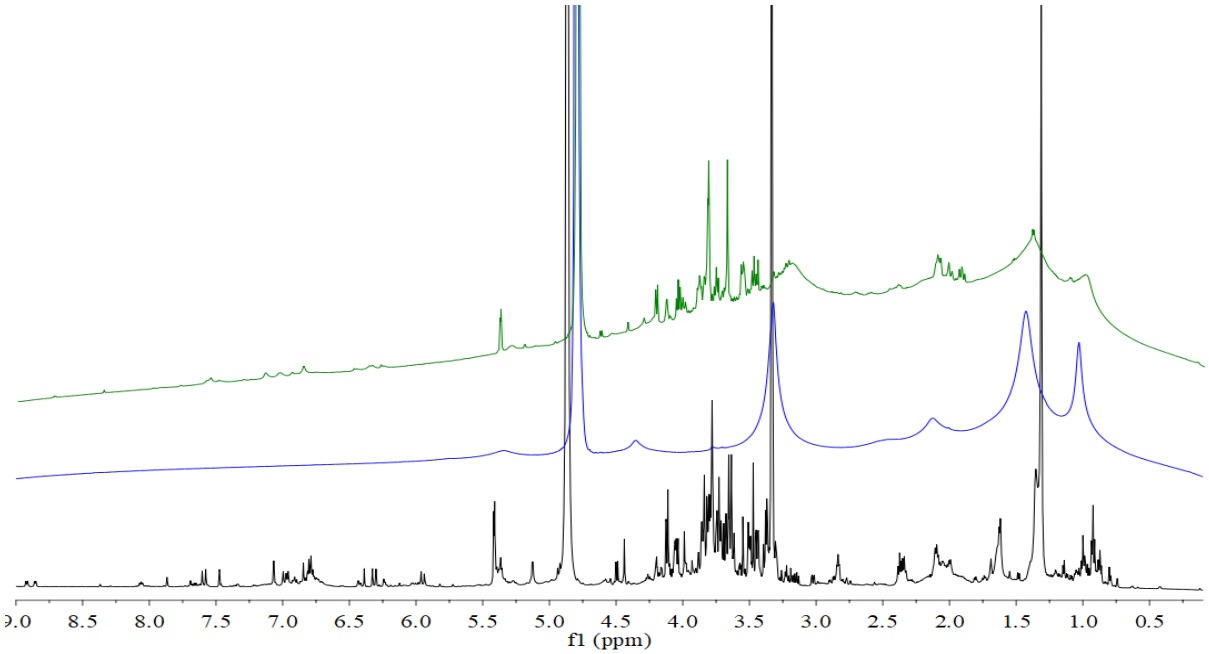

Figure V.15: Stacked ^{1}H NMR spectra for coffee leaves extract (black), empty DOPC-DOTAP liposomes (blue), extract loaded DOPC-DOTAP liposomes (green).

The comparison between the proton spectra of empty and loaded DOPC-DOTAP liposomes highlights the presence of vesicles with sizes exceeding 100 nm in both systems. The proton signals of the phospholipid molecules appear broad and weakly resolved. In the spectrum of DOPC-DOTAP liposomes containing leaves extract, proton signals attributable to the various components present in the extract itself are also evident. Dialysis of the loaded DOPC-DOTAP systems allowed the removal of the excess plant extract. After this process, it can be stated that the proton signals attributable to the extract's components serve as evidence of the successful incorporation of the active ingredients into the vesicles.

In the range of 3.3-4.2 ppm (Fig. V.16), the signals attributed to saccharides don't result in significant changes of their shape and resolution. The behavior of saccharides is ascribed to the different physicochemical properties of the two systems (liposomes and saccharides). Saccharides, being hydrophilic molecules, tend to interact more with the external environment of the liposome than with the phospholipid bilayer. Saccharides are generally associated with the polyphenolic component to which they are linked by glycosidic bonds. The signal intensity suggests their abundant presence inside the extract, a fact confirmed by the high number of glycosylated derivatives found in hydroalcoholic extracts of plant matrices. The signals at 2.37 and 4.47 ppm attributed to malic acid and trigonelline (singlet), respectively, show clear broadening, suggesting a strong interaction with the phospholipid system. Trigonelline is a

zwitterionic molecule, and its encapsulation in vesicles is consistent with an increase in surface charge.

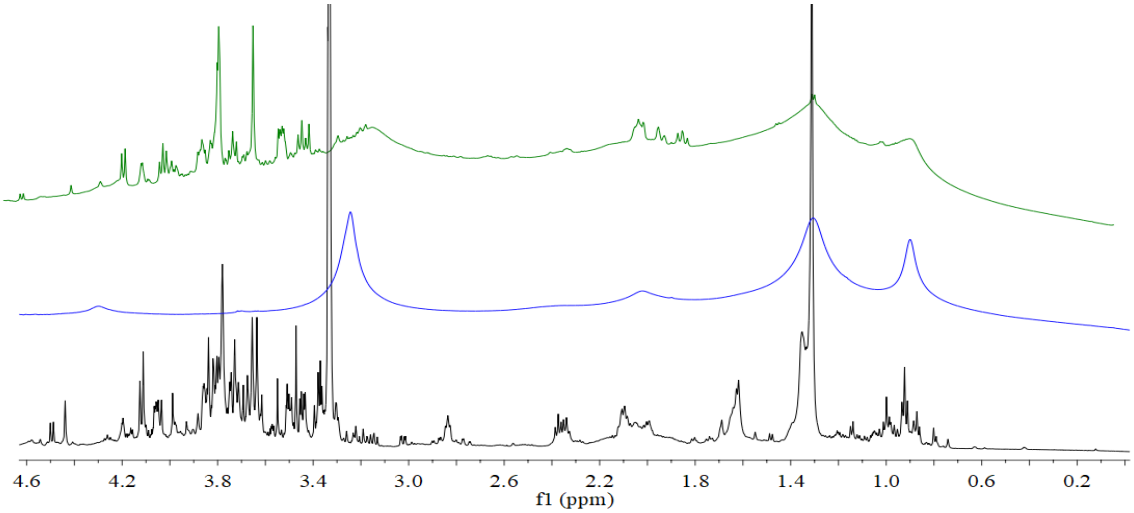

Figure V.16: Stacked ^{1}H NMR spectra for coffee leaves extract (black), empty DOPC-DOTAP liposomes (blue), extract loaded DOPC-DOTAP liposomes (green) in the range 0.0 - 4.6 ppm.

In the range of 5.0 - 7.5 ppm, reported in Figure V17, peaks attributed to chlorogenic acids and polyphenols (mainly rutin and mangiferin) are present, showing strong interactions with the phospholipids of the bilayer. The proton signal at 7.87 ppm (indicative of the presence of caffeine) also exhibits clear broadening of the signal, a loss of intensity, and a shift, suggesting a strong interaction with the phospholipid system.

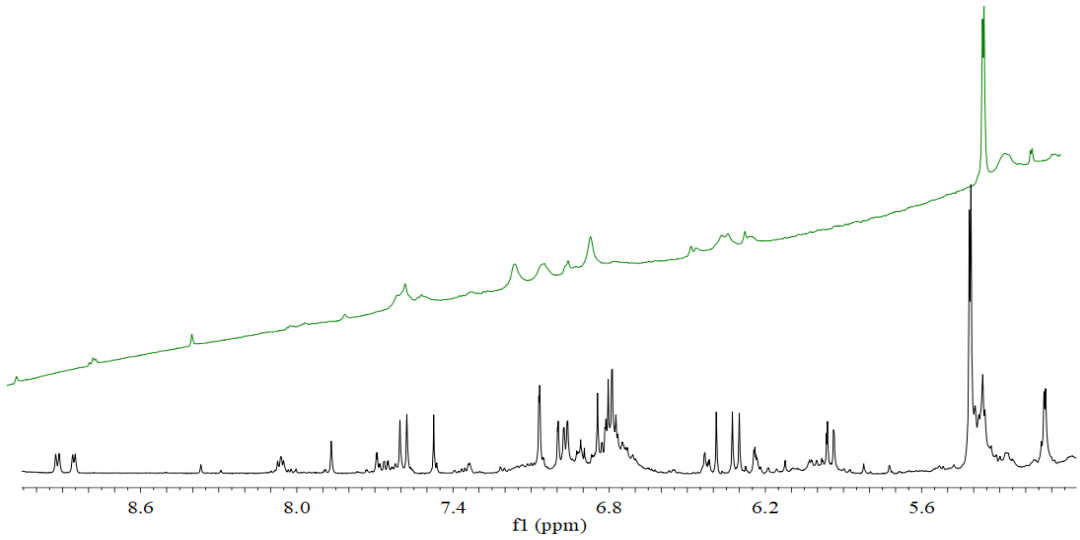

Figure V.17: Stacked ^{1}H NMR spectra for coffee leaves extract (black) and, extract loaded DOPC-DOTAP liposomes (green) in the range 5.0 - 9.0 ppm.

From the analysis of the ^{1}H NMR spectra of DOPC-DOTAP and DOPC-DOTAP liposomes with coffee leaf extracts, it can be observed that there is an actual interaction between the liposomal system and the contents of the plant extract. Specifically, polyphenols, chlorogenic acids, trigonelline, and caffeine are the molecules that can be easily identified, suggesting a specific interaction with the lipophilic environment of the vesicles.

In Figure V.18, the overlay of three proton spectra is presented: chlorogenic acid, empty DOPC/DOTAP liposomes, and CGA-loaded DOPC/DOTAP liposomes.

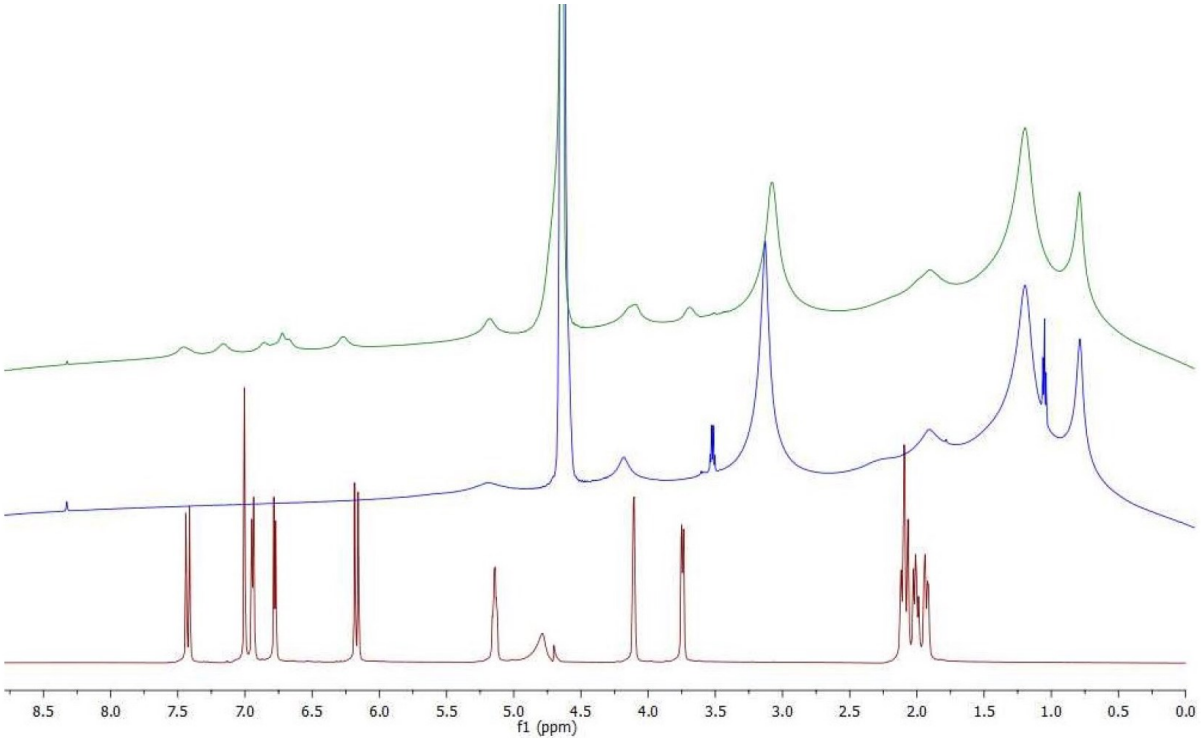

Figure V.18: Stacked ^{1}H NMR spectra for chlorogenic acid in D_2O (red), empty DOPC-DOTAP liposomes (blue), CGA loaded DOPC-DOTAP liposomes (green).

Both NMR spectra of empty and CGA-loaded DOPC/DOTAP liposomes exhibit low signal resolution, typical in the case of macromolecules or aggregates. However, it is possible to identify and assign various signals from phospholipids. In the case of empty liposomes, no detectable signals are present in the aromatic region (6-8 ppm), whereas in the CGA-loaded liposomes, signals attributable to chlorogenic acid can be observed in that region.

In the proton spectra of liposomes containing CGA, the proton signals related to chlorogenic acid are evident at lower fields with broad and poorly resolved signals, suggesting interaction with the phospholipid molecules constituting the phospholipid bilayer. From the comparison made between the spectra of empty DOPC/DOTAP liposomes and those loaded with chlorogenic acid, the presence of peaks derived from chlorogenic acid is evident. Specifically,

the proton signals H8, H6', H5', H2', and H9 of chlorogenic acid are present in the liposomal structure (Fig. V.18).

V.3.2.2 DOPC-DDAB Liposomes

Below is the ^{1}H NMR spectrum of empty DOPC-DDAB liposomes in D_2O (Fig. V.19).

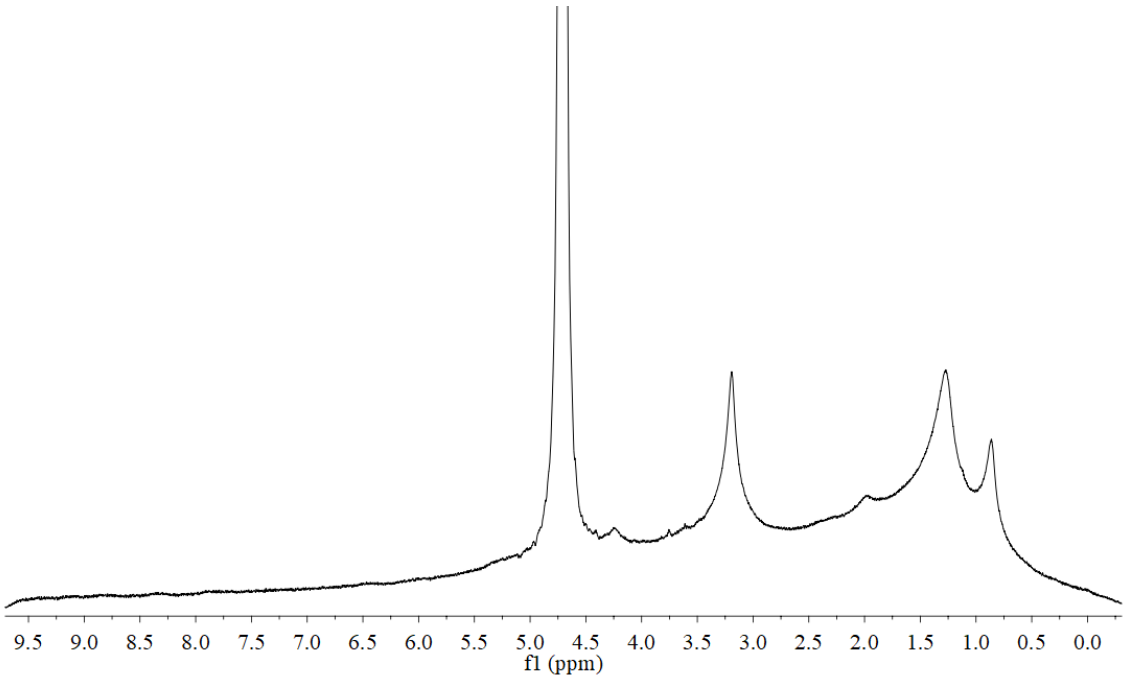

Figure V.19: ^{1}H NMR spectrum of empty DOPC-DDAB liposomes in D_2O.

As already observed for empty DOPC-DOTAP systems, in this case as well, the presence of broad and weakly resolved peaks is evident in the ^{1}H NMR spectrum, attributable to the correct formation of liposomal systems. The assignment of the chemical shift values of the protons to their respective positions in the lipid structure is based on data collected in previous studies (Bonechi et al., 2009).

The assignment of proton peaks is shown in Figure V.20, and the corresponding chemical shift values are reported in Table V.7.

Table V.7: Assignment of chemical shifts values for NMR signals of DOPC-DDAB liposomes.

Hn	Chemical shift (ppm)
H1	0.84
H2	1.24
H3’	1.97
H4	3.19
H5	3.75
H6	4.24

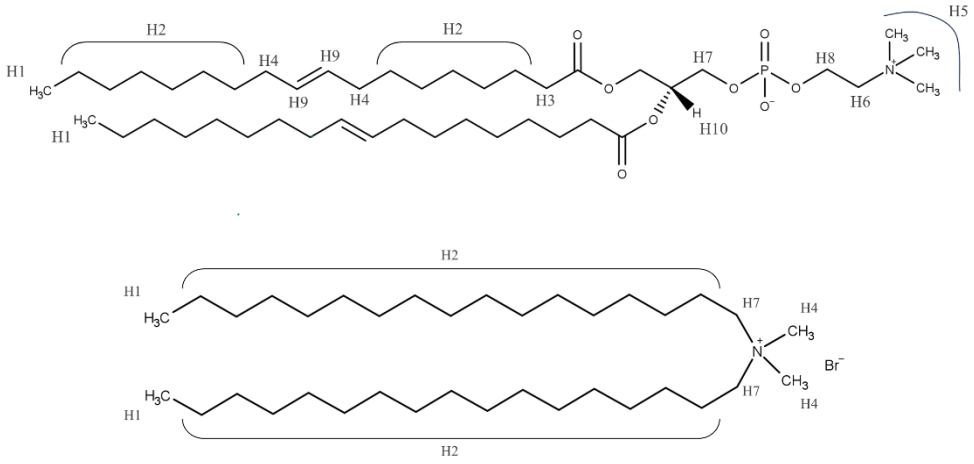

Figure V.20: Structure and assignment of NMR signals for DOPC (a) and DDAB (b).

The DOPC-DOTAP and DOPC-DDAB systems exhibit very similar behavior, both when they are empty and when loaded with the extract. The overlap of the proton spectra of empty DOPC-DDAB liposomes, DOPC-DDAB liposomes loaded (after dialysis), and the spectrum of the coffee leaf extract is shown in Figure V.21. This allows for the analysis of conformational variations in the liposomal system following the loading of the extract.

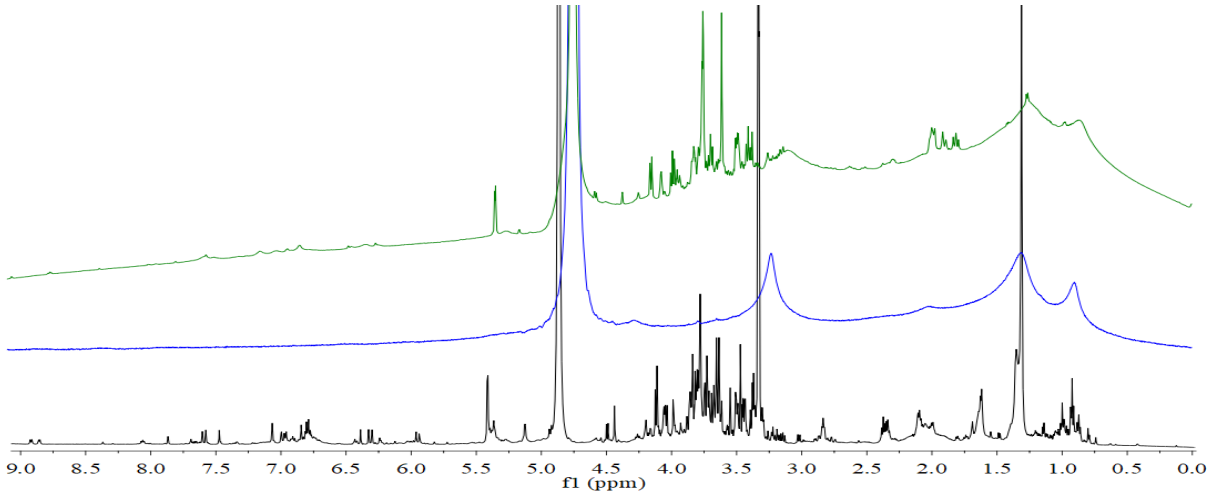

Figure V.21: Stacked ^{1}H NMR spectra for coffee leaves extract (black), empty DOPC-DDAB liposomes (blue), extract loaded DOPC-DDAB liposomes (green).

The discussion of the DOPC-DOTAP systems is fully consistent with the DOPC-DDAB systems. In the spectrum of the loaded liposomes subjected to dialysis, proton signals attributable to various components of the extract can be recognized, confirming the incorporation of active principles into the vesicles. In the range of 0.00 to 5.50 ppm shown in Figure V.22, the peaks assigned to trigonelline and malic acid show a broadening of signals in the liposome loaded with the extract, suggesting a strong interaction with the phospholipid system. Similarly to DOPC-DOTAP liposomes, the peaks assigned to the saccharide group show very little variation. As with DOPC-DOTAP, the encapsulation of trigonelline in the vesicles is consistent with an increase in surface charge.

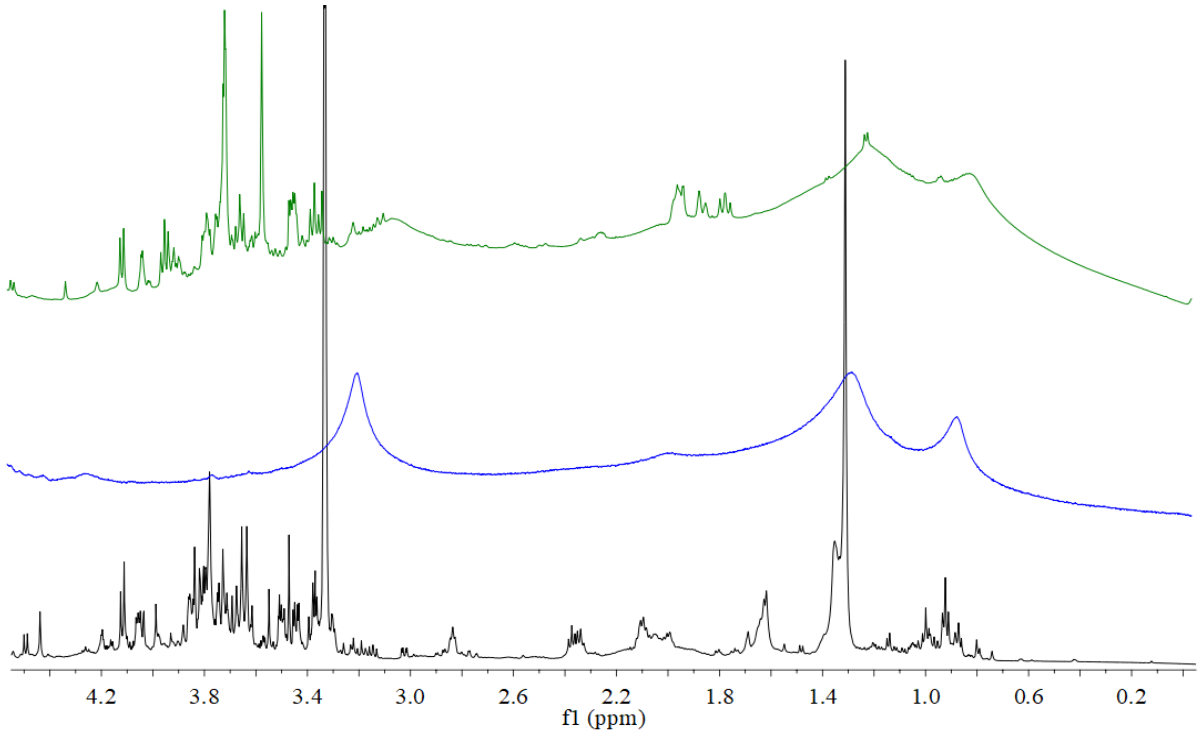

Figure V.22: Stacked ^{1}H NMR spectra for coffee leaves extract (black), empty DOPC-DDAB liposomes (blue), extract loaded DOPC-DDAB liposomes (green) in the range 0.0 - 4.5 ppm.

Even the region of aromatic systems (Fig. V.23) aligns with the analysis previously conducted for DOPC-DOTAP systems. Peaks assigned to chlorogenic acids, polyphenols (rutin and mangiferin), and caffeine exhibit strong interactions with the phospholipids of the bilayer.

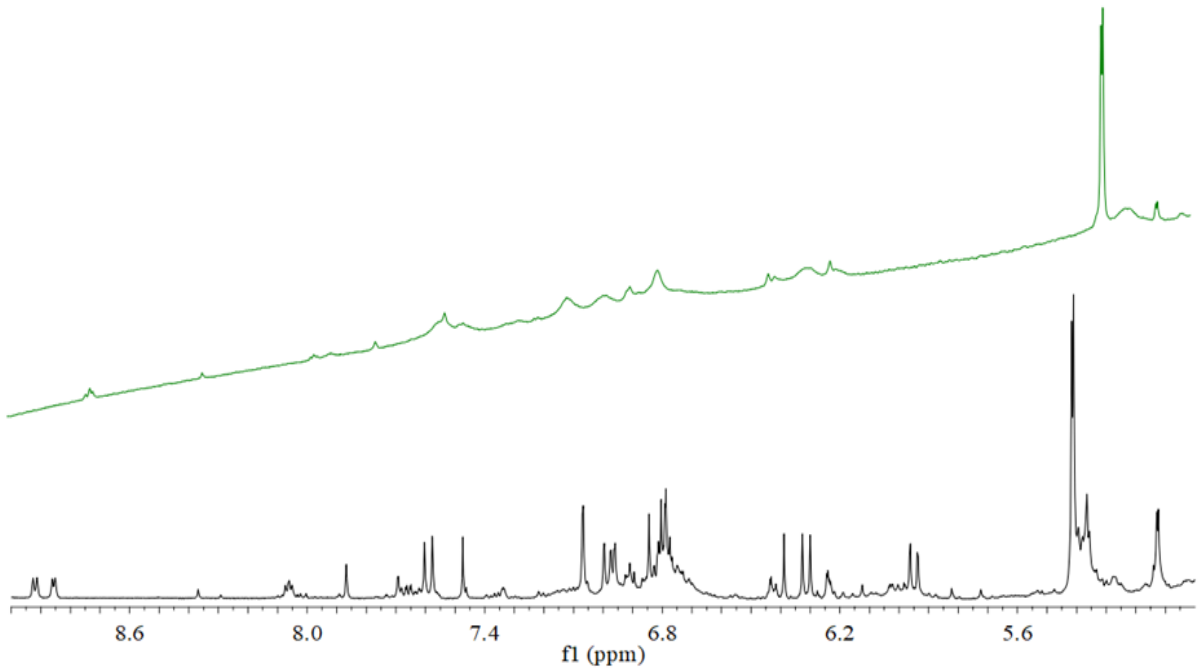

Figure V.23: Stacked 1H NMR spectra for coffee leaves extract (black) and extract loaded DOPC-DDAB liposomes (green) in the range 5.5 - 9.5 ppm.

The ^{1}H NMR analysis of DOPC-DOTAP and DOPC-DDAB liposomes has revealed a strong interaction between certain molecules from the extract and the liposomes. It is also possible to affirm that this study has not detected differences in the behavior of the two different systems. Both liposomes, therefore, prove to be effective in encapsulating molecules belonging to the coffee leaf extract, such as trigonelline, malic acid, chlorogenic acids, caffeine, and polyphenols (mangiferin and rutin).

Regarding the formulation of liposomes enriched with chlorogenic acid, the verification of successful encapsulation and the significance of the dialysis process is crucial when considering the distinct shape of the signals corresponding to chlorogenic acid in the spectra of DOPC/DDAB-CGA liposomes before and after dialysis, as depicted in Figure V.24.

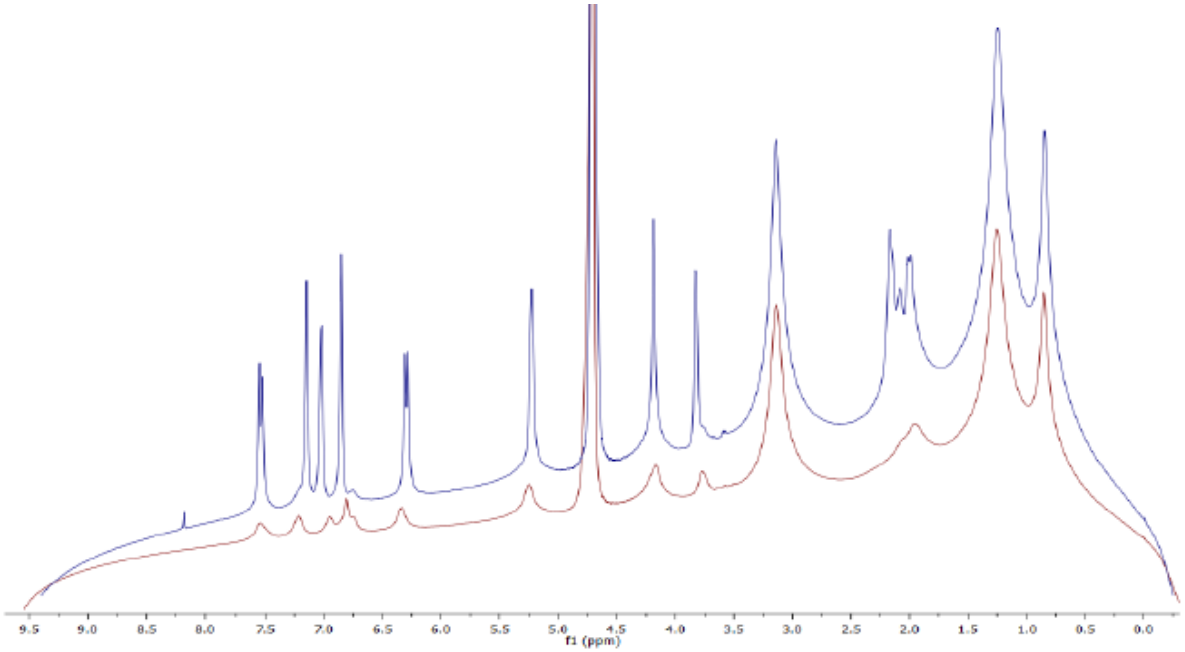

Figure V.24: Overlay of ^{1}H NMR spectra of DOPC-DDAB liposomes loaded with chlorogenic acid before (in blue) and after (in red) the dialysis process.

In the spectrum shown in blue, which corresponds to non-dialyzed liposomes, it is possible to observe that the signals of chlorogenic acid are narrow and well-resolved compared to the signals of phospholipids. This characteristic confirms the presence of chlorogenic acid as a free molecule in solution. After the dialysis process, the signals take on the characteristics of the encapsulated system, and become broader and much less intense. This change is attributed to the removal of non-encapsulated chlorogenic acid and confirm that the dialysis process is optimal for the purification of the liposomes themselves.

The NMR spectra of liposomes formed by empty DOPC/DDAB and DOPC/DDAB-CGA phospholipids exhibit a very similar NMR spectrum to the systems of empty DOPC/DOTAP

and DOPC/DOTAP-CGA described earlier. As in DOPC/DOTAP-CGA, the spectra of DOPC/DDAB-CGA also feature signals attributed to chlorogenic acid. Figure V.25 depicts the overlay of the proton spectra of empty and CGA-loaded DOPC/DDAB liposomes.

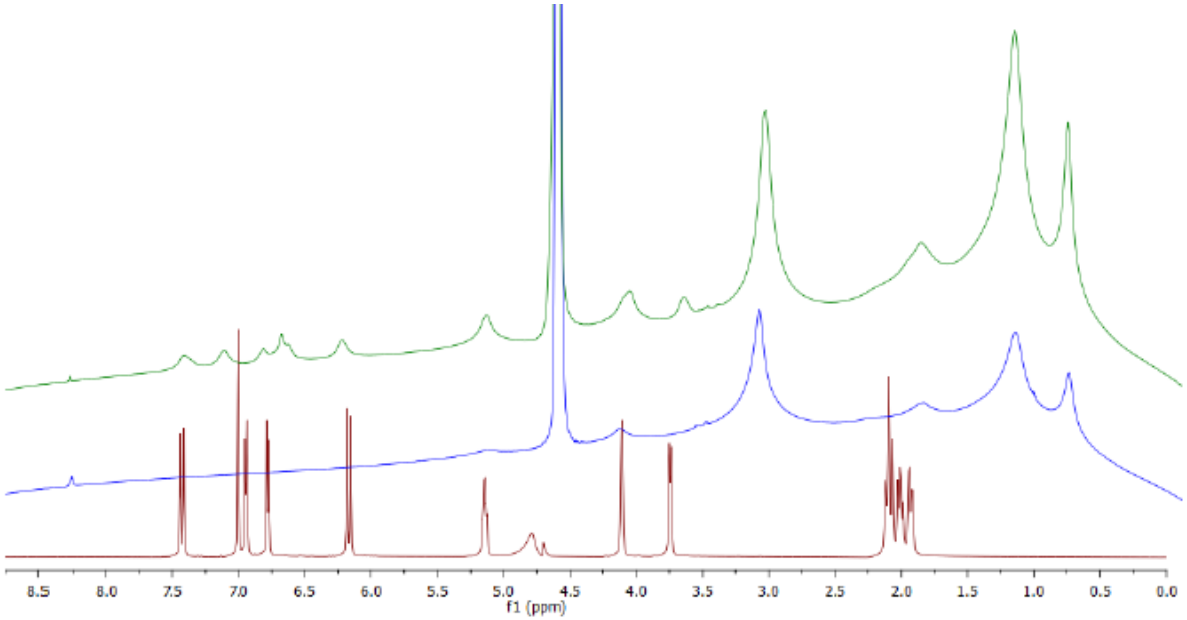

Figure V.25: Stacked ^{1}H NMR spectra for chlorogenic acid in D_2O (red), empty DOPC-DDAB liposomes (blue), CGA loaded DOPC-DDAB liposomes (green).

From the overlay of the three spectra in Figure V.25, it is also evident that the spectra of empty and CGA-loaded DOPC/DDAB liposomes show poor signal resolution. In the case of CGA-loaded liposomes, in the aromatic region (6-8 ppm), signals attributable to chlorogenic acid are observed. Also in this case the shape of the signals at lower fields, generated by the protons of chlorogenic acid, appears broad and of weak intensity, which is consistent with the hypothesis of successful encapsulation. Another important effect could be observed in signals with no multiplicity and shifted after the encapsulation.

V.3.3 Encapsulation efficiency (EE)

With the HPLC-MS analysis, it is possible to obtain the encapsulation efficiency, which measures the liposomes' ability to encapsulate compounds from the plant extract. Quantitative analyses were conducted with a focus on the molecules most abundant in the extract. Compounds belonging to the polyphenols category were expressed as mangiferin equivalents, given the use of mangiferin as the standard for compound quantification.
The encapsulation efficiency values are reported as a percentage in Table V.8, and the retention times associated with each compound coincide with the times indicated in the qualitative analysis.

Table V.8: Encapsulation efficiency for coffee leaves extract in DOPC-DOTAP and DOPC-DDAB liposomes.

Compound	Rt (min)	EE% DOPC-DOTAP	EE% DOPC-DDAB
Chlorogenic acid	7.69	21,61%	19,45%
Catechin/Epicatechin	10.38	13,52%	11,89%
Procyanidin B	11.22	8,11%	8,76%
Isomangiferin	11.63	18,16%	15,80%
Mangiferin	12.42	21,92%	23,82%
Procyanidin A trimer	16.19	10,78%	11,64%
Rutin glycoside	19.89	13,77%	15,01%
Quercetin glycoside	20.59	15,58%	16,20%
Rutin	23.35	13,60%	12,11%
Kaempferol-3-O-rhamno glucoside	25.50	12,96%	13,22%
Trigonelline	28.52	27,44%	25,81%
Caffeine	1.11	16,13%	18,52%

The collected data reveal that the percentages range from 8.11% to 27.44% for DOPC-DOTAP liposomes, while for DOPC-DDAB, the range is from 8.76% to 25.81%. Trigonelline is the substance that shows better encapsulation efficiency for both liposomes (EE% > 25%), consistent with the increased surface charge density recorded in the DLS analyses. On the other hand, procyanidin B appears to have the lowest encapsulation efficiency, and a hypothesis for the low encapsulation rate could be correlated with the physical characteristics of the molecule itself (high molecular weight). DOPC-DOTAP liposomes exhibit an EE% greater than 20% for 5-CGA, mangiferin, and trigonelline.

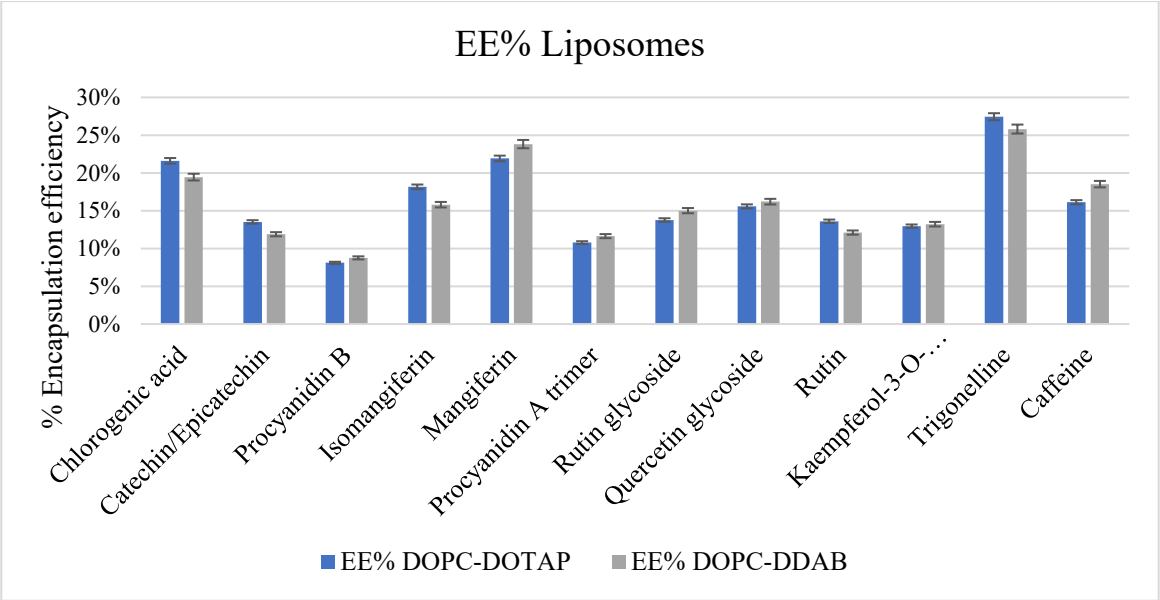

Figure V.26: Encapsulation efficiency for coffee leaves extract in DOPC-DOTAP and DOPC-DDAB liposomes.

Both DOPC-DOTAP and DOPC-DDAB show an average encapsulation efficiency (EE%) for the polyphenol group of 14.27%, while the average EE% for alkaloids prefer DOPC-DDAB liposomes (22.16%) over DOPC-DOTAP (21.79%). The greater difference in encapsulation is observed in caffeine, where DOPC-DDAB liposomes have a 2.39% better EE% compared to DOPC-DOTAP. In terms of absolute quantities (Tab. V.9), DOPC-DOTAP liposomes exhibit a higher encapsulation capacity than DOPC-DDAB.

Table V.9: Total concentrations of encapsulated compound classes in DOPC-DOTAP and DOPC-DDAB liposomes.

Compound class	EE mg/mL DOPC-DOTAP	EE mg/mL DOPC-DDAB
Chlorogenic acid	3.52	3.16
Xhantones	7.55	7.19
Polyphenols	1.09	1.16
Alkaloids	2.51	2.62
TOTAL	**13.57**	**12.98**

The DOPC-DOTAP liposomes appear to be more efficient concerning chlorogenic acid and xanthones, while the DOPC-DDAB liposomes respond better to the classes of polyphenols and alkaloids.

The chlorogenic acid content was calculated using a standard calibration curve(Feng et al., 2016) (Fig. V.29) obtained by recording absorbances at a wavelength λ = 330 nm through a

UV-Visible spectrophotometer. Chlorogenic acid standards were prepared using methanol (CH_3OH) and undergoing appropriate dilutions within a concentration range from 1 to 10 mg/L.

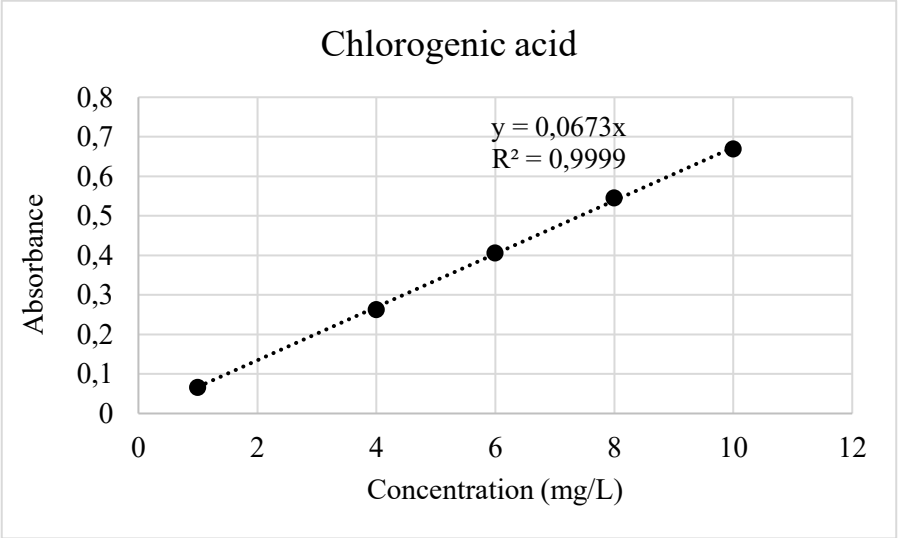

Figure V.27: Calibration curve for chlorogenic acid using UV spectroscopy at 330nm.

Figure V.27 reports the calibration curve obtained from successive dilutions of a standard solution of chlorogenic acid, with the equation Y=0.0673x and an R^2 value of 0.99995. The encapsulation efficiency (EE%) reported in Table V.10 was calculated by considering the amount of substance present in the liposomes after the purification step relative to the initial amount of substance in the liposome synthesis.

Table V.10: Encapsulation efficiency for chlorogenic acid in DOPC.DOTAP and DOPC-DDAB liposomes.

Liposomes	CGA concentration post-dialysis (mg/mL)	CGA start concentration (mg/mL)	Encapsulation Efficiency (EE%)
DOPC/DOTAP CGA	1.36	6.00	22.60%
DOPC DDAB CGA	0.98	6.00	16.26%

From the results, it is noticeable that DOPC/DDAB liposomes exhibit a lower encapsulation efficiency (EE%) compared to DOPC/DOTAP, suggesting that the latter is more effective in encapsulating chlorogenic acid due to its structural characteristics.

Based on the experiments performed in this work with the two liposomal systems, it can be confirmed that the liposomes with the best chemical properties for encapsulating chlorogenic acid are the DOPC/DOTAP systems. Comparing the DLS results, it is evident that DOPC/DOTAP liposomes have a mean size in line with the extrusion process and low PDI

values, indicating the presence of a predominantly monodisperse and thus stable system. For DOPC/DDAB, there is a general stabilization effect due to chlorogenic acid loading, leading to a decrease in surface charge. In addition, increased polydispersity index values are observed for unloaded liposomes, indicating a lower stability of the liposomal systems. The analysis of the NMR spectra and the value of the EE% confirm that the encapsulation process with chlorogenic acid was successfully.

V.4 Conclusions

In this chapter, two different liposome formulations (DOPC-DOTAP and DOPC-DDAB) were synthesized and loaded with *Coffea arabica* leaf extract and chlorogenic acid. The synthesis was based on lipid film formation, rehydration, and subsequent extrusion, obtaining both empty and loaded liposomes (passive loading). The synthesis and loading were confirmed for both formulations by Dynamic Light Scattering (DLS) and ^{1}H Nuclear Magnetic Resonance (NMR) analyses. In particular, nuclear magnetic resonance analyses highlighted the encapsulation of the plant extract and chlorogenic acid in liposomes, which, to avoid interferences, were purified through dialysis with deuterated water.

The encapsulation of the main components of the extract was quantified through High Performance Liquid Chromatography with MS detector (HPLC-MS) analysis, allowing a comparison of the different loading capacities of DOPC-DOTAP and DOPC-DDAB liposomes. Encapsulation of CGA was evaluated using UV-Vis spectroscopy for its speed and simpler set up. Dynamic light scattering results comparing mean hydrodynamic diameter, polydispersity index, and surface charge measurements, show that DOPC-DOTAP liposomes have slightly better properties than DOPC-DDAB liposomes and are therefore more suitable for loading with the desired substances. Loading with *Coffea arabica* leaf extract, given the chemical complexity of the extract, influences both liposomes in the same way, significantly increasing the measured surface charge values.

^{1}H-NMR analyses confirm the encapsulation of the substances of interest in both liposomes, specifically chlorogenic acids, xanthones (mangiferin and isomangiferin), and various flavonoids. At the same time, the interaction of alkaloids such as trigonelline, likely responsible for the increase in surface charge of the systems, has been highlighted.

The data provided by HPLC-MS analyses demonstrate the ability of both systems to encapsulate the substances of interest, with encapsulation efficiency percentages ranging from 8.11% to 27.44%. The higher absolute encapsulation efficiency was attributed to DOPC-DOTAP liposomes, particularly regarding chlorogenic acid and xanthone classes.

In conclusion, DOPC-DOTAP liposomes generally exhibit better properties than DOPC-DDAB liposomes for use as encapsulation systems. Plant extracts, on the other hand, are difficult to encapsulate, making liposomes complex systems that are difficult to manage, as there is a clear alteration of the physicochemical properties of both proposed formulations.

Chapter VI

Conclusions

Plant matrices containing important secondary metabolites (flavonoids, glycoalkaloids, iminosugars and chlorogenic acids) were studied and selected during the present thesis work. The study of these matrices focused on three fundamental phases: the first phase of extraction, the separation of molecules, and their subsequent characterization and quantification. The last chapter focused on the drug delivery of molecules extracted from the previously analyzed matrices. The study of the matrices was based on chromatographic separation techniques coupled with mass detector, capable of conducting quantitative (SIM, SRM) and qualitative studies through data dependent approaches. Chapter II reports the study of an important plant matrix such as coffee leaves. Leaves of *Coffea arabica* represent a significant food alternative to tea leaves for preparing infusions. By combining chromatographic approaches (HPLC-MS) with NMR spectroscopy, it was possible to characterize this matrix rich in nutraceutical compounds. Chapter III presents a study on the extraction of an important compound, 1-deoxynojirimycin, from the leaves of *Morus alba* and *nigra*. The extraction of this crucial compound was optimised using Experimental Design methods. To quantify 1-deoxynojirimycin in this matrix, a chromatographic HILIC method, coupled with a mass detector in SRM mode was developed. The optimization process led to the identification of significant extraction parameters, defining a set of optimal values.

Chapter IV focused on the development of a chromatographic method for quantifying glycoalkaloids in matrices of various plants belonging to the *Solanaceae* family. The recovery of these molecules from matrices usually discarded represents a significant resource from the perspective of the circular economy. The plant matrices under examination are waste generally intended to be buried in the fields or used in biomass processes. By using an internal standard produced from plants belonging to another genus (*Liliaceae*), it is possible to develop a method useful for quantifying glycoalkaloids present in the solanaceous family. The main compounds were separated and quantified in SIM mode using a mass spectrometer coupled with a reverse-phase chromatography system.

The fifth and final chapter concerns the synthesis and passive loading of lipid and liposomal nanoparticles. Cationic liposomes were synthesized in two distinct formulations and subsequently loaded with an extract of coffee leaves previously analyzed in Chapter II and with chlorogenic acid, one of the major components of the extract. The synthesized particles were characterized using physicochemical techniques to investigate their size and surface charge modifications through Dynamic Light Scattering techniques. Through NMR spectroscopy, it was then possible to verify the loading process by modifying the measured signals.

Encapsulation efficiency quantification was carried out using HPLC-MS for the extract, while UV spectroscopy was used for chlorogenic acid.

References

Abu Bakar Siddique, M., & Brunton, N. (2019). Food Glycoalkaloids: Distribution, Structure, Cytotoxicity, Extraction, and Biological Activity. In *Alkaloids - Their Importance in Nature and Human Life*. IntechOpen. https://doi.org/10.5772/intechopen.82780

Akbarzadeh, A., Rezaei-Sadabady, R., Davaran, S., Joo, S. W., Zarghami, N., Hanifehpour, Y., Samiei, M., Kouhi, M., & Nejati-Koshki, K. (2013). Liposome: Classification, preparation, and applications. *Nanoscale Research Letters*, *8*(1). https://doi.org/10.1186/1556-276X-8-102

Alañón, M. E., Palomo, I., Rodríguez, L., Fuentes, E., Arráez-Román, D., & Segura-Carretero, A. (2019). Antiplatelet activity of natural bioactive extracts from mango (Mangifera indica l.) and its by-products. *Antioxidants*, *8*(11). https://doi.org/10.3390/antiox8110517

Angeloni, S., Navarini, L., Khamitova, G., Sagratini, G., Vittori, S., & Caprioli, G. (2020). Quantification of lignans in 30 ground coffee samples and evaluation of theirs extraction yield in espresso coffee by HPLC-MS/MS triple quadrupole. *International Journal of Food Sciences and Nutrition*, *71*(2), 193–200. https://doi.org/10.1080/09637486.2019.1624693

Araujo, P. (2009). Key aspects of analytical method validation and linearity evaluation. *Journal of Chromatography B: Analytical Technologies in the Biomedical and Life Sciences*, *877*(23), 2224–2234. https://doi.org/10.1016/j.jchromb.2008.09.030

Barreto, J. A. C. B., Revisan, M. A. T. S. T., Ull, W. I. E. H., Piegelhalder, B. E. S., & Wen, R. O. W. O. (2008). Characterization and Quantitation of Polyphenolic Compounds in Bark, Kernel, Leaves, and Peel of Mango (Mangifera indica L_) - Journal of Agricultural and Food Chemistry (ACS Publications). *Journal Agricultural and Food Chemistry*, 5599–5610.

Bianco, G., Schmitt-Kopplin, P., De Benedetto, G., Kettrup, A., & Cataldi, T. R. I. (2002). Determination of glycoalkaloids and relative aglycones by nonaqueous capillary electrophoresis coupled with electrospray ionization-ion trap mass spectrometry. *Electrophoresis*, *23*(17), 2904–2912.

Bonechi, C., Donati, A., Tamasi, G., Leone, G., Consumi, M., Rossi, C., Lamponi, S., & Magnani, A. (2018). Protective effect of quercetin and rutin encapsulated liposomes on induced oxidative stress. *Biophysical Chemistry*, *233*, 55–63. https://doi.org/10.1016/J.BPC.2017.11.003

Bonechi, C., Donati, A., Tamasi, G., Pardini, A., Rostom, H., Leone, G., Lamponi, S., Consumi, M., Magnani, A., & Rossi, C. (2019). Chemical characterization of liposomes containing

nutraceutical compounds: Tyrosol, hydroxytyrosol and oleuropein. *Biophysical Chemistry*, *246*, 25–34. https://doi.org/10.1016/j.bpc.2019.01.002

Bonechi, C., Martini, S., Ciani, L., Lamponi, S., Rebmann, H., Rossi, C., & Ristori, S. (2012). Using Liposomes as Carriers for Polyphenolic Compounds: The Case of Trans-Resveratrol. *PLoS ONE*, *7*(8), e41438. https://doi.org/10.1371/journal.pone.0041438

Bonechi, C., Ristori, S., Martini, G., Martini, S., & Rossi, C. (2009). Study of bradykinin conformation in the presence of model membrane by Nuclear Magnetic Resonance and molecular modelling. *Biochimica et Biophysica Acta (BBA) - Biomembranes*, *1788*(3), 708–716. https://doi.org/10.1016/j.bbamem.2008.12.019

Boros, K., Jedlinszki, N., & Csupor, D. (2016). Theanine and Caffeine content of infusions prepared from commercial tea samples. *Pharmacognosy Magazine*, *12*(45), 75–78. https://doi.org/10.4103/0973-1296.176061

Bozzuto, G., & Molinari, A. (2015). Liposomes as nanomedical devices. In *International Journal of Nanomedicine* (Vol. 10, pp. 975–999). Dove Medical Press Ltd. https://doi.org/10.2147/IJN.S68861

Brown, M. S., McDonald, G. M., & Friedman, M. (1999). Sampling leaves of young potato (Solanum tuberosum) plants for glycoalkaloid analysis. *Journal of Agricultural and Food Chemistry*, *47*(6), 2331–2334. https://doi.org/10.1021/jf981124m

Cahill, M. G., Caprioli, G., Vittori, S., & James, K. J. (2010). Elucidation of the mass fragmentation pathways of potato glycoalkaloids and aglycons using Orbitrap mass spectrometry. *Journal of Mass Spectrometry*, *45*(9), 1019–1025. https://doi.org/10.1002/jms.1785

Campa, C., Mondolot, L., Rakotondravao, A., Bidel, L. P. R., Gargadennec, A., Couturon, E., La Fisca, P., Rakotomalala, J.-J., Jay-Allemand, C., & Davis, A. P. (2012). A survey of mangiferin and hydroxycinnamic acid ester accumulation in coffee (Coffea) leaves: biological implications and uses. *Annals of Botany*, *110*(3), 595–613. https://doi.org/10.1093/aob/mcs119

Campbell, R. B., Balasubramanian, S. V., & Straubinger, R. M. (2001). Phospholipid-cationic lipid interactions: influences on membrane and vesicle properties. *Biochimica et Biophysica Acta (BBA) - Biomembranes*, *1512*(1), 27–39. https://doi.org/10.1016/S0005-2736(01)00290-5

Cangeloni, L., Bonechi, C., Leone, G., Consumi, M., Andreassi, M., Magnani, A., Rossi, C., & Tamasi, G. (2022). Characterization of Extracts of Coffee Leaves (Coffea arabica L.) by

Spectroscopic and Chromatographic/Spectrometric Techniques. *Foods*, *11*(16), 2495. https://doi.org/10.3390/foods11162495

Caprioli, G., Cahill, M. G., Vittori, S., & James, K. J. (2014). Liquid Chromatography-Hybrid Linear Ion Trap-High-Resolution Mass Spectrometry (LTQ-Orbitrap) Method for the Determination of Glycoalkaloids and Their Aglycons in Potato Samples. *Food Analytical Methods*, *7*(7), 1367–1372. https://doi.org/10.1007/s12161-013-9758-6

Cataldi, T. R. I., Lelario, F., & Bufo, S. A. (2005). Analysis of tomato glycoalkaloids by liquid chromatography coupled with electrospray ionization tandem mass spectrometry. *Rapid Communications in Mass Spectrometry*, *19*(21), 3103–3110. https://doi.org/10.1002/rcm.2176

Chan, E. W. C., Lim, Y. Y., Wong, S. K., Lim, K. K., Tan, S. P., Lianto, F. S., & Yong, M. Y. (2009). Effects of different drying methods on the antioxidant properties of leaves and tea of ginger species. *Food Chemistry*, *113*(1), 166–172. https://doi.org/10.1016/j.foodchem.2008.07.090

Chen, C., Razali, U. H. M., Saikim, F. H., Mahyudin, A., & Noor, N. Q. I. M. (2021). Morus alba l. Plant: Bioactive compounds and potential as a functional food ingredient. In *Foods* (Vol. 10, Issue 3). MDPI AG. https://doi.org/10.3390/foods10030689

Chen, X. (2019). A review on coffee leaves: Phytochemicals, bioactivities and applications. *Critical Reviews in Food Science and Nutrition*, *59*(6), 1008–1025. https://doi.org/10.1080/10408398.2018.1546667

Chen, X. M., Ma, Z., & Kitts, D. D. (2018). Effects of processing method and age of leaves on phytochemical profiles and bioactivity of coffee leaves. *Food Chemistry*, *249*, 143–153. https://doi.org/10.1016/J.FOODCHEM.2017.12.073

Choung, M. G., Hwang, Y. S., Lee, M. S., Lee, J., Kang, S. T., & Jun, T. H. (2014). Comparison of extraction and isolation efficiency of catechins and caffeine from green tea leaves using different solvent systems. *International Journal of Food Science and Technology*, *49*(6), 1572–1578. https://doi.org/10.1111/ijfs.12454

Clemente, I., Baglioni, M., Bonechi, C., Bisozzi, F., Rossi, C., & Tamasi, G. (2023). Green Hydrogels Loaded with Extracts from Solanaceae for the Controlled Disinfection of Agricultural Soils. *Polymers*, *15*(22), 4455. https://doi.org/10.3390/polym15224455

Clifford, M. N., Johnston, K. L., Knight, S., & Kuhnert, N. (2003). Hierarchical scheme for LC-MSn identification of chlorogenic acids. *Journal of Agricultural and Food Chemistry*, *51*(10), 2900–2911. https://doi.org/10.1021/jf026187q

Clifford, M. N., Kirkpatrick, J., Kuhnert, N., Roozendaal, H., & Salgado, P. R. (2008). LC-MSn analysis of the cis isomers of chlorogenic acids. *Food Chemistry*, *106*(1), 379–385. https://doi.org/10.1016/j.foodchem.2007.05.081

Clogston, J. D., & Patri, A. K. (2011). Zeta Potential Measurement. In *Methods in Molecular Biology* (Vol. 697, pp. 63–70). Humana Press Inc. https://doi.org/10.1007/978-1-60327-198-1_6

Danaei, M., Dehghankhold, M., Ataei, S., Hasanzadeh Davarani, F., Javanmard, R., Dokhani, A., Khorasani, S., & Mozafari, M. (2018). Impact of Particle Size and Polydispersity Index on the Clinical Applications of Lipidic Nanocarrier Systems. *Pharmaceutics*, *10*(2), 57. https://doi.org/10.3390/pharmaceutics10020057

Dantas, C. A. G., Abreu, L. S., da Cunha, H. N., Veloso, C. A. G., Souto, A. L., de Fátima Agra, M., de Oliveira Costa, V. C., da Silva, M. S., & Tavares, J. F. (2021). Dereplication of phenolic derivatives of three Erythroxylum species using liquid chromatography coupled with ESI-MSn and HRESIMS. *Phytochemical Analysis*, *32*(6), 1011–1026. https://doi.org/10.1002/pca.3043

Dar, A., Faizi, S., Naqvi, S., Roome, T., Zikr-ur-Rehman, S., Ali, M., Firdous, S., & Moin, S. T. (2005). Analgesic and Antioxidant Activity of Mangiferin and Its Derivatives: the Structure Activity Relationship. *Biological and Pharmaceutical Bulletin*, *28*(4), 596–600. https://doi.org/10.1248/bpb.28.596

de Almeida, R. F., Trevisan, M. T. S., Thomaziello, R. A., Breuer, A., Klika, K. D., Ulrich, C. M., & Owen, R. W. (2019a). Nutraceutical compounds: Echinoids, flavonoids, xanthones and caffeine identified and quantitated in the leaves of Coffea arabica trees from three regions of Brazil. *Food Research International*, *115*, 493–503. https://doi.org/10.1016/j.foodres.2018.10.006

Distl, M., & Wink, M. (2009). Identification and quantification of steroidal alkaloids from wild tuber-bearing solanum species by HPLC and LC-ESI-MS. *Potato Research*, *52*(1), 79–104. https://doi.org/10.1007/s11540-008-9123-0

Esquivel, P., Viñas, M., Steingass, C. B., Gruschwitz, M., Guevara, E., Carle, R., Schweiggert, R. M., & Jiménez, V. M. (2020). Coffee (Coffea arabica L.) by-Products as a Source of Carotenoids and Phenolic Compounds—Evaluation of Varieties With Different Peel Color. *Frontiers in Sustainable Food Systems*, *4*, 590597. https://doi.org/10.3389/fsufs.2020.590597

Feng, Y., Sun, C., Yuan, Y., Zhu, Y., Wan, J., Firempong, C. K., Omari-Siaw, E., Xu, Y., Pu, Z., Yu, J., & Xu, X. (2016). Enhanced oral bioavailability and in vivo antioxidant activity

of chlorogenic acid via liposomal formulation. *International Journal of Pharmaceutics*, *501*(1–2), 342–349. https://doi.org/10.1016/j.ijpharm.2016.01.081

Ferenczi-Fodor, K., Végh, Z., Nagy-Turák, A., Renger, B., & Zeller, M. (2001). Validation and Quality Assurance of Planar Chromatographic Procedures in Pharmaceutical Analysis. *Journal of AOAC INTERNATIONAL*, *84*(4), 1265–1276. https://doi.org/10.1093/jaoac/84.4.1265

Friedman, M. (2006). Potato Glycoalkaloids and Metabolites: Roles in the Plant and in the Diet. *Journal of Agricultural and Food Chemistry*, *54*(23), 8655–8681. https://doi.org/10.1021/jf061471t

Friedman, M. (2015). Chemistry and Anticarcinogenic Mechanisms of Glycoalkaloids Produced by Eggplants, Potatoes, and Tomatoes. In *Journal of Agricultural and Food Chemistry* (Vol. 63, Issue 13, pp. 3323–3337). American Chemical Society. https://doi.org/10.1021/acs.jafc.5b00818

Friedman, M., & Dao, L. (n.d.). Distribution of Glycoalkaloids in Potato Plants and Commercial Potato Products. In *J. Agric. Food Chem* (Vol. 1002).

Gebhardt, C. (2016). The historical role of species from the Solanaceae plant family in genetic research. In *Theoretical and Applied Genetics* (Vol. 129, Issue 12, pp. 2281–2294). Springer Verlag. https://doi.org/10.1007/s00122-016-2804-1

Giacomino, A., Abollino, O., Malandrino, M., & Mentasti, E. (2011). The role of chemometrics in single and sequential extraction assays: A Review. Part II. Cluster analysis, multiple linear regression, mixture resolution, experimental design and other techniques. In *Analytica Chimica Acta* (Vol. 688, Issue 2, pp. 122–139). https://doi.org/10.1016/j.aca.2010.12.028

Gogna, N., Hamid, N., & Dorai, K. (2015). Metabolomic profiling of the phytomedicinal constituents of Carica papaya L. leaves and seeds by 1H NMR spectroscopy and multivariate statistical analysis. *Journal of Pharmaceutical and Biomedical Analysis*, *115*, 74–85. https://doi.org/10.1016/j.jpba.2015.06.035

Han, W., Chen, X., Yu, H., Chen, L., & Shen, M. (2018). Seasonal variations of iminosugars in mulberry leaves detected by hydrophilic interaction chromatography coupled with tandem mass spectrometry. *Food Chemistry*, *251*, 110–114. https://doi.org/10.1016/j.foodchem.2018.01.058

He, B., Li, Q., Jia, Y., Zhao, L., Xiao, F., Lv, C., Xu, H., Chen, X., & Bi, K. (2012). A UFLC-MS/MS method for simultaneous quantitation of spinosin, mangiferin and ferulic acid in

rat plasma: application to a comparative pharmacokinetic study in normal and insomnic rats. *Journal of Mass Spectrometry*, *47*(10), 1333–1340. https://doi.org/10.1002/jms.3072

Hu, X. Q., Jiang, L., Zhang, J. G., Deng, W., Wang, H. L., & Wei, Z. J. (2013). Quantitative determination of 1-deoxynojirimycin in mulberry leaves from 132 varieties. *Industrial Crops and Products*, *49*, 782–784. https://doi.org/10.1016/j.indcrop.2013.06.030

Jaiswal, R., Sovdat, T., Vivan, F., & Kuhnert, N. (2010). Profiling and characterization by LC-MSn of the chlorogenic acids and hydroxycinnamoylshikimate esters in maté (Ilex paraguariensis). *Journal of Agricultural and Food Chemistry*, *58*(9), 5471–5484. https://doi.org/10.1021/jf904537z

Jungfer, E., Zimmermann, B. F., Ruttkat, A., & Galensa, R. (2012). Comparing procyanidins in selected Vaccinium species by UHPLC-MS 2 with regard to authenticity and health effects. *Journal of Agricultural and Food Chemistry*, *60*(38), 9688–9696. https://doi.org/10.1021/jf303100q

Justesen, U., & Arrigoni, E. (2001). Electrospray ionisation mass spectrometric study of degradation products of quercetin, quercetin-3-glucoside and quercetin-3-rhamnoglucoside, produced by in vitro fermentation with human faecal flora. *Rapid Communications in Mass Spectrometry*, *15*(7), 477–483. https://doi.org/10.1002/rcm.250

Juvik, J. A., & Stevens, M. A. (1982). Inheritance of Foliar α-Tomatine Content in Tomatoes1. *Journal of the American Society for Horticultural Science*, *107*(6), 1061–1065. https://doi.org/10.21273/JASHS.107.6.1061

Kazuno, S., Yanagida, M., Shindo, N., & Murayama, K. (2005). Mass spectrometric identification and quantification of glycosyl flavonoids, including dihydrochalcones with neutral loss scan mode. *Analytical Biochemistry*, *347*(2), 182–192. https://doi.org/10.1016/j.ab.2005.09.020

Khallouki, F., Ricarte, I., Breuer, A., & Owen, R. W. (2018). Characterization of phenolic compounds in mature Moroccan Medjool date palm fruits (Phoenix dactylifera) by HPLC-DAD-ESI-MS. *Journal of Food Composition and Analysis*, *70*(May 2017), 63–71. https://doi.org/10.1016/j.jfca.2018.03.005

Kimura, T., Nakagawa, K., Saito, Y., Yamagishi, K., Suzuki, M., Yamaki, K., Shinmoto, H., & Miyazawa, T. (2004). Determination of 1-Deoxynojirimycin in Mulberry Leaves Using Hydrophilic Interaction Chromatography with Evaporative Light Scattering Detection. *Journal of Agricultural and Food Chemistry*, *52*(6), 1415–1418. https://doi.org/10.1021/jf0306901

Knapp, S., Bohs, L., Nee, M., & Spooner, D. M. (2004). Solanaceae - A model for linking genomics with biodiversity. *Comparative and Functional Genomics*, *5*(3), 285–291. https://doi.org/10.1002/CFG.393

Kozukue, N., Yoon, K. S., Byun, G. I. N., Misoo, S., Levin, C. E., & Friedman, M. (2008). Distribution of glycoalkaloids in potato tubers of 59 accessions of two wild and five cultivated Solanum species. *Journal of Agricultural and Food Chemistry*, *56*(24), 11920–11928. https://doi.org/10.1021/jf802631t

Kumar, K., Srivastav, S., & Sharanagat, V. S. (2021). Ultrasound assisted extraction (UAE) of bioactive compounds from fruit and vegetable processing by-products: A review. In *Ultrasonics Sonochemistry* (Vol. 70). Elsevier B.V. https://doi.org/10.1016/j.ultsonch.2020.105325

Lashermes, P., Combes, M.-C., Robert, J., Trouslot, P., D'Hont, A., Anthony, F., & Charrier, A. (1999). Molecular characterisation and origin of the Coffea arabica L. genome. *Molecular and General Genetics MGG*, *261*(2), 259–266. https://doi.org/10.1007/s004380050965

Lim, H. K., Chen, J., Sensenhauser, C., Cook, K., & Subrahmanyam, V. (2007). Metabolite identification by data-dependent accurate mass spectrometric analysis at resolving power of 60 000 in external calibration mode using an LTQ/Orbitrap. *Rapid Communications in Mass Spectrometry*, *21*(12), 1821–1832. https://doi.org/10.1002/rcm.3024

Maja, L., Željko, K., & Mateja, P. (2020). Sustainable technologies for liposome preparation. In *Journal of Supercritical Fluids* (Vol. 165). Elsevier B.V. https://doi.org/10.1016/j.supflu.2020.104984

Malherbe, C. J., Willenburg, E., De Beer, D., Bonnet, S. L., Van der Westhuizen, J. H., & Joubert, E. (2014). Iriflophenone-3-C-glucoside from Cyclopia genistoides: Isolation and quantitative comparison of antioxidant capacity with mangiferin and isomangiferin using on-line HPLC antioxidant assays. *Journal of Chromatography B: Analytical Technologies in the Biomedical and Life Sciences*, *951–952*(1), 164–171. https://doi.org/10.1016/j.jchromb.2014.01.038

Marchetti, L., Saviane, A., Montà, A. D., Paglia, G., Pellati, F., Benvenuti, S., Bertelli, D., & Cappellozza, S. (2021). Determination of 1-deoxynojirimycin (1-dnj) in leaves of italian or italy-adapted cultivars of mulberry (morus sp.pl.) by hplc-ms. *Plants*, *10*(8). https://doi.org/10.3390/plants10081553

Marcolongo, P., Gamberucci, A., Tamasi, G., Pardini, A., Bonechi, C., Rossi, C., Giunti, R., Barone, V., Borghini, A., Fiorenzani, P., Frosini, M., Valoti, M., & Pessina, F. (2020).

Chemical characterisation and antihypertensive effects of locular gel and serum of Lycopersicum esculentum L. var. “Camone” tomato in spontaneously hypertensive rats. *Molecules*, *25*(16). https://doi.org/10.3390/molecules25163758

Martini, S., Conte, A., & Tagliazucchi, D. (2017). Phenolic compounds profile and antioxidant properties of six sweet cherry (Prunus avium) cultivars. *Food Research International*, *97*, 15–26. https://doi.org/10.1016/j.foodres.2017.03.030

Miao, M., & Xiang, L. (2020). Pharmacological action and potential targets of chlorogenic acid. In *Advances in Pharmacology* (Vol. 87, pp. 71–88). Academic Press Inc. https://doi.org/10.1016/bs.apha.2019.12.002

Milner, S. E., Brunton, N. P., Jones, P. W., O Brien, N. M., Collins, S. G., & Maguire, A. R. (2011). Bioactivities of glycoalkaloids and their aglycones from solanum species. In *Journal of Agricultural and Food Chemistry* (Vol. 59, Issue 8, pp. 3454–3484). https://doi.org/10.1021/jf200439q

Monteiro, Â., Colomban, S., Azinheira, H. G., Guerra-Guimarães, L., Do Céu Silva, M., Navarini, L., & Resmini, M. (2019). Dietary Antioxidants in Coffee Leaves: Impact of Botanical Origin and Maturity on Chlorogenic Acids and Xanthones. *Antioxidants*, *9*(1), 6. https://doi.org/10.3390/antiox9010006

Monteiro, Â., Colomban, S., Azinheira, H. G., Guerra-Guimarães, L., Silva, M. D. C., Navarini, L., & Resmini, M. (2020). Dietary antioxidants in coffee leaves: Impact of botanical origin and maturity on chlorogenic acids and xanthones. *Antioxidants*, *9*(1). https://doi.org/10.3390/antiox9010006

Mullard, G., Allwood, J. W., Weber, R., Brown, M., Begley, P., Hollywood, K. A., Jones, M., Unwin, R. D., Bishop, P. N., Cooper, G. J. S., & Dunn, W. B. (2015). A new strategy for MS/MS data acquisition applying multiple data dependent experiments on Orbitrap mass spectrometers in non-targeted metabolomic applications. *Metabolomics*, *11*(5), 1068–1080. https://doi.org/10.1007/s11306-014-0763-6

Naveed, M., Hejazi, V., Abbas, M., Kamboh, A. A., Khan, G. J., Shumzaid, M., Ahmad, F., Babazadeh, D., FangFang, X., Modarresi-Ghazani, F., WenHua, L., & XiaoHui, Z. (2018). Chlorogenic acid (CGA): A pharmacological review and call for further research. *Biomedicine & Pharmacotherapy*, *97*, 67–74. https://doi.org/10.1016/j.biopha.2017.10.064

Nepal, B., & Stine, K. J. (2019). Glycoalkaloids: Structure, properties, and interactions with model membrane systems. In *Processes* (Vol. 7, Issue 8). MDPI. https://doi.org/10.3390/PR7080513

Ngamsuk, S., Huang, T. C., & Hsu, J. L. (2019a). Determination of phenolic compounds, procyanidins, and antioxidant activity in processed coffea Arabica L. leaves. *Foods*, *8*(9), 1–13. https://doi.org/10.3390/foods8090389

Ngamsuk, S., Huang, T. C., & Hsu, J. L. (2019b). Determination of phenolic compounds, procyanidins, and antioxidant activity in processed coffea Arabica L. leaves. *Foods*, *8*(9). https://doi.org/10.3390/foods8090389

Niggeweg, R., Michael, A. J., & Martin, C. (2004). Engineering plants with increased levels of the antioxidant chlorogenic acid. *Nature Biotechnology*, *22*(6), 746–754. https://doi.org/10.1038/nbt966

Nuengchamnong, N., Ingkaninan, K., Kaewruang, W., Wongareonwanakij, S., & Hongthongdaeng, B. (2007). Quantitative determination of 1-deoxynojirimycin in mulberry leaves using liquid chromatography-tandem mass spectrometry. *Journal of Pharmaceutical and Biomedical Analysis*, *44*(4), 853–858. https://doi.org/10.1016/j.jpba.2007.03.031

Osman, S. F., Herb, S. F., Fitzpatrick, T. J., & Schmiediche, P. (1978). Glycoalkaloid composition of wild and cultivated tuber-bearing Solanum species of potential value in potato breeding programs. *Journal of Agricultural and Food Chemistry*, *26*(5), 1246–1248. https://doi.org/10.1021/jf60219a024

Pan, B., Zhong, W., Deng, Z., Lai, C., Chu, J., Jiao, G., Liu, J., & Zhou, Q. (2016). Inhibition of prostate cancer growth by solanine requires the suppression of cell cycle proteins and the activation of ROS/P38 signaling pathway. *Cancer Medicine*, *5*(11), 3214–3222. https://doi.org/10.1002/cam4.916

Panche, A. N., Diwan, A. D., & Chandra, S. R. (2016a). Flavonoids: an overview. *Journal of Nutritional Science*, *5*, e47. https://doi.org/10.1017/jns.2016.41

Panche, A. N., Diwan, A. D., & Chandra, S. R. (2016b). Flavonoids: an overview. *Journal of Nutritional Science*, *5*, e47. https://doi.org/10.1017/jns.2016.41

Pardini, A., Consumi, M., Leone, G., Bonechi, C., Tamasi, G., Sangiorgio, P., Verardi, A., Rossi, C., & Magnani, A. (2021). Effect of different post-harvest storage conditions and heat treatment on tomatine content in commercial varieties of green tomatoes. *Journal of Food Composition and Analysis*, *96*. https://doi.org/10.1016/j.jfca.2020.103735

Patay, É. B., Bencsik, T., & Papp, N. (2016). Phytochemical overview and medicinal importance of Coffea species from the past until now. In *Asian Pacific Journal of Tropical Medicine* (Vol. 9, Issue 12, pp. 1127–1135). Elsevier (Singapore) Pte Ltd. https://doi.org/10.1016/j.apjtm.2016.11.008

Perrone, D., Donangelo, R., Donangelo, C. M., & Farah, A. (2010). Modeling weight loss and chlorogenic acids content in coffee during roasting. *Journal of Agricultural and Food Chemistry*, *58*(23), 12238–12243. https://doi.org/10.1021/jf102110u

Piao, X., Li, S., Sui, X., Guo, L., Liu, X., Li, H., Gao, L., Cai, S., Li, Y., Wang, T., & Liu, B. (2018). 1-Deoxynojirimycin (DNJ) ameliorates indomethacin-induced gastric ulcer in mice by affecting NF-kappaB signaling pathway. *Frontiers in Pharmacology*, *9*(APR). https://doi.org/10.3389/fphar.2018.00372

Quidde, T., Osbourn, A. E., & Tudzynski, P. (1998). Detoxification of α-tomatine byBotrytis cinerea. *Physiological and Molecular Plant Pathology*, *52*(3), 151–165. https://doi.org/10.1006/pmpp.1998.0142

Ramappa, V. K., Srivastava, D., Singh, P., Kumar, U., & Singh, V. (2020). Mulberry 1-deoxynojirimycin (DNJ): an exemplary compound for therapeutics. *The Journal of Horticultural Science and Biotechnology*, *95*(6), 679–686. https://doi.org/10.1080/14620316.2020.1760738

Resende, F. O., Rodrigues-Filho, E., Luftmann, H., Petereit, F., & De Mello, J. C. P. (2011). Phenylpropanoid substituted flavan-3-ols from trichilia catigua and their in vitro antioxidative activity. *Journal of the Brazilian Chemical Society*, *22*(11), 2087–2093. https://doi.org/10.1590/S0103-50532011001100010

Rockenbach, I. I., Jungfer, E., Ritter, C., Santiago-Schübel, B., Thiele, B., Fett, R., & Galensa, R. (2012). Characterization of flavan-3-ols in seeds of grape pomace by CE, HPLC-DAD-MS n and LC-ESI-FTICR-MS. *Food Research International*, *48*(2), 848–855. https://doi.org/10.1016/j.foodres.2012.07.001

Rodríguez-Gómez, R., Vanheuverzwjin, J., Souard, F., Delporte, C., Stevigny, C., Stoffelen, P., De Braekeleer, K., & Kauffmann, J.-M. (2018). Determination of Three Main Chlorogenic Acids in Water Extracts of Coffee Leaves by Liquid Chromatography Coupled to an Electrochemical Detector. *Antioxidants*, *7*(10), 143. https://doi.org/10.3390/antiox7100143

Rohela, G. K., Shukla, P., Muttanna, Kumar, R., & Chowdhury, S. R. (2020). Mulberry (Morus spp.): An ideal plant for sustainable development. In *Trees, Forests and People* (Vol. 2). Elsevier B.V. https://doi.org/10.1016/j.tfp.2020.100011

Rue, E. A., Rush, M. D., & van Breemen, R. B. (2018). Procyanidins: a comprehensive review encompassing structure elucidation via mass spectrometry. *Phytochemistry Reviews*, *17*(1), 1–16. https://doi.org/10.1007/s11101-017-9507-3

Salerno, R., Casale, F., Calandruccio, C., & Procopio, A. (2016). Characterization of flavonoids in Citrus bergamia (Bergamot) polyphenolic fraction by liquid chromatography–high resolution mass spectrometry (LC/HRMS). *PharmaNutrition*, *4*, S1–S7. https://doi.org/10.1016/j.phanu.2015.10.001

Sánchez-Maldonado, A. F., Schieber, A., & Gänzle, M. G. (2016). Antifungal activity of secondary plant metabolites from potatoes (Solanum tuberosum L.): Glycoalkaloids and phenolic acids show synergistic effects. *Journal of Applied Microbiology*, *120*(4), 955–965. https://doi.org/10.1111/jam.13056

Segheto, L., Santos, B. C. S., Werneck, A. F. L., Vilela, F. M. P., Sousa, O. V. de, & Rodarte, M. P. (2018). Antioxidant extracts of coffee leaves and its active ingredient 5-caffeoylquinic acid reduce chemically-induced inflammation in mice. *Industrial Crops and Products*, *126*, 48–57. https://doi.org/10.1016/J.INDCROP.2018.09.027

Shakya, R., & Navarre, D. A. (2008). LC-MS analysis of solanidane glycoalkaloid diversity among tubers of four wild potato species and three cultivars (Solanum tuberosum). *Journal of Agricultural and Food Chemistry*, *56*(16), 6949–6958. https://doi.org/10.1021/jf8006618

Sharma, A., & Sharma, U. S. (1997). international journal of pharmaceutics Review Liposomes in drug delivery: progress and limitations. In *International Journal of Pharmaceutics* (Vol. 154).

Shih, M.-J., & Kuć, J. (1974). α and β-solamarine in kennebec Solanum tuberosum leaves and aged tuber slices. *Phytochemistry*, *13*(6), 997–1000. https://doi.org/10.1016/S0031-9422(00)91436-5

Shin, J. S., Lee, K. G., Lee, H. H., Lee, H. J., An, H. J., Nam, J. H., Jang, D. S., & Lee, K. T. (2016). α-Solanine Isolated From Solanum Tuberosum L. cv Jayoung Abrogates LPS-Induced Inflammatory Responses Via NF-κB Inactivation in RAW 264.7 Macrophages and Endotoxin-Induced Shock Model in Mice. *Journal of Cellular Biochemistry*, 2327–2339. https://doi.org/10.1002/jcb.25530

Smith, M. C., Crist, R. M., Clogston, J. D., & McNeil, S. E. (2017). Zeta potential: a case study of cationic, anionic, and neutral liposomes. *Analytical and Bioanalytical Chemistry*, *409*(24), 5779–5787. https://doi.org/10.1007/s00216-017-0527-z

Stöggl, W. M., Huck, C. W., & Bonn, G. K. (2004). Structural elucidation of catechin and epicatechin in sorrel leaf extracts using liquid-chromatography coupled to diode array-, fluorescence- ,and mass spectrometric detection. *Journal of Separation Science*, *27*(7–8), 524–528. https://doi.org/10.1002/jssc.200301694

Sun, W., & Miller, J. M. (2003). Tandem mass spectrometry of the B-type procyanidins in wine and B-type dehydrodicatechins in an autoxidation mixture of (+)-catechin and (-)-epicatechin. *Journal of Mass Spectrometry*, *38*(4), 438–446. https://doi.org/10.1002/jms.456

Surianarayanan, R., Gurumallappa Shivakumar, H., Varma Vegesna, N. S. K., & Srivastava, A. (2016). Effect of sample Concentration on the Characterization of Liposomes using Dynamic light Scattering Technique. *Pharmaceutical Methods*, *7*(1), 70–74. https://doi.org/10.5530/phm.2016.7.11

Tam, C. C., Nguyen, K., Nguyen, D., Hamada, S., Kwon, O., Kuang, I., Gong, S., Escobar, S., Liu, M., Kim, J., Hou, T., Tam, J., Cheng, L. W., Kim, J. H., Land, K. M., & Friedman, M. (2021). Antimicrobial properties of tomato leaves, stems, and fruit and their relationship to chemical composition. *BMC Complementary Medicine and Therapies*, *21*(1). https://doi.org/10.1186/s12906-021-03391-2

Tamasi, G., Baratto, M. C., Bonechi, C., Byelyakova, A., Pardini, A., Donati, A., Leone, G., Consumi, M., Lamponi, S., Magnani, A., & Rossi, C. (2019). Chemical characterization and antioxidant properties of products and by-products from *Olea europaea* L. *Food Science & Nutrition*, *7*(9), 2907–2920. https://doi.org/10.1002/fsn3.1142

Tamasi, G., Pardini, A., Bonechi, C., Donati, A., Pessina, F., Marcolongo, P., Gamberucci, A., Leone, G., Consumi, M., Magnani, A., & Rossi, C. (2019). Characterization of nutraceutical components in tomato pulp, skin and locular gel. *European Food Research and Technology*, *245*(4), 907–918. https://doi.org/10.1007/s00217-019-03235-x

Tamasi, G., Pardini, A., Croce, R., Consumi, M., Leone, G., Bonechi, C., Rossi, C., & Magnani, A. (2021). Combined experimental and multivariate model approaches for glycoalkaloid quantification in tomatoes. *Molecules*, *26*(11). https://doi.org/10.3390/molecules26113068

Terahara, N. (2015). Flavonoids in Foods: A Review. *Natural Product Communications*, *10*(3), 1934578X1501000. https://doi.org/10.1177/1934578X1501000334

Traïkia, M., Warschawski, D. E., Recouvreur, M., Cartaud, J., & Devaux, P. F. (2000). Formation of unilamellar vesicles by repetitive freeze-thaw cycles: characterization by electron microscopy and 31 P-nuclear magnetic resonance. *European Biophysics Journal*, *29*(3), 184–195. https://doi.org/10.1007/s002490000077

Troiano, J. M., Olenick, L. L., Kuech, T. R., Melby, E. S., Hu, D., Lohse, S. E., Mensch, A. C., Dogangun, M., Vartanian, A. M., Torelli, M. D., Ehimiaghe, E., Walter, S. R., Fu, L., Anderton, C. R., Zhu, Z., Wang, H., Orr, G., Murphy, C. J., Hamers, R. J., … Geiger, F.

M. (2015). Direct probes of 4 nm diameter gold nanoparticles interacting with supported lipid bilayers. *Journal of Physical Chemistry C*, *119*(1), 534–546. https://doi.org/10.1021/jp512107z

Ulrich, E. L., Akutsu, H., Doreleijers, J. F., Harano, Y., Ioannidis, Y. E., Lin, J., Livny, M., Mading, S., Maziuk, D., Miller, Z., Nakatani, E., Schulte, C. F., Tolmie, D. E., Kent Wenger, R., Yao, H., & Markley, J. L. (2007). BioMagResBank. *Nucleic Acids Research*, *36*(Suppl_1), D402–D408. https://doi.org/10.1093/nar/gkm957

Vial, J., & Jardy, A. (1999). Experimental Comparison of the Different Approaches To Estimate LOD and LOQ of an HPLC Method. *Analytical Chemistry*, *71*(14), 2672–2677. https://doi.org/10.1021/ac981179n

Wang, L., & Weller, C. L. (2006). Recent advances in extraction of nutraceuticals from plants. *Trends in Food Science & Technology*, *17*(6), 300–312. https://doi.org/10.1016/j.tifs.2005.12.004

Wang, Y., Berhow, M. A., Black, M., & Jeffery, E. H. (2020). A comparison of the absorption and metabolism of the major quercetin in brassica, quercetin-3-O-sophoroside, to that of quercetin aglycone, in rats. *Food Chemistry*, *311*(April), 125880. https://doi.org/10.1016/j.foodchem.2019.125880

Wang, Y., Zhang, T., Xu, J., & Du, W. (2011). Comparison of the binding affinity of chlorogenic acid with two serum albumins. *International Journal of Biological Macromolecules*, *48*(1), 81–86. https://doi.org/10.1016/j.ijbiomac.2010.09.015

Wanyonyi, A. W., Chhabra, S. C., Mkoji, G., Eilert, U., & Njue, W. M. (n.d.). *Bioactive steroidal alkaloid glycosides from Solanum aculeastrum*. www.elsevier.com/locate/phytochem

Wei, A. A. J., Joshi, A., Chen, Y., & McIndoe, J. S. (2020). Strategies for avoiding saturation effects in ESI-MS. *International Journal of Mass Spectrometry*, *450*. https://doi.org/10.1016/j.ijms.2020.116306

Wink, M. (2003). Evolution of secondary metabolites from an ecological and molecular phylogenetic perspective. *Phytochemistry*, *64*, 3–19. https://doi.org/10.1016/S0031-9422(03)00300-5

Wishart, D. S., Guo, A., Oler, E., Wang, F., Anjum, A., Peters, H., Dizon, R., Sayeeda, Z., Tian, S., Lee, B. L., Berjanskii, M., Mah, R., Yamamoto, M., Jovel, J., Torres-Calzada, C., Hiebert-Giesbrecht, M., Lui, V. W., Varshavi, D., Varshavi, D., … Gautam, V. (2022). HMDB 5.0: the Human Metabolome Database for 2022. *Nucleic Acids Research*, *50*(D1), D622–D631. https://doi.org/10.1093/nar/gkab1062

Wu, S. B., Meyer, R. S., Whitaker, B. D., Litt, A., & Kennelly, E. J. (2013). A new liquid chromatography-mass spectrometry-based strategy to integrate chemistry, morphology, and evolution of eggplant (Solanum) species. *Journal of Chromatography A*, *1314*, 154–172. https://doi.org/10.1016/j.chroma.2013.09.017

Yuan, Q., & Zhao, L. (2017). The Mulberry (Morus alba L.) Fruit—A Review of Characteristic Components and Health Benefits. *Journal of Agricultural and Food Chemistry*, *65*(48), 10383–10394. https://doi.org/10.1021/acs.jafc.7b03614